Understanding Fibroblast Behaviour in an Electrospun Microfibrous Scaffold

Joe Peter Woodley

A thesis submitted to The University of Sheffield in fulfilment of the requirements for the degree of

Doctor of Philosophy

The School of Clinical Dentistry

Faculty of Medicine, Dentistry, and Health

7th July 2023

Acknowledgements

I could not have undertaken this project without the guidance and unwavering support of my supervisors Dr. Ilida Ortega Asencio and Prof. Daniel Lambert. Thank you for encouraging me to publish my work and your crucial role in conceptualising, reviewing and editing many draft manuscripts. Ilida, I could not have hoped for a more enthusiastic or supportive primary supervisor, being part of your research group has been so much fun. Dan, thank you for your wisdom and all the 'kudos' on Strava, you now know exactly how much time I spent running when I should have been working!

I would like to thank the technical and administrative staff at the University of Sheffield School of Clinical Dentistry. I am especially indebted to Lisa Chang, Matthew Worsley, Brenka McCabe, Kirsty Franklin and Jason Heath. I was also lucky enough to receive technical help from Dr Christopher Hill in the Firth Court electron microscope facility, Dr Oday Hussein in the characterisation small research facility and Linden Drezet in the water engineering laboratory. I am grateful to have shared this experience with the Dental School research community, especially my dear friends Hatim, Rayan, Ali, Martina and Cathy.

I would like to thank my house mates, Dr Joe Law, Grace Kelleher, Erin and Kes. Thank you for putting up with me. When Erin is a grumpy teen, I will remind her that she has the best housemates on the planet. Thanks to Joe, Alex, Cynog, Ben, Ed, Harriet and Tim for all the runs, rides and climbs in the wonderful Peak District. Thanks also to Hallamshire Harriers and Dark Peak Fell Runners – British relay champions!

Finally, thank you to my wonderful family, especially my parents and sister who have always been my greatest educators. Thank you for investing so much time and energy into supporting me in everything I do. Thank you for letting me and Antonia move home during COVID, it was a special time.

Antonia, thank you for everything you do, I love you and our life together.

Joe Woodley

Abstract

Fibroblasts are connective tissue cells with multiple functions in health and disease. They are responsible for maintenance of the extracellular matrix and become activated during the wound healing response. Persistently active fibroblast populations are implicated in the development of fibrotic tissue and have come under increasing scrutiny as key constituents of the tumour stroma. Given their complex roles in health, regeneration and disease and accounting for the fibrous matrix in which fibroblasts reside in vivo, these cells have been extensively studied in three-dimensional tissue culture models.

The aim of this thesis was to explore the behaviour of fibroblast cells cultured on 3D electrospun polycaprolactone scaffolds. The hypothesis that scaffolds mimic the microarchitecture of the extracellular matrix and are sufficient to maintain a population of low activity in-vivo like fibroblasts was tested with scaffolds fabricated at the University of Sheffield, School of Clinical Dentistry. These scaffolds were characterised using SEM image analysis, water contact angle and uniaxial mechanical testing and mercury intrusion porosimetry. Fibre widths and orientation resembled the arrangement of collagen in the extracellular matrix.

Fibroblasts were seeded onto electrospun scaffolds and 2D tissue culture plastic controls. On scaffolds fewer normal oral fibroblasts (NOF) expressed the proliferation marker Ki67 and qPCR revealed that this was due to cellular quiescence, not senescence. On scaffolds qPCR showed that the expression of activation marker α-SMA and ECM protein coding genes collagen 1, fibronectin and versican was reduced compared to 2D controls. Next generation RNA sequencing revealed that the MAPK pathway was suppressed in scaffold grown fibroblasts. Finally, cancer associated fibroblasts (CAF) cultured on electrospun scaffolds showed reduced expression of CAF markers ACTA2, PDGFR, TNC and VCAN. These results indicate that electrospun polycaprolactone scaffolds can trigger a reduction in the activation behaviour of NOF and CAF. In the future this model can be used to develop our understanding of fibroblast diseases and to seek novel therapeutic targets.

Outputs

Publications

Woodley JP, Lambert DW, Asencio IO. **Understanding Fibroblast Behaviour in 3D Biomaterials.** Tissue Eng Part B Rev. 2022 Jun; 28(3):569-578. Doi: 10.1089/ten.TEB.2021.0010.

Woodley JP, Lambert DW, Asencio IO. **Reduced Fibroblast Activation on Electrospun Polycaprolactone Scaffolds.** Bioengineering. 2023; 10(3):348. Doi: 10.3390/bioengineering10030348

Licenses have been acquired for the reproduction of published materials listed above.

Presentations

University of Sheffield School of Clinical Dentistry Postgraduate Research Day 2023

1st place: “Gone in 60 seconds”. Students are challenged to condense three years of research into a 60 second video that communicates the project background, research methods and major scientific findings.

The University of Sheffield Extracellular Matrix and Stroma Group April Meeting 2022

A presentation on “Reduced fibroblast activation on electrospun polycaprolactone scaffolds”.

White Rose Biomaterials and Tissue Engineering Group Annual Meeting 2020 (online)

A presentation on “Understanding fibroblast behaviour in 3D fibrous biomaterials”.

Posters

UK Society for Biomaterials Annual Meeting 2022

11th World Biomaterials Congress 2020 (Online)

Contents

Abbreviations

AFM - Atomic Force Microscopy

AM - Acetoxymethyl

α-SMA - Alpha-Smooth Muscle Actin

BCA - Bicinchoninic Acid

β-gal - Beta-galactosidase

BSA - Bovine Serum Albumin

B2M - Beta-2-Microglobulin

CAF - Cancer Associated Fibroblasts

Cdc42 - Cell Division Cycle 42

cDNA - Copy DNA

CT – Cycle Threshold

DCM - Dichloromethane

DE - Differentially Expressed

DMEM - Dulbecco’s Modified Eagle's Medium

DMF - Dimethylformamide

DNase - Deoxyribonuclease

dNTP- Deoxynucleotide Triphosphate

dsDNA - Double Stranded DNA

ECL - Enhanced Chemiluminescence

EDTA - Ethylenediaminetetraacetic

EMT - Epithelial-Mesenchymal Transition

ERK - Extracellular Signal-Regulated Kinase

ES - Electrospun

EtOH - Ethyl Alcohol (Ethanol)

F-actin - Filamentous Actin

FBS - Foetal Bovine Serum

FDA - Food and Drug Administration

FDR - False Discovery Rate

FGF - Fibroblast Growth Factor

GAG - Glycosaminoglycan

GAPDH - Glyceraldehyde 3-Phosphate Dehydrogenase

GO - Gene Ontology

Grb2 - Growth factor receptor-bound protein 2

GSEA - Gene Set Enrichment Analysis

GTPase - Guanosine Triphosphate Hydrolase

GU - Gauge

HER2 - Human Epidermal Growth Factor Receptor Type 2

HGF - Hepatocyte Growth Factor

IgG - Immunoglobulin G

IMS - Industrial Methylated Spirit

IN - Inch

KEGG - Kyoto Encyclopedia of Genes and Genomes

LM - Lower Marker

LPA - Lysophosphatidic Acid

mAb - Monoclonal Antibody

MAPK - Mitogen-Activated Protein Kinase

MIP - Mercury Intrusion Porosity

MMP - Matrix Metallopeptidase

M_n - Molecular Weight (number average)

NGS - Next Generation RNA-Sequencing

MOPS - 3-(N-morpholino) Propane Sulfonic Acid

NF-κB - Nuclear Factor Kappa-B

NIH - National Institutes of Health

NOF - Normal Oral Fibroblasts

OSCC - Oral Squamous Cell Carcinoma

PANTHER - Protein Analysis Through Evolutionary Relationships

PBS - Phosphate Buffered Saline

PCA - Principal Component Analysis

PCL - Polycaprolactone

PC1 - Principal Component 1

PEG - Polyethylene Glycol

PLGA - Poly(Lactic-co-Glycolic Acid)

PLLA - Poly (L-Lactic acid)

PMMA - Polymethyl Methacrylate

P-p44/p42 - Phosphorylated-p44/42

qPCR - Quantitative Polymerase Chain Reaction

RAC - Ras-related C3 Botulinum Toxin Substrate

RCF - Relative Centrifugal Force

RPM - Revolutions Per Minute

RhoA - Ras Homolog Family Member A

RIPA - Radioimmunoprecipitation Assay

RNA - Ribonucleic Acid

RNase - Ribonuclease

RPM - Revolutions Per Minute

RQN - RNA Quality Number

RT - Reverse Transcription

RTK - Receptor Tyrosine Kinase

SASP - Senescence-Associated Secretory Phenotype

SDS - Sodium Dodecyl Sulphate

SEM - Scanning Electron Microscope

SHC - Src Homology 2 Domain Containing Adapter Protein

TBS - Tris-buffered Saline

TBST - Tris-buffered Saline with Tween

TCP - Tissue Culture Plastic

TGF-β - Transforming Growth Factor Beta

TME - Tumour Microenvironment

WCA - Water Contact Angle

YAP - Yes Associated Protein

2D - Two Dimensional

3D - Three Dimensional

List of Figures

Figure 4.8. Representative images of water droplets on tissue culture plastic and 15% PCL electrospun scaffolds.

Figure 4.9. (A) PrestoBlue and (B) PicoGreen assay data for 3T3 fibroblasts cultured on TCP and ES PCL scaffolds. GraphPad Prism software was used to generate graphs. *** $p < 0.001$, ** $p < 0.01$, * $p < 0.05$. Error bars represent standard deviation, n=3.

Figure 4.10. (a) PrestoBlue and (b) PicoGreen assay data for NOF fibroblasts cultured on TCP and ES PCL scaffolds. GraphPad Prism software was used to generate graphs. *** $p < 0.001$, ** $p < 0.01$, * $p < 0.05$. Error bars represent standard deviation, n=3.

Figure 4.11. Representative Live/Dead staining of NOF grown on TCP and scaffolds. Images were taken 1, 4 and 7 days post seeding. ImageJ was used to enhance all images equally using the 'subtract background' function and brightness increase tool. Live cells are stained green (cytoplasm) and dead cells are stained red (nucleus). The white scale bar is equal to 200 μm.

Figure 5.1. Representative Ki67 immunofluorescence images. Ki67 positive nuclei appear purple whilst Ki67 negative nuclei appear blue due to DAPI counterstaining of all nuclei. All images had the same enhancement using ImageJ software to subtract background fluorescence and increase brightness. Superimposed pie-charts show the proportion of proliferative (Ki67+) cells in purple and non-proliferative (Ki67−) cells in blue. The nuclei in a total of 27 images were counted for each pie-chart with 3 images taken from each of 3 technical replicates cut from 3 biological replicates. White scale bar is equal to 100 μm.

Figure 5.2 (A). Representative β-gal staining in NOF after senescence induction using 500 μM H_2O_2. White arrows point to some of the areas of blue β-gal staining. (B) Confluent cells used as a model of quiescence.

Figure 5.3. Fold changes in expression of senescence-associated genes versus senescent NOF. Error bars represent standard deviation. ** $p < 0.01$, ** $p < 0.05$. TCP and scaffold

biological replicates = 9, technical replicates = 3. Senescent and quiescent biological replicates = 3, technical replicates = 3.

Figure 5.4. QPCR results for cytoskeletal gene expression of (A) ACTA2 and (B) VIM, versus TCP grown NOF. * $p < 0.05$, ** $p < 0.01$, **** $p < 0.0001$. Error bars show standard deviation. TCP and Scaffold biological replicates = 9, technical replicates = 3. Senescent and Quiescent biological replicates = 3, technical replicates = 3. TGF-β TCP and Scaffold biological replicates = 6, technical replicates = 3.

Figure 5.5. QPCR results for ECM gene expression of (A) VCAN (V1), (B) COL1A, (C) COL3A, versus TCP grown NOF. ** $p < 0.01$, *** $p < 0.001$, **** $p < 0.0001$. Error bars show standard deviation. TCP and Scaffold biological replicates = 9, technical replicates = 3. Senescent and Quiescent biological replicates = 3.

Figure 5.6. QPCR results for ECM gene FN1 expression, versus the average TCP expression. ** $p < 0.01$. Error bars show standard deviation. Per day, biological replicates = 3, technical replicates = 3.

Figure 5.7. Representative SEM Images taken after 1, 4 and 7 days of culture. Images have been magnified 2000x and each image contains a scale bar. Adobe Photoshop 2021 was used to artificially colour NOF red.

Figure 5.8. Representative immunofluorescent images of NOF grown on scaffolds, glass and flat PCL membranes. White arrows point to examples of focal adhesion sites. White scale bars are 100 μm long in x20 magnification images and 50 μm long in x40 magnification images. The same image enhancement has been performed in all images, using ImageJ to subtract background fluorescence and increase brightness.

Figure 6.1. Ponceau staining (pink) identifies protein transferred from a polyacrylamide electrophoresis gel to a nitrocellulose membrane by electroblotting. Cells were lysed using TRI reagent or RIPA buffer. Western blotting was conducted using antibodies directed towards GAPDH and p44/p42 MAPK.

List of Tables

Chapter 1: Introduction

This project was conceptualised in response to observations made by Dr Amanpreet Kaur, working under the supervision of Dr Ilida Ortega Asencio. When seeded onto electrospun polycaprolactone scaffolds, 3T3 fibroblasts attached and were metabolically active, however they had significantly reduced growth rates when compared with fibroblasts grown on two-dimensional (2D) tissue culture plastic. Conversely, rat mesenchymal stem cells grew at comparable rates on both the 2D plastic and three dimensional (3D) scaffolds. In vivo adult fibroblasts reside within the extracellular matrix (ECM) where they have low activity until activated in response to physical and chemical stimuli. This research project was therefore formulated to investigate the hypothesis that aspects of the electrospun scaffold's fibrous microarchitecture contribute to the maintenance of a quiescent in vivo-like fibroblast population. This work is significant due to the role of activated fibroblasts in diseases such as cancer and fibrosis as well as the growing desire to incorporate stromal support cells into tissue engineered constructs to increase their in vivo-like credentials.

Before experimental research could begin a literature review was completed. It became clear that the current portrait of fibroblast behaviour in 3D culture models was a complex one. In the 1990's, studies in collagen gels elucidated a role for cellular mechanotransduction in the governance of fibroblast activation behaviour. As the first 3D culture system used to investigate fibroblast activation, natural hydrogels were limited by their rapid degradation and the difficulties associated with controlling their properties. More recently advanced synthetic and hybrid hydrogels have renewed efforts to isolate specific aspects of the culture environment and dissect their roles in controlling fibroblast behaviour. Alongside hydrogels many modern studies have taken advantage of the microfabrication methods that are commonly used in tissue engineering to mimic architectural and mechanical properties of the extracellular matrix. These studies have shown that scaffold architecture including porosity, fibre size and orientation can influence fibroblast behaviour. The surface properties of 3D culture environments that include binding site availability and surface charge also contribute to the

regulation of cellular behaviour. Reviewing this literature is a challenge as fibroblasts are regularly used to assess the biocompatibility of new materials and the literature is therefore replete with studies that briefly mention fibroblast behaviour in 3D biomaterials. Furthermore, due to the large number of competing studies in different systems and the added complexity arising from fibroblast heterogeneity, much of the research has opposing results. As a result, the literature review focuses on research centred on the fundamental biology governing fibroblast activation behaviour. It identifies the requirement for one highly versatile model that can provide clarity in the evaluation of fibroblast activation in a relevant 3D environment. It also highlights how a greater understanding of activation cues in vitro can be translated to therapeutic opportunities in the treatment of cancer and other fibrotic diseases.

Electrospinning is one of the techniques that has been used to produce ECM-like scaffolds. Electrospun scaffold properties can be independently tuned, they promote cell spreading and facilitate cell-cell contacts, they are not subject to extensive remodelling and do not cause cellular encapsulation as seen in hydrogels. Furthermore, electrospinning is easily scalable and many Food and Drug Administration (FDA) approved polymers are compatible with the manufacturing process, enhancing the translatability of work conducted in this model. For these reasons electrospun scaffolds represent a good model system in which to investigate fibroblast activation.

To test the hypothesis that the microfibrous electrospun scaffold simulates the micro-architecture of collagen fibres in the extracellular matrix, thus maintaining a population of low activity in vivo-like fibroblasts, experimental data is presented over three results chapters. The first chapter covers scaffold manufacture and characterization, it is followed by an exploration of the scaffold fibroblast phenotype in the second chapter. The final results chapter investigates the molecular pathways that govern activation behaviour and considers applications for the scaffold in disease modelling. The scaffold was characterised using a variety of techniques including SEM image analysis, mercury intrusion porosimetry, water contact angle testing and mechanical testing. This data was used to confirm inter-batch

consistency in scaffold properties and to provide information on the fibrous micro-architecture of the scaffold. Immunofluorescent imaging and quantitative polymerase chain reaction (qPCR) were two of the techniques used to observe and quantify aspects of fibroblast activation behaviour on the scaffold and 2D control surfaces. Data was gathered on fibroblast proliferation, gene expression and morphology. In the final results chapter, the genetic regulation of scaffold behaviour was investigated using next generation ribonucleic acid (RNA) sequencing and bioinformatic analysis. Exploration of the impact of scaffold culture on disease activated cancer associated fibroblasts (CAF) was also completed, using qPCR to quantify the expression of CAF markers.

The thesis concludes with a general discussion of the results gathered and considers any limitations of the experimental work conducted. Finally, the perspectives for future work emanating from this research project are explored.

Chapter 2: Literature Review

2.1. Introduction

Fibroblasts are heterogeneous cells found in stromal tissues throughout the body. The diverse lineage and lack of unique markers for fibroblasts has hindered research since their first characterization in the mid-1800s. Modern techniques such as single-cell sequencing have shed more light on the array of tissue and subtype specific fibroblast functions in both health and disease. Adult fibroblasts are low activity ECM architects that when activated have a complex and multifunctional role in the wound healing response. In cancer distinct fibroblast populations have both tumour suppressive and supportive roles and in fibrosis fibroblasts are the main effectors of disease.

Given their complex functionality in health and disease, a significant amount of research has been focussed on the fibroblast. As stromal cells, fibroblasts exist in a three-dimensional (3D) matrix, without the polarity of epithelial or endothelial cells. For this reason, research has focused on the use of 3D biomaterials that more accurately recapitulate the fibroblasts' native environment. Early studies began in collagen hydrogels and looked at the impact of mechanical tension on fibroblast phenotypes. The explosion of modern biomaterial research and the advent of new manufacturing techniques over the last 20 years has heralded a new era of fibroblast research.

This literature review considers what is known about fibroblasts in vivo and summarises the major relevant findings of in vitro analyses conducted to date. We focus on studies concerned with fibroblast activation, a process that when deregulated is a major driver of disease. Natural and synthetic hydrogels, ECM derivatives and polymer scaffolds have been used extensively to investigate the impact of micro-architectural and mechanical properties on fibroblast behaviour. This review includes a look at the key manufacturing and bioengineering approaches taken, with a focus on electrospinning, the technique used to create fibrous scaffolds for this research thesis.

2.2. Fibroblasts In Vivo

2.2.1. Introduction

As heterogeneous stromal cells, fibroblasts have roles in ECM deposition and turnover, they are involved in inflammation and immunity and also the wound healing response. Fibroblasts are implicated in many diseases including fibrosis and cancer. A high degree of heterogeneity based on fibroblast lineage, location and function has made studying these cells a complex task, however recent breakthroughs in subtype characterisation may yield therapeutic opportunities.

2.2.2. Defining Fibroblasts

Fibroblasts were first observed in the 1800s and yet even today there remains a lack of specific molecular markers for these cells (Chang, Chi et al. 2002, Lendahl, Muhl et al. 2022). For this reason, spindle-like morphology and the absence of epithelial markers or specific markers for other stromal cells have become common determinants of fibroblast cells (Chang, Chi et al. 2002, Lendahl, Muhl et al. 2022). Recently RNA sequencing and single cell transcriptomics have improved our ability to investigate these cells. However, a high degree of heterogeneity between fibroblast populations at different locations throughout the body and even within the same tissue, has made characterising fibroblasts a challenge (Muhl, Genove et al. 2020)

2.2.3. Fibroblast Heterogeneity

Most connective tissue fibroblasts have their origins in the embryonic mesoderm and subsequent mesenchyme (LeBleu and Neilson 2020). Although, some fibroblasts including those in the head derive from the neuroectoderm (neural crest) (Lendahl, Muhl et al. 2022). Alongside quiescent fibroblasts the adult mesenchyme hosts many cells that give rise to fibroblast-like cells during the response to injury, they include epithelial cells, perivascular cells and adipocytes to name a few (LeBleu and Neilson 2020). Furthermore, fibroblasts differ in form and function depending on their location within the body (Driskell and Watt 2015). The most well characterised example of adjacent fibroblast populations exhibiting different morphology, physiology and function comes from the dermis of the skin (Tracy, Minasian et al.

2016). Papillary fibroblasts proliferate more rapidly than reticular fibroblasts when explanted from human skin (Harper and Grove 1979) and are subject to less contact inhibition at confluence (Schafer, Pandy et al. 1985, Sorrell, Baber et al. 2004). Furthermore, reticular fibroblasts have been found to contract collagen gels quicker than papillary fibroblasts (Schafer, Pandy et al. 1985, Sorrell, Baber et al. 1996). Beyond site specificity fibroblasts are subject to age-related changes (Lynch and Watt 2018). Age-related decline is likely to be subtype dependent in adult fibroblasts, where age has been observed to have a greater impact on the functional decline of papillary fibroblasts than reticular fibroblasts (Mine, Fortunel et al. 2008). Furthermore, during development fibroblast phenotypes change, with foetal scar free healing observed in many mammalian species but lost in adulthood (Colwell, Longaker et al. 2003). Human foetal explants retained their remarkable healing capabilities when transplanted into immuno-deficient nude mice, suggesting that this ability is tissue intrinsic (Lorenz, Longaker et al. 1992). Lynch and Watt suggested that this could be the result of foetal fibroblasts that are lost in adult skin (Lynch and Watt 2018). Fibroblast heterogeneity is also present throughout the body in disease-activated populations (LeBleu and Neilson 2020).

Heterogeneity in diseased fibroblast populations must be taken into account when considering therapeutic interventions for diseases from cancer to fibrosis (Lynch and Watt 2018). Epigenetic heterogeneity has been observed in fibroblasts derived from fibrotic and healthy tissues (Lynch and Watt 2018) with fibroblasts taken from keloid tissue accumulating epigenetic changes that are not present in healthy tissue (Russell, Russell et al. 2010). Epigenetic changes such as histone modification and DNA methylation have also been found in synovial fibroblasts taken from rheumatoid arthritis patients (Karouzakis, Gay et al. 2009). Finally, there is a high degree of heterogeneity in cancer associated fibroblasts (CAF) (Nurmik, Ullmann et al. 2020) although it is unclear whether this reflects the subtypes seen in healthy tissue (Lynch and Watt 2018). The phenotype of myofibroblastic and inflammatory CAF subtypes was recently shown to be fluid in collagen-alginate gels and highly dependent on matrix mechanical properties (Cao, Cheng et al. 2021).

2.2.4 Fibroblasts and the Extracellular Matrix

The extracellular matrix (ECM) is a vital and multifaceted structure that not only provides mechanical support to tissues but has a regulatory role in controlling cell-cell and cell-matrix interactions (Hu, Ling et al. 2022). The ECM is made up of structural proteins like collagen and fibronectin alongside proteoglycans and glycoproteins that facilitate matrix hydration and regulate signalling (Kresse and Schonherr 2001, Tracy, Minasian et al. 2016). Fibroblasts are the main producers of ECM components including collagen, the core structural protein upon which the other matrix constituents assemble. Collagen and other fibrillary proteins such as fibronectin, elastin and vitronectin confer rigidity and elasticity to the matrix (Tracy, Minasian et al. 2016). Fibroblasts also produce glycoproteins and proteoglycans, hydrophilic molecules that when hydrated fill most of the interstitial space and act as shock absorbers. They also have important roles in mediating cell-ECM and cell-cell interactions (Cattaruzza and Perris 2005, Tracy, Minasian et al. 2016).

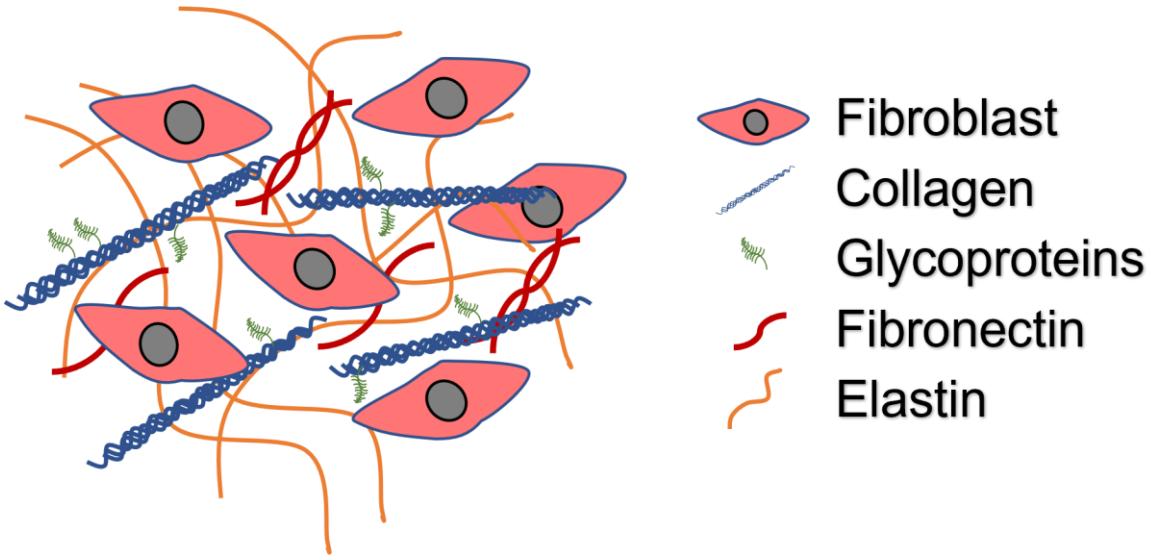

Figure 2.1. *A schematic representation of the key proteins of the extracellular matrix.*

2.2.5. Fibroblasts and Wound Repair

Alongside their roles in ECM production and maintenance, fibroblasts play a crucial role in the wound healing response. Wound healing has four overlapping and interdependent phases; haemostasis, inflammation, proliferation and remodelling (Figure 2.2) (Guo and DiPietro 2010, Wang, Huang et al. 2018). Monocytes populate the wound bed during the inflammatory stage and recruit quiescent fibroblasts through the secretion of cytokines. Fibroblast migration is likely to occur along fibronectin fibrils (Bainbridge 2013). Once fibroblasts arrive at the wound site they produce matrix metalloproteinases (MMPs) which degrade collagen fragments and other debris (Halloran and Slavin 2002) as well as existing basement membranes to enhance the infiltration of inflammatory cells (Wynn 2008). Activated fibroblasts proliferate and begin to produce large amounts of collagen III, which is quicker to produce than collagen I and is preferentially deposited during the proliferation phase (Halloran and Slavin 2002). The collagen I isoform has greater tensile properties and forms in the days and weeks following injury, emphasising the prolonged presence of fibroblasts during the remodelling phase (Halloran and Slavin 2002). Collagen I is the most abundant collagen and the main collagen found in tendons, ligaments, skin and most connective tissues where it confers tensile strength and torsional stiffness (Gelse, Poschl et al. 2003). Collagen III is present in the same tissues as collagen I apart from bone and is especially abundant in elastic tissues (Gelse, Poschl et al. 2003). Activated fibroblasts also express alpha-smooth muscle actin (α-SMA), taking on a smooth muscle-like phenotype in order to aid wound contracture (Halloran and Slavin 2002). The functional dexterity of fibroblasts is highlighted through their many roles in wound healing. However, with such diverse functionality, fibroblasts are implicated in a wide range of diseases.

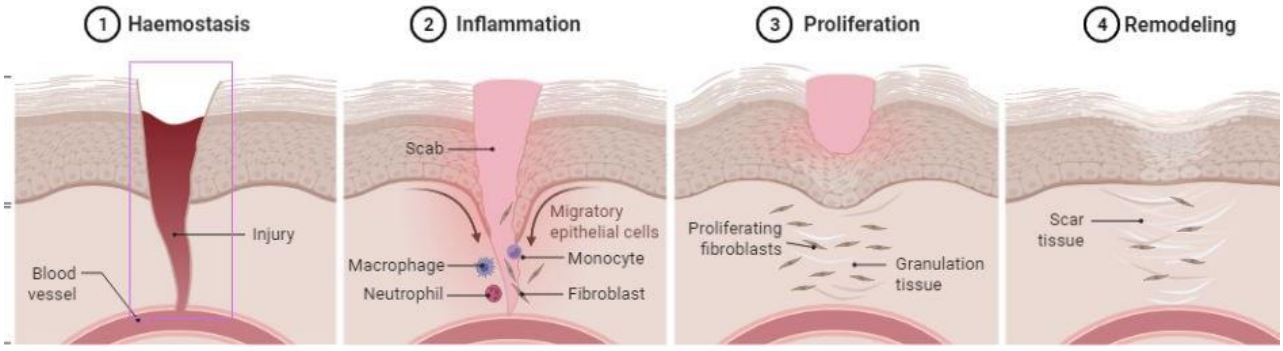

Figure 2.2. *The four stages of wound healing. Once recruited, activated fibroblasts have roles in matrix remodelling and deposition as well as maintenance and regulation of the inflammatory environment. Adapted from "Wound Healing" template, by BioRender.com (2023). Retrieved from https://app.biorender.com/biorender-templates.*

2.2.6. Fibroblasts in Inflammation and Immunity

As their role during the inflammatory phase of wound healing suggests, fibroblasts are implicated in the regulation of both inflammation and immunity. This functionality stretches beyond just the wound healing response to the immune response in cancer and the maintenance of inflammatory states in tissues throughout the body (Davidson, Coles et al. 2021). The role of inflammation and immune regulation is often perturbed during disease states with fibroblast involvement like fibrosis and cancer.

2.2.7. Fibrotic Disease

Fibrosis can occur in tissues throughout the body and is characterised by the excessive accumulation of ECM products. It is a disease of fibroblast activation (Wynn and Ramalingam 2012). In fibrosis an abnormal or prolonged inflammatory response drives disease. Such inflammation can be triggered by tissue injury, autoimmune or allergenic reactions and chemical insult. Despite diverse triggers, the outcome is generally characterised by scarring, hardening and tissue overgrowth (Wynn 2007). Recruited by inflammatory mediators, activated fibroblasts are responsible for producing fibrotic tissue. In normal wound healing a balance between MMP production and collagen deposition ensures appropriate levels of granulation tissue form (Pardo and Selman 2006). The process becomes pathogenic when

excessive collagen production overcomes the antagonistic action of MMPs which degrade and remodel the immature ECM (Pardo and Selman 2006). Not only are fibroblasts recruited in response to inflammation but they are able to secrete immune modulating chemokines that attract leukocytes and perpetuate the inflammatory environment (Davidson, Coles et al. 2021). Once again, fibroblast heterogeneity plays a role in fibrosis. Wynn suggests that identification of pro-fibrotic sub-populations and the mechanisms by which they are recruited could provide a therapeutic opportunity to limit fibroblast activation (Wynn 2008). For example, alongside stromal fibroblasts, circulating mesenchymal stem cells (Bucala, Spiegel et al. 1994) and tissue specific stem cells such as hepatic stellate cells in the liver (Friedman 2004) may contribute to activated fibroblast populations in fibrosis.

2.2.8. Fibroblasts in Cancer

The tumour microenvironment (TME), also known as the desmoplastic reaction or tumour stroma is a name for all non-cancer cell components of the tumour (Kalluri 2016). It includes immune cells, blood vessels, basement membrane, ECM and activated fibroblasts (Kalluri 2016). In the TME perpetually activated fibroblasts are referred to as cancer associated fibroblasts (CAF). CAF are derived from many sources (Ishii, Ochiai et al. 2016) and may also arise from epithelial cells that have undergone epithelial-mesenchymal transition (EMT) (Kalluri and Zeisberg 2006). As with fibroblasts in fibrotic tissue, CAF are heterogeneous in form and function (Li, Courtois et al. 2017, Ohlund, Handly-Santana et al. 2017, Costa, Kieffer et al. 2018). Fibroblasts may be involved from the very early stages of cancer initiation. Non-CAF skin fibroblasts isolated from cancer patients with a range of cancers were shown to be more proliferative than fibroblasts from non-cancer patients, suggesting their altered behaviour could contribute to cancer formation (Kopelovich 1982, Schor, Haggie et al. 1986). Of perhaps greater significance was a study in which the overexpression of transforming growth factor-β (TGF-β) and/or hepatocyte growth factor (HGF) in transplanted normal human fibroblasts caused tumorigenesis in healthy human mammary epithelial cells integrated into ‘humanised’ mouse breast tissue (Kuperwasser, Chavarria et al. 2004). It has been easier to

elucidate the role of CAF in tumour progression. The injection of CAF was shown to stimulate the growth of breast carcinoma cells to a greater extent than normal fibroblasts did in a mouse xenograft (Orimo, Gupta et al. 2005). In addition, transplanted CAF promoted angiogenesis through the recruitment of endothelial progenitor cells (Orimo, Gupta et al. 2005). CAF increased the invasiveness of non-invasive cancers (Dimancheboitrel, Vakaet et al. 1994) and through the production of MMPs, CAF may enhance metastasis (Kalluri 2016). Interestingly, whilst CAF are involved in tumour promotion, they also appear to have tumour suppressing capabilities. When α-SMA positive myofibroblasts were depleted in transgenic mice, pancreatic ductal adenocarcinomas (PDAC) formed that were more invasive and survival rates fell (Ozdemir, Pentcheva-Hoang et al. 2014). PDAC are associated with fibrosis and the presence of activated myofibroblasts. Patients with fewer tumour associated myofibroblasts had a lower survival rate (Ozdemir, Pentcheva-Hoang et al. 2014). It is evident from this research that CAF do not represent a 'silver bullet' for cancer therapy and our understanding of their complex roles in cancer is still developing.

2.2.9. Fibroblasts in vivo summarised

Fibroblasts are mesenchymal cells with vital functions during development of the ECM. In adult tissue despite being the most abundant cell in the stroma they have low activity. Despite a high degree of functional and site-specific heterogeneity, the ability to activate in response to physical and chemical cues is conserved. In activation fibroblasts transition from their quiescent low activity state to highly proliferative, motile cells which produce ECM proteins, matrix remodelling MMPs, cytokines and growth factors. Despite new evidence of heterogeneity in activated fibroblast populations, understanding the conditions that prevail in deregulated fibroblast activation has great therapeutic potential in diseases like fibrosis and cancer. When studying activation, it is vital to remember that fibroblasts exist in a 3D matrix without the apical-basolateral polarity of epithelial or endothelial cells. For this reason, a great deal of research has been conducted using 3D biomaterials that better recapitulate features of the ECM than traditional two-dimensional (2D) culture surfaces. Furthermore, as tissue

engineers seek better materials and manufacturing techniques to mimic the ECM, incorporating fibroblasts will enhance the biomimicry of engineered models and therapeutics.

2.3. Fibroblasts in 3D culture

2.3.1. Introduction

In vitro studies in 3D began as early as the 1950s with collagen-based hydrogels (Ehrmann and Gey 1956) and by the turn of the century, natural-hydrogels of mostly type 1 collagen had been used extensively to investigate several aspects of fibroblast behaviour (Cukierman, Pankov et al. 2002). This included changes to morphology, proliferation, motility and gene expression, all features associated with activation (Hinz 2007). Other natural gels included fibrin (Niewiarowski and Goldstein 1973) and hyaluronan (Masters, Shah et al. 2004, Tibbitt and Anseth 2009). Much of the research in collagen hydrogels focussed on the impact of hydrogel tension on fibroblast mechanoregulation and activation. However, certain features such as cell entanglement (Jiang and Grinnell 2005) and confinement (Smithmyer, Cassel et al. 2019) alongside gel contraction, limited the utility of the collagen-based models. Very few studies included 2D controls which made ascertaining whether changes in fibroblast behaviour were a result of mechanical and microarchitectural properties or collagen receptor binding difficult. Furthermore, when using collagen hydrogels, it was challenging to control and isolate specific features like porosity or stiffness (Tibbitt and Anseth 2009), to understand their individual effects on fibroblast behaviour. Attention therefore turned to novel hydrogel systems, both natural and synthetic, as well as decellularized matrices (Tibbitt and Anseth 2009). Despite extensive research using a broad spectrum of culture techniques and manufacturing methods, conflicting results, different characterization methodologies and different cell lines lead to an inconsistent picture of fibroblast behaviour throughout the early 2000s.

Over the last decade an expansion in the number of novel biomaterials and manufacturing techniques designed for tissue engineering purposes has resulted in a new age of fibroblast

research. Due to their robust nature and easy isolation fibroblasts are often used to test the biocompatibility of novel materials. Where initial research centred on cellular mechanisms of control in 3D environments, a desire to incorporate functionality and control into engineered constructs has overtaken the field. Here we will present a comprehensive review of the 3D culture strategies used in the study of fibroblast behaviour. A graphical summary of the techniques employed in fibroblast research in vitro is presented below (Figure 2.3).

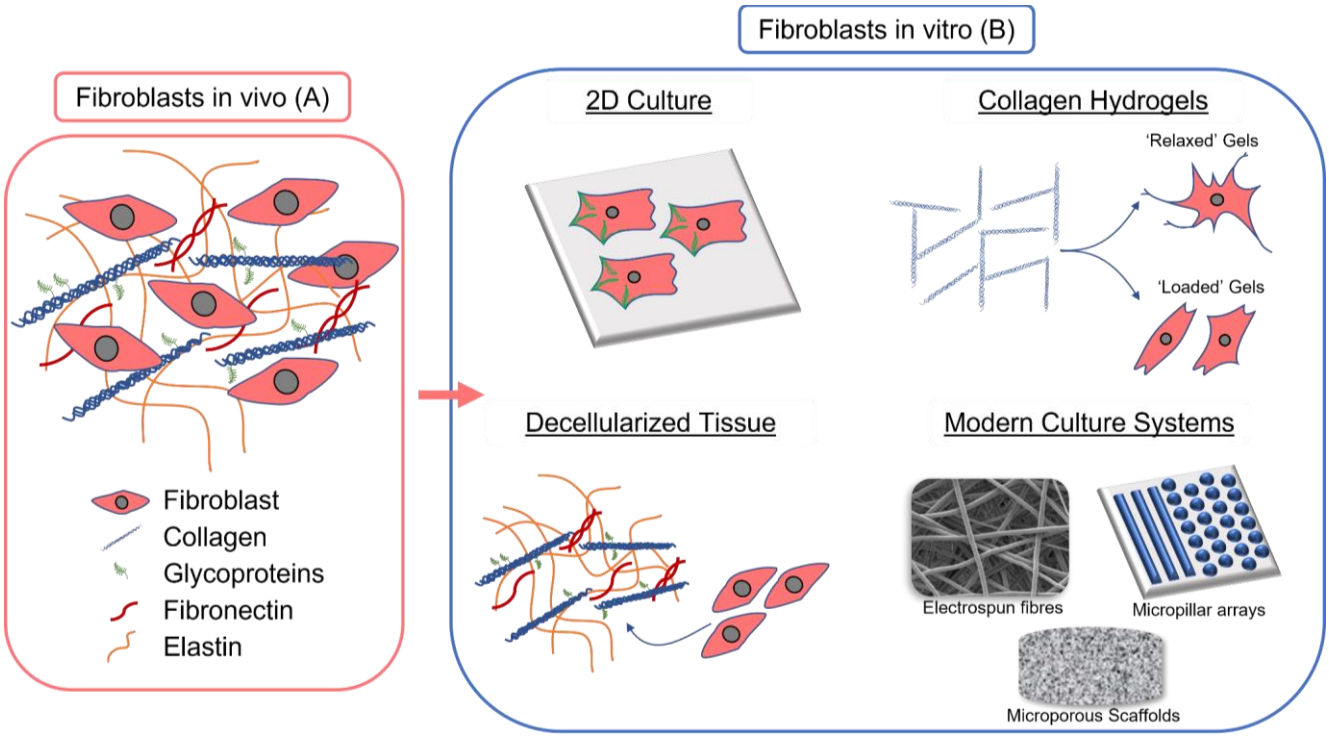

Figure 2.3. *(A) In vivo fibroblasts reside in the ECM. (B) Fibroblasts were first cultured in vitro in 2D monolayers on glass or plastic. 3D cultures including hydrogels, decellularized matrices and an array of modern biomaterials have since taken priority. On stiff 2D surfaces fibroblasts became partially activated, expressing α-SMA stress fibres, focal adhesions and a spread cytoplasm. Collagen hydrogel studies indicated that in relaxed gels without isometric tension, fibroblasts become quiescent with low proliferation rates and a dendritic morphology. Loaded gels gave rise to bi-polar fibroblasts with higher proliferation rates and α-SMA expression. Tissue sections and ECM derivatives can be decellularized to create 3D models with a high degree of biomimicry. Finally, modern culture systems have provided new opportunities to study fibroblast behaviour in vitro.*

2.3.2 Fibroblast Behaviour in Collagen Hydrogels

The first use of collagen hydrogels for cell culture took place in 1956 and included fibroblast cells (Ehrmann and Gey 1956). This was followed in 1972 by the first study to document changes to fibroblast morphology and proliferation rate in a collagen gel (Elsdale and Bard 1972). Fibroblasts formed bipolar protrusions that aligned with collagen fibres and proliferated at a slower rate than cells seeded onto plastic (Elsdale and Bard 1972). The 1990s heralded a new era in which studies went beyond observational science to probe the mechanisms that control fibroblast behaviour in collagen gels. Table 2.1 summarises the first wave of these studies.

Table 2.1. The First Studies Investigating Fibroblast Behaviour in Collagen Hydrogels.

Fibroblast	3D Environment	2D Environment	Key Findings	Reference
Foreskin fibroblasts	Collagen gels	Monolayer	ERK signalling was disrupted in unloaded gels causing a fall in proliferation.	(Rosenfeldt and Grinnell 2000)
Foreskin fibroblasts	Collagen gels	Monolayer and Poly(Hema) coated monolayer	Collagen synthesis is reduced in hydrogel culture and poly-Hema coated plates.	(Ivarsson, McWhirter et al. 1998)
Foetal lung fibroblasts	Collagen gels	Monolayer	Less proliferation in response to IGF and PDGF. Hydrogel contraction alters experimental conditions.	(Mio, Adachi et al. 1996)
Review	Collagen gels	-	Relaxed ‘vs’ loaded gels.	(Grinnell 1994)
Dermal fibroblasts	Collagen gels	Monolayer	FGF and EGF responses are maintained in hydrogels.	(Geesin, Brown et al. 1993)
Dermal fibroblasts	Collagen gels	Monolayer	G0/1 arrest led to less proliferation in 3D culture.	(Kono, Tanii et al. 1990)
Dermal fibroblasts	Collagen gels	Monolayer	Growth factor responses in monolayer, relaxed and loaded gels.	(Nakagawa, Pawelek et al. 1989)
Dermal fibroblasts	Collagen gels	Monolayer	There was less proliferation and less collagen was produced in 3D.	(Mauch, Hatamochi et al. 1988)

EGF, Epidermal growth factor. ERK, extracellular signal-regulated kinase. FGF, fibroblast growth factor. IGF, insulin growth factor. PDGF, platelet-derived growth factor.

The early studies listed in Table 2.1 consistently observed lower proliferation rates in 3D collagen hydrogels than in monolayers formed on tissue culture plastic (TCP). This appeared to be the result of growth phase (G0/1) arrest, which reduced the number of cells entering S phase (Kono, Tanii et al. 1990). At the time, Kono *et al*. hypothesised that this was due to cell-collagen receptor binding and was not necessarily a result of the architectural or mechanical features of the 3D culture environment (Kono, Tanii et al. 1990).

Kono *et al.* were correct and evidence of integrin α1 dependent collagen binding stimulating proliferation was later found (Pozzi, Wary et al. 1998). However, collagen studies also indicated a role for the mechanoregulation of fibroblast phenotypes. Unless collagen hydrogels are restrained, fibroblasts naturally contract them, giving rise to two distinct hydrogel states. The first is a relaxed state that occurs after fibroblasts have contracted an unrestrained (floating) gel. The second occurs when fibroblasts try to contract a gel that has been anchored to the well plate walls. The gel becomes mechanically loaded as it resists fibroblast contractile activity. In relaxed gels fibroblasts became dendritic in morphology and had low proliferation rates whilst in loaded gels the fibroblasts had higher proliferation rates and formed stellate or bipolar projections along the lines of tension (Grinnell 1994).

In the years that followed, extracellular regulated kinase (ERK) signalling was shown to be vital in the mechanoregulation of fibroblasts in collagen gels (Rosenfeldt and Grinnell 2000). ERK 1 and 2 (p44 mitogen activated protein kinase (MAPK) and p42 MAPK respectively) are activated when phosphorylation increases their enzymatic activity (Zhang and Liu 2002). In “unloaded” gels where a previously anchored gel is released, fibroblasts would switch to the relaxed gel phenotype (Rosenfeldt and Grinnell 2000). In both “unloaded” and relaxed gels ERK phosphorylation was significantly reduced compared to in loaded gels. Furthermore, if ERK signalling was inhibited in loaded gels, DNA synthesis would stall (Rosenfeldt and Grinnell 2000). Platelet-derived growth factor receptors (PDGFR) are cell surface receptors that can stimulate ERK phosphorylation and were proposed as a possible point of ERK inhibition in loaded gels. However, using phorbol esters to stimulate the ERK pathway

downstream of cell surface receptors like PDGFR, did not trigger normal ERK phosphorylation. This suggested that other downstream pathway components were disrupted in collagen hydrogel cultures (Rosenfeldt and Grinnell 2000).

Earlier studies had identified that cells detached from monolayer culture stop proliferating and are unable to phosphorylate ERK 1 and 2 when stimulated with growth factors (Zhu and Assoian 1995, Lin, Chen et al. 1997, Renshaw, Ren et al. 1997). Fibroblasts in relaxed and "unloaded" cultures remain attached to the collagen hydrogel but still exhibit disruption to ERK signalling. Therefore, the study by Rosenfeldt and Grinnell suggested that tension may be more important than adhesion or polarity in proliferation control (Rosenfeldt and Grinnell 2000). It was hypothesised that integrin association with Src homology 2 domain containing adapter protein (SHC), could be a potential route for the integration of mechanical signalling in the collagen gel (Rosenfeldt and Grinnell 2000). SHC has been shown to associate with integrins and in turn activate growth factor receptor-bound protein 2 (Grb2), a known upstream activator of ERK, in endothelial cells in response to shear stress (Chen, Li et al. 1999).

Mechanoregulation seems to have a strong influence on fibroblast proliferation rates and can also influence growth factor responses (Grinnell 1994, Rosenfeldt and Grinnell 2000). However, the data regarding growth factor responses from studies listed in Table 2.1 was not always definitive. Insulin growth factor (IGF) and platelet-derived growth factor (PDGF) stimulated proliferation in monolayer cultures but their effects were reduced and abolished respectively in 3D (Mio, Adachi et al. 1996). Growth inhibitor Prostaglandin E2 was still able to reduce proliferation in collagen gels (Mio, Adachi et al. 1996). Mio *et al.* concluded that fibroblast proliferation fell in collagen gels as fibroblasts remained responsive to growth inhibitors but had a reduced response to growth stimulators in 3D. Mio *et al.* used support gels to ensure that the contracting collagen gel could not detach from the well and become relaxed. The growth factor response has also been tested and compared in loaded and relaxed collagen gels (Nakagawa, Pawelek et al. 1989). In loaded collagen gels fibroblast proliferation is reduced in comparison to monolayer cultures, whilst in relaxed gels proliferation halts almost

entirely. As such a difference in growth factor responses would be expected. Fibroblast Growth Factor (FGF) stimulated growth in loaded gels in a manner similar to monolayer culture whilst responses to PDGF, interleukin-1 and transforming growth factor-β (TGF-β) were lost (Nakagawa, Pawelek et al. 1989). In relaxed gels the response to all growth factors including FGF was lost (Nakagawa, Pawelek et al. 1989). Taken together these results suggest that FGF response may be subject to mechanoregulation. The response to other factors including PDGF, IGF and interleukin-1 were diminished in 3D gels though they did not appear to be subject to mechanoregulation.

The studies listed in Table 2.1 also reported on fibroblast collagen deposition rates in collagen hydrogels. Fibroblasts cultured in relaxed gels produced less collagen (Mauch, Hatamochi et al. 1988, Ivarsson, McWhirter et al. 1998) although deposition in response to ascorbic acid stimulation was found to be equal to monolayer cultures (Geesin, Brown et al. 1993). Interestingly Ivarsson *et al.* compared a relaxed collagen gel with both monolayer culture and a poly(2-hydroxyethyl methacrylate) (poly(hema)) coated 2D surfaces. At a concentration of 0.3% poly(hema) enables cells to attach to the 2D substrate but not to spread (Ivarsson, McWhirter et al. 1998). In both hydrogels and poly(hema) cultures the production of collagen-1 was downregulated. Fewer focal adhesions formed in poly(hema) and gel culture than in monolayers and this may have influenced collagen production (Ivarsson, McWhirter et al. 1998). Collagen messenger RNA (mRNA) levels fell in the 3D gels but remained unaffected in 2D collagen or poly(hema) coated substrates (Ivarsson, McWhirter et al. 1998). These results suggested that collagen production is influenced at the translational level in poly(hema) cultures where spreading is limited. In collagen gels collagen production was limited at the transcriptional level (Ivarsson, McWhirter et al. 1998).

Since 2000, many more studies have compared the behaviour of fibroblasts in collagen hydrogels and monolayer cultures (Table 2.2). The group of Frederick Grinnell continued to work with collagen gels, however their focus turned towards cellular morphology, motility and matrix interactions. In line with earlier observations, well spread fibroblasts formed focal

adhesions and lamellar extensions on stiff plastic surfaces used for monolayer culture (Grinnell, Ho et al. 2003). Fibroblasts in loaded collagen gels formed stellate or bipolar extensions (Grinnell, Ho et al. 2003). Grinnell *et al.* introduced a new seeding technique in which a low density (10^5/ml) of cells were seeded into a collagen gel (Grinnell, Ho et al. 2003). At these densities fibroblasts did not contract the matrix and would become dendritic in morphology (Grinnell, Ho et al. 2003). In vivo fibroblasts are a phagocytic cell and on collagen coated 2D coverslips they are able to ingest fibronectin-coated beads (Jiang and Grinnell 2005). However, when fibroblasts became dendritic in relaxed collagen gels they were unable to ingest beads, due to the formation of fibrillar tangles between gel collagen fibres and fibroblast projections (Jiang and Grinnell 2005). Dendritic fibroblast-matrix attachments were integrin-independent and the cells could not be detached using trypsin-EDTA or integrin blocking antibodies (Jiang and Grinnell 2005).

Fibroblast motility and collagen gel matrix remodelling were also investigated. In loaded hydrogels where fibroblasts were subject to tension, the addition of growth factor lysophosphatidic acid (LPA) and fetal bovine serum (FBS) was more effective at stimulating matrix contraction than PDGF (Rhee and Grinnell 2007). In relaxed gels PDGF, LPA and FBS were all equally effective. This study provided further evidence of a role for cellular tension and morphology in the regulation of growth factor responses, both of which are governed by collagen gel conditions (Rhee and Grinnell 2007).

Table 2.2. Collagen Hydrogel Studies After 2000 With a Focus on Morphology and Motility.

Fibroblast	3D Environment	2D Environment	Key Findings	Reference
Review	Collagen gels	-	Fibroblast morphology and migration vary with changes to gel stiffness and tension.	(Rhee 2009)
Foreskin fibroblasts	Collagen gels	Monolayer	Greater MMP1+3 expression and less proliferation in 3D.	(Li, Rezakhanlou et al. 2009)
Human fibroblast	Collagen gels	Collagen-coated glass coverslip	Investigated migration and cellular morphology in response to gel conditions and growth factors.	(Rhee and Grinnell 2007)
Dermal fibroblast	Collagen gels (nested)	-	Migration occurs into adjacent gels.	(Grinnell, Rocha et al. 2006)
Foreskin fibroblast	Collagen gels	-	Cell entanglement inhibits phagocytosis.	(Jiang and Grinnell 2005)
Foreskin fibroblast	Collagen gels	Collagen-coated glass coverslip	Cellular morphology and attachments were investigated.	(Grinnell, Ho et al. 2003)
Review	Collagen gels	-	Review on 3D gels.	(Cukierman, Pankov et al. 2002)

MMP, Matrix Metalloproteinase.

2.3.2.1 Fibroblast Activation in Collagen Hydrogels

Amongst the studies listed in Table 2.1 and 2.2, several aspects of fibroblast activation behaviour were characterised. In vivo fibroblast activation involves increased proliferation, motility, expression of α-SMA and the increased deposition of ECM proteins such as collagen (Hinz 2007). Activated fibroblasts are also known as myofibroblasts (Hinz 2007). Deregulated activation can become pathological in cases of fibrosis, hypertrophic scarring and cancer (Gabbiani 2003, Desmouliere, Guyot et al. 2004, Desmouliere, Chaponnier et al. 2005, Kalluri and Zeisberg 2006). Figure 2.4 provides a summary of the data gathered from collagen gel studies on fibroblast activation traits, focussing on gel mechanical properties. The collagen hydrogel studies helped to identify a role for ECM tension and cellular mechanotransduction in fibroblast activation.

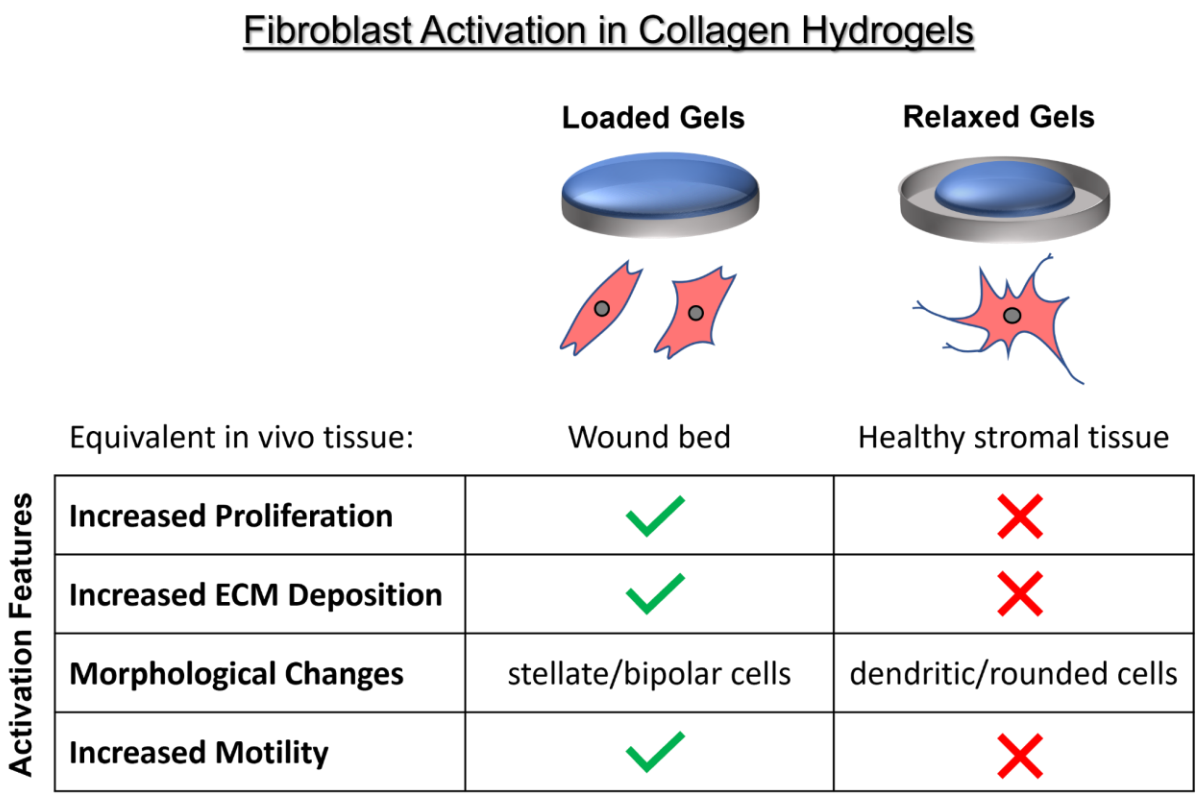

Figure 2.4. *Fibroblasts in the body become activated in response to injury. The responses of fibroblasts to changing mechanical environments in collagen hydrogels give rise to phenotypes that resemble activated and quiescent fibroblasts.*

2.3.2.2. Collagen hydrogel summary

Collagen gels were the first model with enhanced biomimetic properties and were used to study fibroblast behaviour in a more physiologically relevant 3D system. They showed that traditional monolayer cultures on glass or plastic give rise to partially activated fibroblasts and provided a wealth of data on the control of fibroblast phenotypes in a 3D system. Despite this, collagen gel studies had limitations. Cell encapsulation limited initial spreading until sufficient levels of matrix degrading proteases could be produced (Smithmyer, Cassel et al. 2019). Furthermore, while gel contraction provided opportunities for studies into mechanotransduction in relaxed, loaded and unloaded gels, it made extended experiments challenging due to the changing matrix conditions. It is also clear that fibroblast collagen entanglement creates attachments that are not in keeping with normal in vivo matrix

attachments and therefore may alter cell behaviour considerably (Jiang and Grinnell 2005). Finally, some of the behaviours observed may be the result of collagen receptor binding and the use of collagen-coated 2D controls could have acted as a more suitable control in many of the studies. The known collagen receptors include integrins (α1β1, α2β1, α10β1 and α11β1), discoidin domain receptors and some members of the mannose receptor family, they have been reviewed in detail (Leitinger and Hohenester 2007). The collagen receptors have many biological functions in the regulation of cellular phenotype including the control of fibroblast activation, MMP expression and collagen synthesis (Elango, Hou et al. 2022). Research using collagen gels became less frequent during the last 15 years with the arrival of new synthetic and hybrid polymer hydrogels that enabled better control of microarchitecture and mechanical properties. Furthermore, synthetic gels do not suffer from rapid degradation and resorption in the same manner as natural ones (Matera, Lee et al. 2021). Gel control allowed researchers to isolate individual aspects of 3D culture and identify their effect on fibroblast behaviour.

2.3.3. Fibroblast behaviour in synthetic and hybrid hydrogels

Synthetic and composite hydrogels are highly tunable and their mechanical and microarchitectural properties can be readily controlled (Gonzalez-Diaz and Varghese 2016). Polyacrylamide and alginate-collagen composite gels have been used to study the impact of stiffness, hardness and porosity on fibroblast motility and morphology (Pelham and Wang 1997, Yeung, Georges et al. 2005, da Cunha, Klumpers et al. 2014). More recently, synthetic gels have been used to investigate the roles of polarity and cell spreading on fibroblast phenotype (Smithmyer, Cassel et al. 2019). Other studies have highlighted how advanced composite hydrogels are being modified to enable even greater control of gel properties (Hui, Moretti et al. 2021, Farrell, Aliabouzar et al. 2022).

3T3 fibroblasts became less motile as polyacrylamide gel stiffness was increased (Pelham and Wang 1997) and became rounder and displayed less spread cytoplasm as polyacrylamide gel flexibility was increased (Yeung, Georges et al. 2005). The opposite was seen when dermal fibroblasts were grown on alginate-collagen composite gels, becoming rounder with increasing gel stiffness (da Cunha, Klumpers et al. 2014). The use of different gel systems and cell types could explain the difference in fibroblast morphology. These studies emphasise the challenge of comparing results between studies where different materials, cells and experimental conditions have been used.

A new study that took advantage of tunable hydrogel properties, used modified hyaluronic acid gels to investigate the effect of gel stiffness on fibroblast adhesion. Engineered fibronectin fragments that allowed for the preferential binding of either integrin *αvβ*3 or *α*5*β*1 were incorporated into gels with viscoelastic properties equivalent to fibrotic and healthy tissue (Hui, Moretti et al. 2021). In gels with fibrotic viscoelasticity, preferential *αvβ*3 binding promoted cell spreading, stress fibre and focal adhesion formation. Preferential *α*5*β*1 binding suppressed spreading, stress fibre and focal adhesion formation. In gels that mimicked healthy tissue, spreading and focal adhesion formation was reduced, regardless of binding site availability (Hui, Moretti et al. 2021). Another highly customized hydrogel which incorporated a phase-shift emulsion embedded within a fibrin hydrogel was used to investigate the effect of gel stiffness (Farrell, Aliabouzar et al. 2022). When locally directed ultrasound waves were applied, gas bubbles formed within the perfluorocarbon emulsion, causing radial compaction of the surrounding fibrin. This decreased porosity and increased local stiffness by up to 70%. In stiffened matrix areas there was a significant increase in the expression of α-SMA, indicative of fibroblast activation (Farrell, Aliabouzar et al. 2022). These studies highlight the shift towards modern highly tunable biomaterial solutions to develop our understanding of fibroblast behaviour.

In another recent study polyethylene glycol (PEG)-based hydrogels were used to tackle one of the problems previously associated with hydrogel culture (Smithmyer, Cassel et al. 2019).

In 2D monolayer culture, polarisation along the apico-basolateral axis is forced upon cells as they attach to the surface in only one plane (Smithmyer, Cassel et al. 2019). As cells form contacts with gels on all sides, this apico-basolateral polarity is reduced (Smithmyer, Cassel et al. 2019). Alongside a reduction in polarity, cells cultured in hydrogels become encapsulated, leading to reduced cell spreading. To decouple polarity changes from cell confinement, Smithmyer *et al.* sandwiched fibroblasts between two PEG hydrogel layers to create a "2.5D" culture environment. As part of the contractile apparatus in myofibroblasts, α-SMA was used as a marker of fibroblast activation (Hinz, Celetta et al. 2001). Despite a reduction in polarisation in 2.5D culture compared to 2D monolayer culture, α-SMA was expressed by fibroblasts in both. In normal 3D PEG hydrogels α-SMA expression was significantly reduced (Smithmyer, Cassel et al. 2019). This suggested that cell shape and spreading, which is altered in 3D culture, but not 2.5D culture, influenced the expression of α-SMA (Smithmyer, Cassel et al. 2019). Whilst there was some similarity in α-SMA expression levels between 2D and 2.5D culture, 2.5D culture did cause changes in Yes-associated protein (YAP) 1 nuclear localisation and CDH11 expression, which reflects changes to mechanosensing and cell-cell signalling respectively (Smithmyer, Cassel et al. 2019). This study aimed to distinguish if behavioural differences in hydrogel culture were due to individual properties of ECM mimicry such as a reduction in polarisation or if they were the result of hydrogel encapsulation. As such the study identifies the need for innovative biomaterial approaches to isolate individual properties and consider their role in behavioural regulation (Smithmyer, Cassel et al. 2019).

2.3.4. Fibroblast Behaviour in "Cell-Cleared" Matrices

Cell-cleared matrices, also known as decellularized tissue, were used in the same era as collagen hydrogels to imitate the ECM and investigate fibroblast behaviour in 3D. Both fibroblast-derived matrices deposited in vivo and then cleared of cells and mouse tissue sections decellularized ex vivo were used to grow fibroblasts (Cukierman, Pankov et al. 2001). Of note was evidence that the decrease in fibroblast proliferation seen when collagen gels

were compared to 2D plastic or glass cultures was not observed in 3D cell-cleared matrices (Cukierman, Pankov et al. 2001). Rather than comparing 3D ECM derived matrices to unaltered plastic surfaces, ECM extracts were used to coat the 2D plastic. In this study the 3D matrix gave rise to fibroblasts that were twice as proliferative as they were on any 2D surface coated with fibronectin or laminin and even when compared to a weight-flattened area of the 3D matrix (Cukierman, Pankov et al. 2001). The increased rate of fibroblast proliferation in 3D was entirely dependent on the cell's expression of α5 integrin, as evidenced through its inhibition (Cukierman, Pankov et al. 2001). The rate of proliferation was reduced when the matrix was flattened to 2D but so was the dependence on α5 integrin expression. This suggested that increased proliferation in the decellularized ECM matrix required integrin binding availability in 3D (Cukierman, Pankov et al. 2001). This study once again showed the importance of appropriate controls when studying 3D interactions.

Whilst decellularized tissue represents a scaffold with high structural and chemical similarity to the ECM, the model is not without flaws. As these scaffolds are naturally produced it is not possible to easily control matrix composition or individual features like pore and fibre size or matrix stiffness. Furthermore, the matrices are subject to remodelling and degradation, which gives rise to a changing environment throughout experiments (Badylak, Freytes et al. 2009). For these reasons it is difficult to investigate the impact of specific contextual cues on fibroblast behaviour in cell-cleared scaffolds.

2.3.5. Fibroblast Behaviour in Modern Culture Systems

In the last decade, many novel or repurposed manufacturing techniques and materials have been used to mimic the ECM. The literature is saturated with ECM alternatives for use in fundamental research and for therapeutic application. Fibroblasts are routinely used in initial biocompatibility and cytotoxicity tests for new 3D biomaterials, due to the ready availability of well-established and robust immortal cell lines such as the National Institutes of Health (NIH) 3T3 and L929 murine fibroblasts. Although, given that the materials being tested are often designed as part of a therapeutic application incorporating human cells, such immortalised

non-human cells are not an appropriate equivalent (Thonemann, Schmalz et al. 2002). In addition to immortalised cell lines, the relative accessibility of primary fibroblasts and their in vivo ECM incorporation has made their use commonplace. For these reasons it is not possible to list every study that has reported on some aspect of fibroblast behaviour in a 3D biomaterial. The behavioural features that are regularly used to support the suitability of new materials include scaffold penetration, fibroblast attachment, morphology, metabolic activity and proliferation rates. Studies tend to observe and record these features, often in response to a variety of material modifications. In general however, they are not concerned with understanding the cause or importance of specific fibroblast behaviours, rather they wish to demonstrate the suitability of a material or manufacturing process for future tissue engineering applications. The studies that attempt to complete a more focused behavioural review that centres on fibroblast behaviour are listed in Table 2.3.

Table 2.3. Studies That Focus on Controlling Fibroblast Behaviour in 3D Biomaterials.

Fibroblast Type	Biomaterial	Fabrication technique	Aspects of behaviour investigated	Reference
Human Dermal	PolyL-lactide with Polycaprolactone (PCL)	Electrospinning	Migration and phenotype.	(Chen, Lui et al. 2019)
NIH 3T3	Polydimethylsiloxane (PDMS)	Photolithography and soft lithography	Migration in response to elasticity.	(Nan, Zheng et al. 2019)
NIH 3T3	Bacterial Cellulose-Gelatin	Casting and Leaching	Adhesion, proliferation and MMP expression.	(Khan, Ul-Islam et al. 2016)
Human Vaginal	PLGA PCL blend	Electrospinning	Activation, proliferation, ECM deposition.	(Vashaghian, Zandieh-Doulabi et al. 2016)
Human Dermal	Titanium	Alkali-heat treatment	Morphology, proliferation, ECM deposition and Cytokine expression.	(Yamada, Kato et al. 2016)
NIH 3T3	Silicon	Low pressure furnace Vapour-Liquid-Solid mechanism	Adhesion, proliferation, morphology, gene and protein expression.	(Yang, Wen et al. 2016)
NIH 3T3	Polyurethane Acrylate	Photolithography	Morphology, orientation and fibronectin secretion.	(Bae, Kim et al. 2015)
Human Vocal Fold	Tecoflex ™	Electrospinning	Activation, proliferation, alignment and gene expression.	(Hughes, Gaston et al. 2015)
NIH 3T3	Polyethylene Glycol (PEO) – PCL	Electrospinning	Attachment, migration, morphology, proliferation and gene expression.	(Li, Gregersen et al. 2015)
Human Foreskin	PDMS	Micro-textured polymer gel	Morphology, adhesion, gene and protein expression.	(Stanton, Rankenberg et al. 2014, Stanton, Parrillo et al. 2015)
Human Corneal	Silk	Micro-patterned silk	Alignment, gene expression, metabolism, morphology and proliferation.	(Gil, Park et al. 2010)
NIH 3T3	PDMS micropillar arrays	Photolithography	Adhesion, contractility, migration, morphology.	(Ghibaudo, Trichet et al. 2009)
NIH 3T3	PCL	Electrospinning	The impact of fiber size on proliferation and attachment.	(Chen, Patra et al. 2007)

ECM, extracellular matrix; MMP, matrix metalloproteinase; PCL, polycaprolactone; PDMS, Polydimethylsiloxane; PEO, polyethylene glycol.

2.3.5.1 Controlling Fibroblast Behaviour for Tissue Engineering Applications

The studies in Table 2.3 focus on quantifying and controlling specific and desirable features of fibroblast behaviour. For example, when designing a material for vocal fold reconstruction and repair, fibroblasts should produce a highly ordered ECM (Hughes, Gaston et al. 2015). Or when creating a wound healing scaffold, the presence of aligned fibres that induce fibroblast activation and migration could be used to stimulate wound contracture at the onset of wound healing. Furthermore, limiting this response through the release of matricellular proteins like angiopoietin-like-4 could curtail the wound healing function of the scaffold and reduce the chance of chronic activation causing scarring or fibrosis (Chen, Lui et al. 2019).

Despite these studies going beyond basic biocompatibility testing, their primary focus is on cellular response in the context of material choice or manufacturing method, which limits their scope in terms of understanding fibroblast biology. A small subset of articles, however, go beyond behavioural observations to investigate the mechanisms behind fibroblast phenotype. The studies listed in Table 2.4 investigate fibroblast activation and the signalling cascades at work in 3D culture in a manner similar to initial collagen studies. They focus on the fundamental biology involved in common fibroblast-based diseases rather than creating a new tissue engineered construct.

Table 2.4. Studies That Investigate Fibroblast Biology in 3D Biomaterials.

Fibroblast Type	Biomaterial	Fabrication technique	Aspects of behaviour investigated	Reference
Human Lung	Dextran vinyl sulfone (DexVS)	Electrospun fibres encapsulated in hydrogels	Migration, proliferation, spreading and Rac1, RhoA Cdc42 activity.	(Matera, Wang et al. 2019, Matera, Lee et al. 2021)
Human Cardiac	PLLA	Electrospinning	Adhesion, metabolism, proliferation and proteomics.	(Muniyandi, Palaninathan et al. 2020)
L929 Mouse	Microporous PLLA with PLGA	Lyophilization	Adhesion, migration, morphology and proliferation.	(Bahcecioglu, Hasirci et al. 2018)
Human Fetal Lung	Polyethylene Terephthalate	Electrospinning	NF-κβ signalling.	(Htwe, Harrington et al. 2015)
Human Dermal	Silicone and collagen	Micro-printed	Viability, morphology, α-SMA/ hydroxyproline expression.	(Jiang, Lu et al. 2011)
Human Diploid	Polyethylene-co-vinyl alcohol	Casting	Senescence in Biomaterials due to hydrophilicity.	(Lou, Chiu et al. 2010)
NIH 3T3	PLGA	Electrospinning	Stress response due to surface modifications.	(Park, Lee et al. 2010)
Human Dermal	PMMA	Electrospinning	Adhesion, proliferation, integrin expression and migration.	(Liu, Ji et al. 2009)
NR6 Mouse	Collagen-GAG	Lyophilization	Cell migration in relation to pore size and strut modulus.	(Harley, Kim et al. 2008)
Primary Cardiac	Nylon	Weave	Activation and ECM production.	(Poobalarahi, Baicu et al. 2006)
NIH 3T3	Polyamide	Electrospinning	Morphology, Adhesions and RAC/Rho K activation.	(Nur-E-Kamal, Ahmed et al. 2005)
NIH 3T3	Polyacrylamide	Polymer casting	Adhesions in 3D.	(Beningo, Dembo et al. 2004)

A-SMA, Alpha Smooth Muscle Actin, GTPase, guanosine triphosphate hydrolase; NF-κB, Nuclear Factor Kappa-B; PLGA, poly(lactic-co-glycolic acid); PLLA, poly (l-lactic acid); PMMA, Polymethyl methacrylate. RAC, Ras-related C3 Botulinum Toxin Substrate; RhoA, Ras Homolog Family Member A; Cdc42, Cell Division Cycle 42.

2.3.5.2. Fibroblast Activation in Modern Culture Systems

The conflicting findings of studies in natural and synthetic hydrogels as well as ECM derived matrices were the result of different culture conditions, materials and fibroblast types. This experimental variation is exacerbated by the huge variety of materials and manufacturing processes in use for tissue engineering purposes today. Amongst the studies in Table 2.4 Harley *et al.* used collagen-glycosaminoglycan (GAG) scaffolds to investigate fibroblast motility (Harley, Kim et al. 2008). NR6 fibroblasts were grown on lyophilized collagen-GAG scaffolds where they had a biphasic response to changes in strut stiffness. When strut stiffness was increased from 5 to 12 MPa, cell motility increased, however at 39 MPa, motility was reduced (Harley, Kim et al. 2008). Finding consensus between these results and those gathered in polyacrylamide gels (Pelham and Wang 1997) is challenging given the use of different materials, cells and even methods for measuring stiffness. In the collagen-GAG scaffolds strut stiffness was measured whilst for polyacrylamide scaffolds, whole gel stiffness was used. Furthermore, whilst NR6 fibroblast are derived from 3T3 fibroblasts which were also used in the polyacrylamide gels, they were selected as they lack the epidermal growth factor response normally present in fibroblasts (Pruss and Herschman 1977). The impact of pore size on fibroblast motility was also investigated. The collagen-GAG scaffolds had pore sizes between 96 and 150 μm, in this range cell motility decreased as pore size increased (Harley, Kim et al. 2008). Once again, it can be challenging to draw comparisons between these results and those gathered in hydrogel studies. In a collagen gel as pore size increased from 1.1 to 2.2 μm fibroblast motility increased (Miron-Mendoza, Seemann et al. 2010). In this case the vast difference in pore size range makes comparison difficult. Pores in the collagen-GAG scaffold were larger than the cells and fibroblasts therefore interacted with single struts whilst the fibroblasts in collagen hydrogels were much larger than the pores and would spread across multiple struts and pores.

Another of the studies in Table 2.4. Showed that fibroblasts grown on electrospun PLLA scaffolds had twice the proliferative capacity of those grown on tissue culture plastic

(Muniyandi, Palaninathan et al. 2020). In contrast, fibroblasts grown on electrospun PMMA scaffolds proliferated at the same rate as fibroblasts grown on 2D PMMA films (Liu, Ji et al. 2009). Muniyandi *et al.* used Ki67 antibodies to identify which cells were proliferating, as the marker is expressed in all proliferating cells except those in cell cycle phase G0. The PLLA scaffolds were also modified using ECM proteins including collagen, fibronectin, gelatin and poly L lysine (Muniyandi, Palaninathan et al. 2020). Interestingly none of the coatings altered the proliferation rate significantly, and proliferation rates were significantly elevated compared to 2D tissue culture plastic. This result opposes most collagen gel studies that saw a fall in proliferation rates in 3D (referenced in Tables 2.1 and 2.2). It also contradicts the study conducted by Kono *et al.* in which the number of cells in S phase was reduced in 3D collagen gels (Kono, Tanii et al. 1990). These results suggest that questions remain around the mechanism of fibroblast activation and the counter state of quiescence in different 3D environments. Despite the differences between studies, mechanoregulation, cellular encapsulation and polarity as well as the chemical nature of a material including the availability of integrin binding sites are all key factors in the regulation of fibroblast behaviour.

Fibroblast activation is a key target in fibrosis and cancer research and therefore research that generates a clearer picture of the mechanisms that govern activation in a biologically relevant model could be of great value. Examples of studies that investigate the pathways integrating the mechanical, architectural and chemical signals that govern fibroblast activation in 3D models, include early work that identified that reductions in ERK signalling in collagen hydrogels were the result of mechanoregulation (Rosenfeldt and Grinnell 2000). This has yet to be explored in a system other than the collagen hydrogel. One example of a study that investigated signalling pathways in a modern biomaterial, used electrospun polyethylene terephthalate to understand the role of NF-κβ on fibroblast activation (Htwe, Harrington et al. 2015). NF-κβ is implicated in the release of proinflammatory signals by fibroblasts in inflammatory lung diseases including asthma, chronic obstructive pulmonary disease and idiopathic lung fibrosis (Htwe, Harrington et al. 2015). Other studies presented in Table 2.4

investigate Ras-related C3 botulinum toxin substrate (RAC) activation, senescence, ECM deposition and the stress response.

2.3.5.3 Cellular Nutrition and Oxygen Consumption in 3D Culture

Finally, it is important to acknowledge that 3D cultures are subject to greater variability in nutrient and oxygen distribution than traditional 2D cultures (Tse, Gardner et al. 2021). The degree of porosity can affect the buildup of cellular waste products whilst also creating nutrient gradients across models. In hydrogel culture the ability of small molecules to diffuse through the gel has been estimated to be up to 50% reduced compared to diffusion in solution (McMurtrey, 2016). Such factors have an impact on cellular metabolism and therefore cannot be discounted when comparing growth rates and behaviour between 2D and 3D and between different 3D models.

2.3.6. Fibroblasts in 3D culture summary

Studies conducted in collagen hydrogels were the first to shape our understanding of fibroblast behaviour in in vitro 3D environments. They were followed by a range of more versatile synthetic and hybrid hydrogels where the ability to control mechanical properties and scaffold microarchitecture afforded better control over individual features such as porosity or stiffness. Much of the early work focussed on establishing the role of mechanical tension in regulating the fibroblast activation phenotype and this was well characterised in collagen gels. However, since then there has been a lack of cohesion between studies conducted in a diverse array of modern biomaterials. This has made it a challenge to draw conclusions about the most critical features of 3D culture environments and their impact on fibroblast behaviour. These studies have also suggested that cell encapsulation which limits cell spreading may have had a greater impact on hydrogel studies than previously appreciated.

Fibroblasts have been perhaps the most used cells for early biocompatibility testing in novel biomaterials. ISO 10993: Biological Evaluation of Medical Devices - Part 5 (tests for in vitro cytotoxicity) endorses 7 cell lines for use in the testing of medical devices, of which 6 are

fibroblasts (L929, BALB/3T3 clone A31, MRC-5, WI-38, BHK-21, V79 379A). This has led to a vast number of studies that briefly report on fibroblast activity in 3D, whilst remaining focused on their main objective, to explore material properties and manufacturing techniques. However, given the complex functionality of fibroblasts in health and disease, some modern studies have moved beyond basic biocompatibility testing to investigate fibroblast behaviour once more. Amongst the modern studies, no consensus has formed on the culture features that control fibroblast activation and proliferation. Studies utilising different 3D culture systems have recorded changes in cell shape, spreading, motility and attachments, often in response to a variety of matrix changes that have shown an inverse effect in other studies.

Given the lack of consensus among studies, the use of one highly tunable system would be of great value. Electrospinning is a technique that can be manipulated to control individual matrix features including pore size, fibre diameter and alignment. There are many standardised approaches for the mechanical and physical characterisation of electrospun scaffolds and it is possible to generate 2D controls. For these reasons electrospinning could be used to address questions concerning mechanoregulation and how micro and macro-features combine to influence fibroblast behaviour in 3D. Disseminating the true causative factors that govern fibroblast behaviour remains a challenge when an array of chemical and physical properties converge in 3D culture models. However, informed by previous studies and with the ability to control as many variables as possible in modern biomaterials, it should be possible to build on our current knowledge.

2.4. Electrospinning

Several of the studies listed in Tables 2.3 and 2.4 used electrospinning as a manufacturing method to produce highly fibrous scaffolds for use in fibroblast culture. Electrospinning has a long history and has been used and modified for many purposes over the last century (Greiner and Wendorff 2007). Here we review the history, application and recent advances that make this versatile technique so valuable for the study of fibroblasts.

2.4.1 The History of Electrospinning

The first patents for electrospinning apparatus were filed in 1902 (Cooley 1902, Morton 1902) however it wasn't until the 1990's that the process gained popularity (Cipitria, Skelton et al. 2011). Reneker demonstrated the ability to produce fibres with diameters in the nano-to-micrometre range using up to 20 different polymers (Doshi and Reneker 1995, Reneker and Chun 1996). Since the publication of this work in 1995 the amount of literature regarding the technique of electrospinning has expanded rapidly (Figure 2.5). This is in part due to the technique's versatility. Electrospinning has been used in the textiles industry, in the production of filters with tunable pore sizes, in medical devices and for tissue engineering research (Greiner and Wendorff 2007). In the rapidly growing field of tissue engineering, electrospun fibres have been used to mimic the microarchitecture of the ECM (Jiang, Carbone et al. 2015).

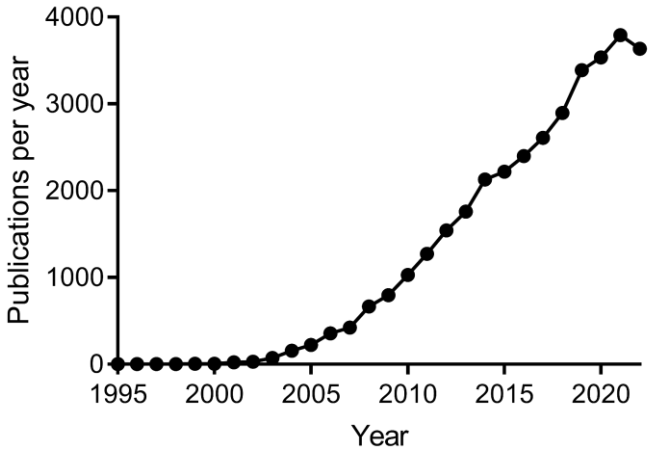

Figure 2.5. *The number of publications per year that were returned when searching for the topic 'electrospinning' on Web of Science on 31/05/2023. Results were refined to only include articles. https://www.webofscience.com/wos/woscc/basic-search*

2.4.2. The Electrospinning Process

A high voltage current is applied to the end of a syringe tip, overcoming the surface tension of an extruded polymer solution to generate an ultra-fine stream of charged polymer (Figure 2.6) (Taylor 1969). Solvent evaporates from the polymer stream as it travels towards a grounded collector, where it is deposited as a non-woven mat of fibres (Doshi and Reneker 1995).

Details of the custom electrospinning setup used at the University of Sheffield, School of Clinical Dentistry can be found in the materials and methods section 3.1. The electrospinning process can be manipulated through the control of polymer and solvent makeup and total volume, the distance to the collector, the voltage and rate of delivery (Reneker and Chun 1996). Basic parameter changes have given way to more advanced scaffold enhancements for use in tissue engineering applications (Jiang, Carbone et al. 2015). Modifications include surface functionalization using plasma treatment and protein addition alongside fibre alignment and growth factor incorporation (Jiang, Carbone et al. 2015).

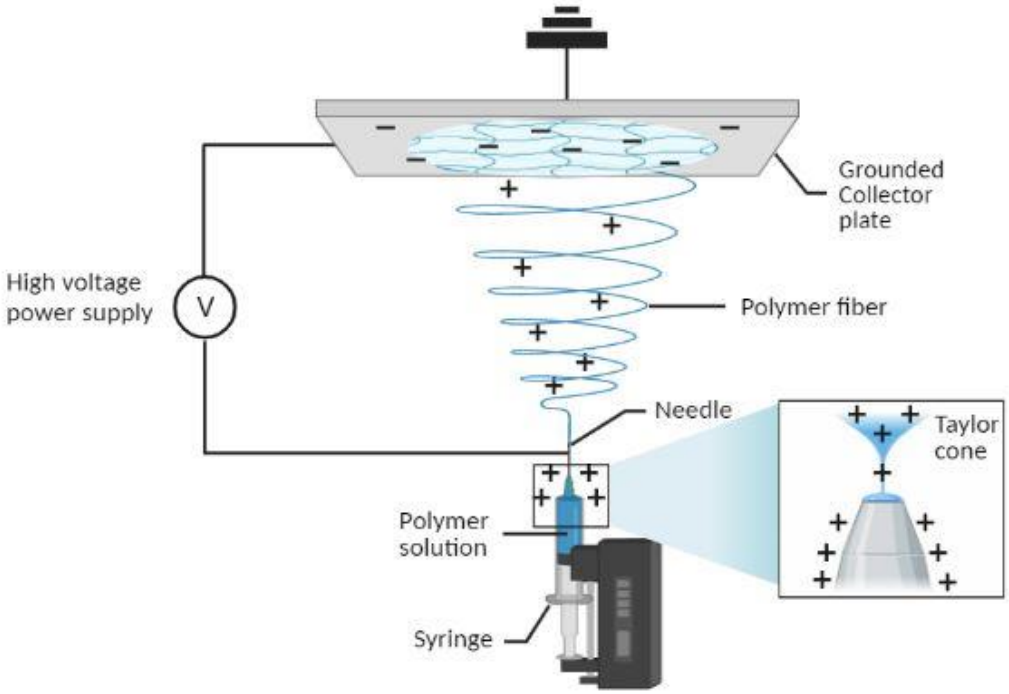

Figure 2.6. *The electrically charged polymer forms a Taylor cone from which the polymer stream is expelled. Adapted from "Principle of electrospinning system" template, made by Dillon Wagay using BioRender.com (2023). Retrieved from https://app.biorender.com/biorender-templates.*

2.4.3. Applications and Advances

Electrospun scaffolds have been used for nerve, ligament, bone, cartilage, skin and skeletal muscle tissue engineering as reviewed by Jiang *et al.* (Jiang, Carbone et al. 2015). Alongside architectural modifications such as changes to fibre size and alignment and the incorporation

of macro-features like grooves and ridges, growth factors and small molecules have been used in electrospun scaffolds (Jiang, Carbone et al. 2015). An example of a highly modified electrospun scaffold being used for tissue engineering purposes is in models of the tendon to bone interface. This complex region of connective tissue contains transitional ECM where highly ordered fibres in the tendon give way to less organised bone matrix. Scaffolds with aligned and unaligned fibres have been used to mimic this area (Xie, Li et al. 2010). As well as changes to the ECM architecture, as tendon gives way to bone there is a tissue mineralization gradient, mimicking this gradient is also possible using electrospun fibres coated in calcium phosphate (Li, Xie et al. 2009).

2.5. Concluding Remarks

Fibroblasts are heterogeneous cells found in the stroma of tissues throughout the body. They activate in response to injury, with the wound healing response a well characterised example of the diverse roles of activated fibroblasts. Activated fibroblasts express α-SMA, part of the contractile apparatus, deposit ECM proteins like collagen and proliferate rapidly. Activated fibroblasts also contribute to disease states in fibrosis and cancer. Activation is triggered by physical and chemical signals that when deregulated, lead to chronic activation and disease.

As stromal cells with a complex functional role in health and disease there has been a significant amount of research using ECM mimicking 3D culture environments to elucidate the physical and chemical cues that govern fibroblast behaviour. Our literature review focused on studies that have compared fibroblast activation behaviour between 2D and 3D cultures or that use 3D culture to investigate fibroblast phenotype. The first studies began in collagen hydrogels before progressing into synthetic and hybrid hydrogels. A clear role for mechanical tension in the regulation of fibroblast phenotype and activation characteristics was established in these systems. Subsequent studies using modern biomaterials have allowed for better control of microarchitectural and mechanical properties. Despite the extensive body of literature, the complex interplay between cell spreading, attachments and polarity in 3D cultures has often led to conflicting results. Furthermore, understanding how disease states

deregulate fibroblast activation in more relevant 3D models remains a key therapeutic target for diseases from cancer to fibrosis.

We conclude that electrospinning is a highly versatile manufacturing technique with the ability to independently control aspects of 3D architecture and investigate their impact on fibroblast behaviour. Furthermore, electrospun scaffolds do not encapsulate cells or limit their ability to spread as with hydrogel culture. They are also slow to degrade and therefore stable culture conditions can be maintained for longer time course experiments. Finally, electrospun polymers have been used in medical trials and therapeutic applications which will make for easier translation to the clinic if required. As such, this investigation will use electrospun scaffolds to further develop our knowledge of fibroblasts in a 3D environment.

2.6. Hypothesis, Aims and Objectives

Based on our literature review we aim to manufacture and characterise a basic electrospun scaffold; the scaffold will be used to grow fibroblast cells and explore their behaviour in a fibrous 3D environment. Once we have fully characterised the scaffold and the fibroblast phenotype, we aim to explore the cellular mechanisms that govern behaviour and test the scaffold for potential applications in disease modelling.

This work is significant due to the lack of cohesion between previous studies and experimental limitations of the hydrogel system. Furthermore, a great deal is still unknown about the nature of cellular control in 3D environments. Once this model is established, modifying scaffold properties could isolate individual environmental cues, making the study of their impact on fibroblast behaviour possible. The data obtained in this project will be key in the future development of complex tissue regeneration and cancer progression models where fibroblasts are an essential component. Due to the roles of fibroblasts in diseases such as fibrosis and cancer this work will have a significant therapeutic impact. The thesis hypothesis is outlined below alongside the specific experimental aims and objectives which will be addressed over the course of 3 results chapters.

2.6.1. Hypothesis

The hypothesis for this research is that when grown on the electrospun scaffold which provides a greater degree of ECM structural mimicry than 2D surfaces, fibroblasts will exhibit reduced activation characteristics, with reduced proliferation rates and reduced expression of activation associated genes such as α-SMA and versican.

2.6.2 Specific Experimental Aims and Objectives

1) To manufacture fibrous polycaprolactone scaffolds using a custom vertical electrospinning rig at The University of Sheffield, School of Clinical Dentistry and to characterise the scaffolds and seed them with fibroblast cells.

    A) Optimise spinning conditions using medical grade polycaprolactone.
    B) Characterise fibre diameter and angle, scaffold porosity, mechanical and physical properties. This will be conducted using SEM image analysis, mercury intrusion porosimetry, water contact angle testing and a mechanical tester.
    C) Quantify 3T3 and NOF fibroblast viability and growth rate using PrestoBlue, Picogreen and Live-dead assays.

2) To investigate how cellular behaviour changes when fibroblasts are grown on the PCL electrospun scaffolds and how cells attach and interact with the scaffold.

    A) Stain Ki67 to quantify proliferation and use qPCR to test for senescence associated gene expression.
    B) Use qPCR to quantify the expression of genes associated with fibroblast activation, including α-SMA, Collagen and Versican.
    C) Use immunofluorescence and SEM images to investigate fibroblast morphology and attachments.

3) To investigate which molecular pathways control the fibroblast phenotype on electrospun scaffolds and to explore potential scaffold applications in regulating fibroblast activation in disease states.

    A) Use western blotting to investigate the MAPK pathway.
    B) Use RNA sequencing to understand the genetic regulation of fibroblast phenotypes on the electrospun scaffold.
    C) Understand how the scaffold impacts the expression levels of genetic markers of cancer associated fibroblasts.

Chapter 3: Materials and Methods

3.1. Fabrication of Electrospun (ES) Scaffolds

Electrospinning was conducted in a custom rig at the University of Sheffield, School of Clinical Dentistry (Figure 3.1). The set-up contained a vertically aligned PHD2000 syringe pump (Harvard Apparatus, UK) connected to an Alpha IV Brandenburg power source (Brandenburg Limited, UK). Ejected polymer was collected on a grounded collection plate positioned above the syringe pump. The collection plate was wrapped in baking parchment to ensure the appropriate detachment of the fibrous membrane from the collector (methodology previously optimised in our research group).

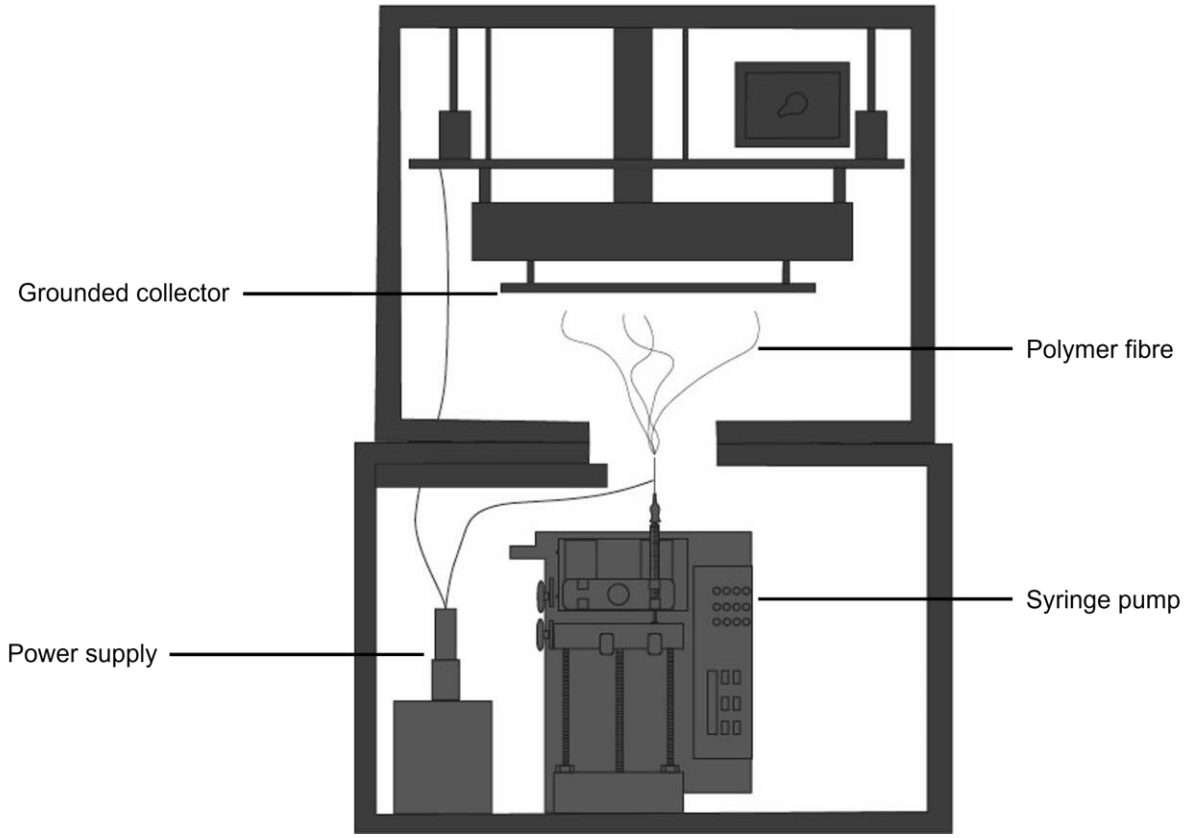

Figure 3.1. *A schematic diagram of the electrospinning rig at the University of Sheffield, School of Clinical Dentistry.*

Polymer solutions were prepared using Sigma polycaprolactone (PCL) with an M_n (number average molecular weight) of 80,000 (440744 Sigma Aldrich, US) or Purasorb PC 12 polycaprolactone (Corbion®, NL). The Purasorb PC 12 is a medical grade polymer and was selected to ensure results would be relevant in the case of clinical translation. Polymers were dissolved in a solvent solution containing 92.66% dichloromethane (DCM) (Fisher Scientific, UK) and 7.34% dimethylformamide (DMF) (Fisher Scientific, UK) and left to mix overnight with a magnetic stirrer. The polymer solution was loaded into a 1 ml polypropylene syringe (Henke-Sass Wolf, DE) with a blunt tip 20-gauge (ga) 1 inch (in) metal needle (Fisnar, US). The metal needle was attached to the power supply using a crocodile clip. The grounded collector was positioned 17 cm from the needle tip. The syringe was reloaded until 2 ml of the polymer solution had been expelled. Polymer was dispensed at a rate of 1.5 ml per hour with a voltage of 21.08 kV applied to the syringe tip. PCL scaffolds were left in a fume hood overnight to ensure solvent evaporation. Scaffolds were stored in sealed bags with desiccant sachets (Merck KGaA, DE) inside a Secador ™ desiccant chamber (SP Bel-Art, USA) until use.

Table 3.1. Electrospinning Conditions for Scaffold Fabrication.

Polymer Used	Polymer Concentration (weight/weight) (w/w)	Solvent Solution	Volume spun (ml)	Conditions (kV) (ml/hr)
Sigma Polycaprolactone (Sigma Aldrich)	10%	DCM:DMF 92.66:7.34	2	21.08 kV 1.5 ml
Purasorb PC 12 Polycaprolactone (Corbion)	10% 12% 15%	DCM:DMF 92.66:7.34	2	21.08 kV 1.5 ml

DCM, dichloromethane; DMF, dimethylformamide.

3.2. Scaffold Characterisation

3.2.1. Scanning Electron Microscope (SEM) Imaging of ES Scaffolds

A Tescan Vega 3 SEM (Tescan-UK Ltd. UK) situated at the University of Sheffield Biomedical Sciences Electron Microscopy Facility was used to image scaffolds. Prior to imaging, samples were gold-coated for 2 minutes with an Edwards S150B Sputter-Coater (Edwards Vacuum UK, UK). For the characterisation of scaffold fibre diameter, fibre angle and porosity, 3 scaffolds were fabricated on 3 different days under the same conditions. Samples were taken from 3 locations within each scaffold including peripheral and central sites (Figure 3.2). A cork borer with a diameter of 8 mm was used to cut scaffolds for SEM analysis whilst a 12 mm borer was used to cut samples for culture with cells. All SEM images were analysed using ImageJ v1.52p (National Institutes of Health, USA).

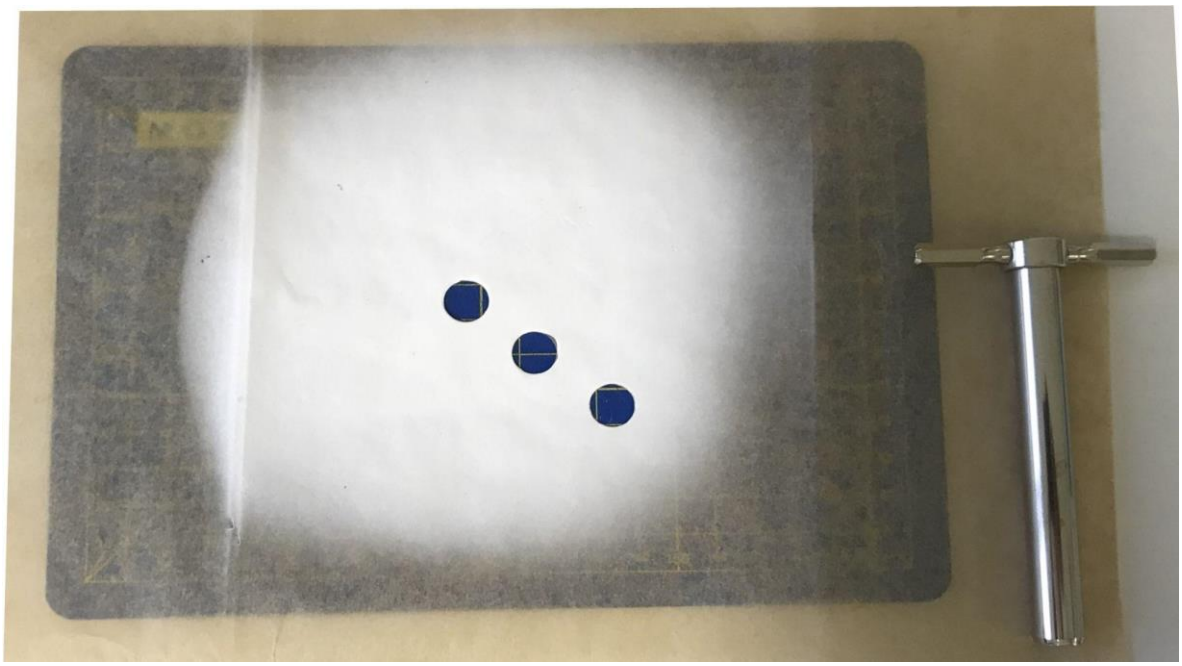

Figure 3.2. *An ES scaffold on baking parchment displaying characteristic sample locations for SEM imaging and the cork borer used to cut scaffold samples.*

3.2.2. Calculating Fibre Diameter and Angle from SEM Images

Each sample was imaged in 3 different places moving from the image periphery to the centre. 10 fibres in the foremost plane of each SEM image were measured with a total of 270 fibres measured for both fibre diameter and angle. To normalise fibre angles the mean fibre angle of each scaffold was subtracted from all individual fibre angles. This process rotated the mean fibre angle for each scaffold to zero. To achieve more accurate alignment values, angles that deviated by more than ∓ 90 ° from the mean were corrected by the addition of 180 °. This correction step accounts for those fibres that are less aligned (mean ∓ > 90 °) in the measured axis (left to right) but are more aligned if measured from right to left. Individual fibre alignment was then calculated using the following equation: $\left|1 - \left(\frac{|mean - angle|}{90}\right)\right| \; x \; 100$. Finally, average fibre alignment was calculated from the individual alignment values.

3.2.3. Calculating Porosity from SEM Images

Surface pore sizes were measured using ImageJ v1.52p. Surface porosity was estimated using the following equation: $\left(\frac{Surface\ pore\ area}{Image\ area}\right) \; x \; 100$. Surface pore area was equivalent to the sum of all surface pore areas within an image.

3.2.4. Mercury Intrusion Porosimetry

Mercury intrusion porosimetry (MIP) was conducted by Dr Oday Hussein at the Characterisation Small Research Facility at the University of Sheffield. An Autopore V 9600 (Micromeritics Instrument Corporation, US) machine was used with Micro-Active software (Micromeritics Instrument Corporation, US). Mercury temperature was 25.34 ℃ and the report range was 0.1 to 61,000 psia. A sample mass of 0.0260 g was used for MIP. Porosity data was presented as the differential pore volume (dV) divided by the differential log pore diameter (dlogD) (dV/dlogD) against the log pore diameter (logD) to visualise the pore size distribution. V is the intrusion volume (pore volume) in ml per gram of sample and D is the pore diameter in μm.

3.2.5. Mechanical Testing

Three scaffolds produced on different days under the same conditions were tested on a Lloyd LRX universal testing machine (Lloyd Instruments Ltd, UK). A 50 N load cell was used with a crosshead speed of 10 mm/min. The test was conducted at room temperature. Two test samples from each scaffold were prepared to ASTM D882 standards with dimensions of 70 mm x 10 mm x 0.25 mm (length x width x thickness). A Mitutoyo 293-816 digital micrometre (Mitutoyo UK Limited) with a resolution of 0.001 mm was used to measure thickness. Nexygen 4.1 software (Lloyd Instruments Ltd, UK) was used to generate stress-strain curves from which the tensile strength and elastic modulus of each specimen was estimated. Sample stress (σ) was determined by the applied load (F) divided by cross-sectional area (A0); $\sigma = A0/F$. Change in gauge length (ΔL) divided by initial gauge length (L0) gives unitary deformation or strain ($\varepsilon = \Delta L/L0$). Consequently, the elastic modulus (E) was calculated from the elastic phase of each sample's stress-strain curve ($E = \Delta\sigma/\Delta\varepsilon$).

3.2.6 Scaffold Water Contact Angle

Water contact angle (WCA) was used to assess scaffold and tissue culture plastic surface wettability. WCA was calculated using a KRUSS DSA100S Drop Shape Analyser (Kruss, DE) with Kruss software DSA3. WCA (θ) was calculated as shown in Figure 3.3. Samples were cut from polystyrene multiwell culture plates (Greiner Bio-One, UK) and PCL scaffolds and were approximately 2 cm^2 in size.

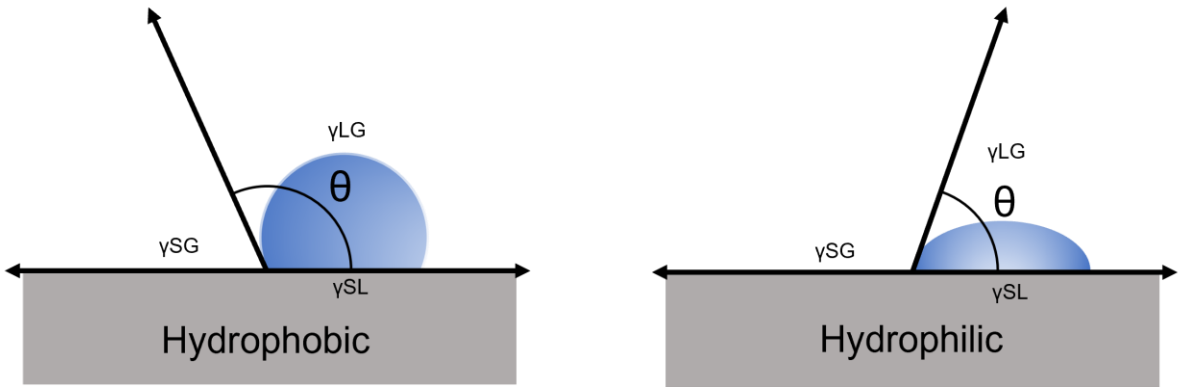

Figure 3.3. *Diagram showing the relationship between WCA (θ) and the liquid gas (γLG), solid gas (γSG) and solid liquid (γSL) interface energies.*

3.3. Fabrication of Flat PCL Membranes

In addition to electrospun scaffolds, the same polymer solution (15% Purasorb PC 12 Polycaprolactone (Corbion) in a 92.66% DCM 7.34% DMF solution) was used to create flat PCL membranes. A 60 mm x 60 mm glass slide held in place with a custom-made 3D printed holder was placed centrally on the chuck of a spin coater (Ossila limited, UK). 2 ml of PCL solution was placed centrally on the glass slide and the spin coater was set to rotate at 1500 revolutions per minute (rpm) for 30 seconds.

3.4. Cell Types Used in This Investigation

Mouse embryonic NIH 3T3 fibroblasts (ATCC® CRL-1658™) were used between passage number 10 and 40. Primary human normal oral fibroblasts (NOF) were donated by Dr Helen Colley (Colley, Hearnden et al. 2011). NOF were isolated from a buccal biopsy taken with written informed consent under ethical approval number 09/H1308/66. This was previously described in (Hearnden, Lomas et al. 2009). NOF were acquired and used between passage number 6 and 12. Primary human cancer associated fibroblasts (CAF) were obtained from oral squamous cell carcinoma (OSCC) resection specimens (Elmusrati, Pilborough et al. 2017) at Sheffield Teaching Hospitals NHS Foundation Trust (Sheffield Research Ethics Committee reference number 13/NS/0120, STH17021). CAF were used between passage number 7 and 11. 3T3 cells were used for initial viability testing with PrestoBlue, PicoGreen and Live/Dead assays. NOF were used to repeat the preliminary viability assays and in all subsequent cell behaviour studies. CAF were used in qPCR RNA expression assays.

Table 3.2. Cell Types, Their Abbreviations, Species of Origin and the Passage Range Used.

Cell Name	Abbreviation	Species	Passage Range
Cancer associated fibroblast	CAF	Human (Primary)	7 - 11
NIH 3T3 fibroblast	3T3	Mouse (embryonic)	10 - 40
Normal oral fibroblast	NOF	Human (Primary)	6 - 12

3.5. Routine Culture

All cells were grown in T75 flasks (Greiner Bio-One, UK) and incubated at a temperature of 37 °C in 95% air and 5% CO_2 in a CellXpert ® C170i incubator (Eppendorf, DE). All cell work including media preparation was conducted in sterile Class 2 laminar flow hoods (Walker, UK) cleaned with 70% industrial methylated spirit (IMS) (Fisher Scientific, UK) in deionized water. All cells were grown in high glucose Dulbecco's Modified Eagle's Medium (DMEM) (Sigma Aldrich, UK) with 10% (volume/volume) (v/v) foetal calf serum (Sigma Aldrich, UK), penicillin-streptomycin (50 IU/ml penicillin, 50 µg/ml streptomycin) (Sigma Aldrich, UK) and 2 mM L-glutamine (Sigma Aldrich, UK). Media was refrigerated at 4 °C and pre-warmed before use. When cells reached approximately 80% confluence they were passaged. To passage cells, old media was removed before the cells were washed twice with phosphate buffered saline (PBS) (Sigma Aldrich, UK). Once washed, 3 ml of Trypsin Ethylenediaminetetraacetic (EDTA) (0.5 g/l porcine trypsin and 0.2 g/l EDTA:4Na in Hanks Balanced Salt Solution with phenol red) (Sigma Aldrich, UK) was added to the cells. The cells were then incubated with the Trypsin/EDTA for 4 minutes at 37 °C with 5% CO_2. Following incubation, cell detachment was visually confirmed with a Nikon Eclipse TS100 microscope. Trypsin/EDTA was then inactivated with 3 ml of culture media before the cell suspension was centrifuged for 10 minutes at 192 relative centrifugal force (RCF). The supernatant was removed from the resultant cell pellet before the cells were resuspended in fresh media. NOF and CAF cells were routinely split 1 in 3 and passaged weekly, whilst 3T3 cells were split 1 in 5 and passaged weekly. Cells were grown in 10 ml of culture medium.

3.6. Cell seeding

3.6.1. Scaffold Seeding

Electrospun scaffolds were cut to a diameter of 12 mm using a 12mm cork-borer and then sterilised in 100% ethanol (EtOH) (Fisher Scientific, UK) for 15 minutes and rinsed 3 times in PBS. A custom-made stainless-steel ring with a central diameter of 10mm produced at the University of Sheffield Department of Chemical and Biological Engineering, Engineering

Workshop was used to hold the scaffold in place and to prevent it from floating. The metal rings were autoclaved before use. The scaffold and rings were placed in 12 well plates (Greiner Bio-One, UK) for seeding and subsequent culture. Cells were counted using a haemocytometer (Hirschmann, DE) and unless otherwise stated 10,000 cells were seeded onto ES scaffolds. 3T3 cells were delivered using a bead-seeding or diffusion-seeding method (Figure 3.4). For bead-seeding 10,000 cells suspended in 10 µl of media were placed onto the surface of the scaffold. After 5 minutes 800 µl of media was added to the scaffold. For diffusion-seeding 800 µl of media was added to the scaffold prior to the bead of cells being released into the media above the scaffold surface. 800 µl was the maximum volume of media that could be held within the metal ring placed on top of the scaffold. NOF and CAF were seeded using only the diffusion seeding technique.

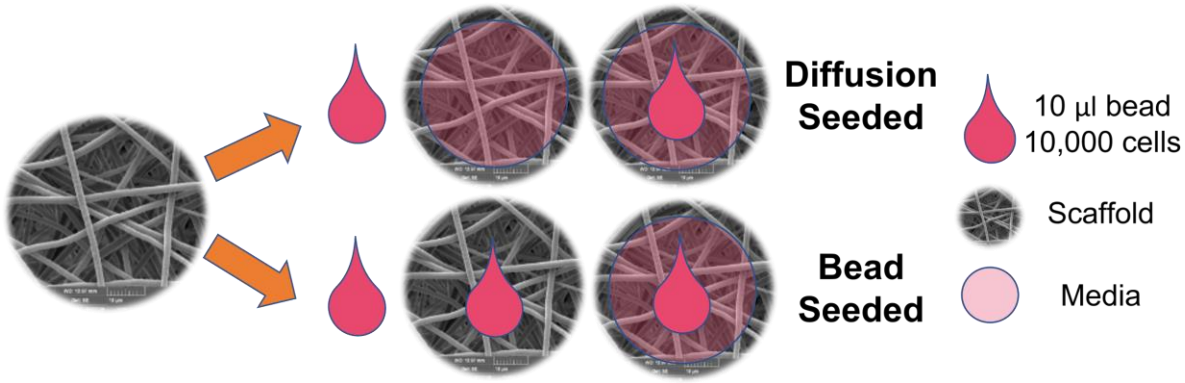

Figure 3.4. *Schematic diagram of the diffusion and bead seeding techniques.*

3.6.2 Tissue Culture Plastic Seeding

Tissue culture plastic (TCP) was used as a control for all experiments unless otherwise stated. All cell types were seeded onto TCP 12 well plates (Greiner Bio-One, UK) using the diffusion seeding method. Unless otherwise stated 12 well plates were used for all TCP experiments.

3.6.3 Glass Coverslip Seeding

NOF were seeded onto circular glass coverslips of 13 mm diameter (Academy Science, UK) using the diffusion seeding method to deliver 10,000 cells for immunofluorescence imaging

during Ki67 proliferation and actin cytoskeleton and focal adhesion staining assays. In these assays glass coverslips were used as the control rather than TCP.

3.7. Inducing Senescence in NOF

Hydrogen peroxide solution (30% (w/w) H_2O_2 in water) (Sigma Aldrich, UK) was diluted in culture media to make a 500 μM H_2O_2 solution. Cells were grown to 60% confluency in a T75 flask before they were incubated in 10 ml of the 500 μM H_2O_2 solution for 2 hours at 37 °C in 95% air and 5% CO_2. After incubation the H_2O_2 solution was removed and cells were washed 3 times with PBS (Sigma Aldrich, UK). Cells were cultured with normal culture media for at least 7 days before the senescent phenotype was confirmed using β-galactosidase (β-gal) staining.

3.7.1 Senescence Associated β-Galactosidase Staining

This assay was completed using a Senescence β-Galactosidase Staining Kit #9860 (Cell Signalling Technology, US). Before staining, cells in T75 flasks were washed in PBS then fixed with 3 ml of fixative solution (Cell Signalling Technology, US) for 20 minutes. The fixative was removed and the flask washed twice with PBS. Next the flask was incubated with 4 ml of staining solution. Staining solution contained 1 mg/ml of X-gal in 1 X Staining Solution (#11675), 1 X Solution A (#11676), 1 X Solution B (#11677) (all Cell Signalling Technology, US). Flasks were incubated overnight in parafilm and wrapped in foil at 37 °C. Cells were imaged with a Nikon Eclipse TS100 microscope attached to a Spot idea ™ digital camera (Spot Imaging, US) and blue staining indicated cellular senescence. Blue staining was not observed in untreated cells and when detected in treated flasks, at least 90% of cells were stained.

3.8. NOF Activation with TGF-β1

Transforming growth factor beta (TBF-β1) was used to activate NOF in culture. 5 ng/ml of TGF-β1 (R&D Systems, UK) in 10 ml of culture media was added to scaffold and TCP grown NOF, 1 day after seeding. NOF were then harvested on day 3 or day 6 after stimulation with TGF-β1 (day 4 or day 7 post seeding).

3.9. Confluence as a Model for Quiescence

NOF were grown to confluence in a T75 flask and then maintained at confluence for 7 days before they were harvested for quantitative polymerase chain reaction (qPCR). Media was refreshed after confluence was reached.

3.10. Fibroblast Viability Assays

3.10.1 PrestoBlue™ Assay

A PrestoBlue™ Assay (Invitrogen, UK) was used to assess the metabolic activity of 3T3 and NOF in culture. PrestoBlue™ is a resazurin based product and as such is reduced by viable cells to produce the fluorescent pink resorufin. Media was removed from cells and 1 ml of a 10% (v/v) PrestoBlue solution in culture media was added to each well which was then incubated in the dark for 1 hour at 37 °C with 95% air and 5% CO_2. The 12 well plate was wrapped in foil and all subsequent work was carried out in an unlit hood. 200 µl of the cultured media was removed in triplicate and placed in a 96 well plate. The resultant fluorescence was measured using a Tecan M200 plate reader (Tecan, CH) with Magellan V7.2 analysis software. An excitation wavelength of 550 nm and an emission wavelength of 590 nm was used to record resorufin fluorescence.

3.10.2. Live/Dead™ Assay

A Live/Dead™ assay kit (Thermofisher, UK) was used to look for evidence of cell death in NOF grown on ES scaffolds and TCP. Samples were rinsed with PBS (Sigma Aldrich, UK) 3 times before they were incubated with 0.05% (v/v) Calcein acetoxymethyl (AM) (Thermofisher, UK) and 0.2% (v/v) Ethidium homodimer-1 (Thermofisher, UK) diluted in 500 µl of PBS per well. After being kept dark wrapped in foil for 20 minutes at room temperature, samples were imaged using an Axioplan 2 (Zeiss, DE) fluorescent microscope.

3.10.3. PicoGreen™ dsDNA Quantification

A Quant-iT PicoGreen™ double stranded DNA (dsDNA) assay kit (Thermofisher, UK) was used to estimate the amount of dsDNA present in cells cultured on ES scaffolds and TCP. NOF

were rinsed with PBS before 500 µl of 1% (v/v) Triton X-100 (Sigma Aldrich, UK) in distilled water was added to each well. Cells were then rapidly frozen at −80 °C for 30 minutes and thawed at room temperature for 30 minutes. This was repeated 3 times. During the freeze-thaw cycles, TCP wells were scraped and scaffolds were manually agitated to ensure NOF lysis. After the final thaw 100 µl of each sample was added to a 96 well plate in triplicate. 100 µl of 0.005% (v/v) Quant-iT PicoGreen™ reagent (Thermofisher, UK) diluted in 5% (v/v) 20 x TE buffer (Thermofisher, UK) in distilled water, was added to each sample. 96 well plates were wrapped in foil and left for 5 minutes at room temperature until they were read using an M200 plate reader (Tecan) and Magellan analysis software (Version V7.2) with an excitation wavelength of 480 nm and an emission wavelength of 520 nm. A Lambda DNA standard (Thermofisher, UK) was used to create a standard curve. The standard curve was used to convert relative fluorescence into dsDNA concentrations.

3.12. Assessing NOF Morphology

3.12.1. NOF Dehydration Using Hexamethyldisilazane

Hexamethyldisilazane (HMDS) was used to dehydrate NOF grown on scaffolds and glass coverslips for SEM imaging. Scaffolds and coverslips were treated in 12 well plates. First, culture media was removed and cells were washed twice with PBS for 5 minutes. Next 1 ml of 2.5% (v/v) Glutaraldehyde in PBS was added and incubated with samples for 1 hour. Samples were then washed in PBS for 15 minutes 3 times. After the final wash samples were washed once more in distilled water for 5 minutes. The next stage required 15-minute incubations with 1 ml of EtOH at increasing concentrations of 35%, 60%, 80%, 90% and 100% (v/v) in distilled water. Next 1 ml of HMDS mixed with EtOH (1:1) was incubated with each sample for 1 hour, after which samples were incubated with 1 ml of 100% HMDS for 5 minutes twice. HMDS was removed and samples were air dried for 1 hour. Prior to SEM imaging samples were gold coated for 2 minutes with an Edwards S150B Sputter-Coater. A Tescan Vega 3 scanning electron microscope situated at the University of Sheffield Electron Microscopy Facility was used to image samples.

3.12.2. Actin Cytoskeleton and Focal Adhesion Staining

Scaffold and TCP cultured NOF were washed with PBS twice and fixed with 400 µl of 4% paraformaldehyde (Alfa Aesar, Thermo Fisher, UK). Paraformaldehyde was removed and scaffolds were washed 3 times for 15 minutes in PBS. Non-specific binding sites were blocked in 400 µl of blocking buffer containing 5% (v/v) donkey serum (Jackson ImmunoResearch, US) and 0.3% (v/v) triton X-100 (Sigma Aldrich, UK) diluted in PBS. Blocking buffer was removed and 400 µl of 1 mg/ml Vinculin (purified clone 7F9) Monoclonal Antibody (mAb) (Merck Millipore, UK) diluted 1:350 in blocking buffer was added per sample for 1 hour at room temperature. The samples were then washed 3 times for 10 minutes with a wash buffer containing 0.05% tween-20 (Sigma Aldrich, UK) in PBS. Samples were then incubated for 45 minutes with Fluorescein Isothiocyanate (FITC)-conjugated AffiniPure Donkey Anti-Mouse igG (H+L) secondary antibody, (Jackson ImmunoResearch, US) diluted 1:1000 in PBS which also contained TRITC-conjugated Phalloidin (60 µg/ml) (Merck Millipore, UK) diluted 1:1000 and DAPI (Merck Millipore, UK) diluted 1:2000. Samples were imaged using an Axioplan 2 (Zeiss) fluorescent microscope and Image-Pro Plus software™.

3.13. Quantifying Fibroblast Activation

3.13.1. Ki67 Immunofluorescence to Identify Proliferating Cells

Immunofluorescent detection of Ki67 was used to identify what proportion of NOF were proliferative (Ki67+) and what proportion were non-proliferative (Ki67−). Fibroblasts were cultured on scaffolds or glass coverslips for 1, 4 or 7 days before they were fixed with 4% Paraformaldehyde (Alfa Aesar, Thermo Fisher, UK) for 15 minutes. Next, NOF were washed 3 times with PBS for 5 minutes each before being covered with 400 µl of blocking buffer per well for 60 minutes. Blocking buffer contained 5% (v/v) goat serum (Jackson ImmunoResearch, UK) and 0.3% (v/v) triton X-100 (Sigma Aldrich, UK) diluted in PBS. The blocking buffer was removed and NOF were incubated with the primary antibody overnight at 4 °C on a rocker plate. The primary antibody Ki-67 (D3B5) Rabbit mAb (Cell Signalling Technology, US) was diluted 1:400 in antibody dilution buffer (PBS, 1% bovine serum albumin

(BSA) (Sigma-Aldrich, UK), 0.3% triton X-100). After incubation the primary antibody was removed and the NOF were washed 3 times in PBS for 5 minutes each. Next, the samples were incubated with a fluorochrome conjugated secondary antibody, Anti-rabbit Immunoglobulin G (IgG), F(ab')2 Fragment (Alexa Fluor® 594 Conjugate) (Cell Signalling Technology, US). The antibody was diluted 1:1000 in the same antibody dilution buffer used for the primary antibody and samples were kept in the dark for 75 minutes on a rocking plate. After incubation samples were washed 3 times with PBS for 5 minutes each. At this point scaffolds were removed from their well plate and placed on an Epredia™ SuperFrost Plus™ microscope slide (Fisher Scientific, UK) with a drop of VECTASHIELD™ antifade mounting medium with DAPI (Vector Laboratories, UK) and a cover slip was applied. NOF grown on coverslips were also removed and placed face down on a microscope slide onto a drop of VECTASHIELD™ antifade mounting medium with DAPI. Slides were imaged using an Axioplan 2 (Zeiss) fluorescent microscope and Image-Pro Plus software™. Cell counting was performed in ImageJ v1.52p. For both glass and scaffold grown NOF, 3 images were taken and counted from 3 scaffolds or coverslips for every time point (days 1, 4 and 7 in culture). This was repeated 3 times on different days for biological repeats with a total of 9 images taken from 3 samples per repeat.

3.13.2. RNA Extraction

Ribonucleic acid (RNA) extraction was first attempted using the Monarch® Total RNA Miniprep Kit (New England BioLabs, US). However, Monarch® RNA lysis buffer (New England BioLabs, US) alone, or with mechanical abrasion of the scaffold surface, was unable to extract sufficient levels of RNA when analysed using the Nanodrop 1000 (Thermo Scientific, US). Subsequent RNA extraction was performed using a Direct-Zol RNA miniprep kit (Zymo Research, US). RNA was extracted from NOF cultured on ES scaffolds or TCP for 1, 4 or 7 days with 3 repeats for each timepoint. To increase RNA yield 4 scaffolds or 4 seeded TCP wells were grouped together at each timepoint. PBS was used to wash scaffolds and TCP wells 3 times to remove excess culture media. Next, 4 scaffolds per time point were placed into a 1.5 ml Eppendorf

tube and 400 µl of TRI Reagent® (Zymo Research, US) was added for 10 minutes to dissolve the scaffolds and lyse the cells. 100 µl of TRI Reagent® was used per well plate. Each well was covered with TRI Reagent® for 5 minutes before being scraped with a pipette tip to ensure complete cell detachment and lysis. At this point the TRI Reagent® was transferred from the wells into a 1.5 ml eppendorf tube as for the ES scaffolds. Next 400 µl of 100% ethanol (Fisher Scientific, UK) was added to the 1.5 ml tubes and mixed. Samples were then transferred to a Zymo-Spin IICR Column (Zymo Research, US) with an attached collection tube and centrifuged in a GenFuge 24D microcentrifuge (Progen Scientific, UK). All centrifuge steps take place at 16.3 x gravity for 30 seconds unless otherwise noted. At this point column elution could be processed to extract protein (described in 3.13.2). After removing the elution, RNA wash buffer (Zymo Research, US) was added to the column and it was centrifuged. Next 5 µl of deoxyribonuclease (DNase) 1 (1 U*/µl) diluted in 35 µl of DNA digestion buffer (Zymo Research, US) was added to the column and left at room temperature for 15 minutes. 400 µl of Direct-Zol™ RNA Prewash (Zymo Research, US) was added and the column centrifuged to remove the DNase. This step was repeated to ensure complete washing of the column. Finally, 700 µl of RNA wash buffer was added and the column was spun for 1 minute. After this the column was transferred into a clean eppendorf tube and 15 µl of DNase/ribonuclease (RNase)-free water (Thermo Scientific™ Water, nuclease-free) (Thermofisher, UK) was added. The tube was centrifuged and RNA was eluted into the eppendorf tube. RNA purity and concentration was estimated using the Nanodrop 1000 (Thermo Scientific, US). RNA was stored at −80 °C before use. ** Unit definition – one unit increases the absorbance of a high molecular weight DNA solution at a rate of 0.001 A260 units/ml of reaction mixture at 25 °C (Zymo Research, US).*

3.13.3. cDNA Library Preparation

Complementary DNA (cDNA) was prepared from 250 ng of RNA in 10 µl of nuclease free water. This water was mixed with 10 µl of 2 x reverse transcription (RT) master mix. Per reaction the RT master mix contained 2 µl of 10 x RT Buffer, 0.8 µl of 25 x deoxynucleotide triphosphate (dNTP) mix (100 mM), 2 µl of 10 x RT random primers, 1 µl of MultiScribe™

reverse transcriptase and 4.2 µl of nuclease free water (Thermofisher, UK). All reagents apart from nuclease free water are part of the High-Capacity cDNA Reverse Transcription Kit (Thermofisher Scientific, UK). This mixture was added to a PCR tube (VWR, US) and heated using an AB 2720 thermal cycler (Applied Biosystems, UK). The mixture was heated at 25 °C for 10 minutes, 37 °C for 2 hours and 85 °C for 5 minutes. Resultant cDNA was stored at −80 °C before use in qPCR.

3.13.4. qPCR

For each reaction qPCR master mix contained 5 µl of qPCRBIO probe blue mix Lo-ROX (PCR Biosystems, UK), 0.5 µl human B2M (beta-2-microglobulin) endogenous control assay (Applied Biosciences, Thermo Fisher Scientific, US), 0.5 µl TaqMan target gene expression assay (Applied Biosciences, Thermo Fisher Scientific, US) and 3 µl of nuclease free water (Invitrogen, Thermo Fisher Scientific, US). B2M was selected at the endogenous control (housekeeping) gene as there was no statistically significant difference between B2M expression in flat and scaffold grown NOF. This was tested 3 times during ACTA2, VIM and VCAN experiments with P values of 0.13, 0.08 and 0.66 respectively. TaqMan target gene expression assays are listed in Table 3.3. For each cDNA sample 9 µl of master mix was added in triplicate to a qPCR strip tube (Qiagen, DE). 1 µl of cDNA was added in triplicate to the strip tubes. Tubes were loaded into a Rotor-Gene Q 2plex (Qiagen, DE) for qPCR. A two-step cycling profile was used with a 10-minute hold at 95 °C followed by 40 cycles consisting of 45 seconds at 60 °C followed by 10 seconds at 95 °C. VIC labelled B2M was detected under the yellow channel (excitation 530 nm ± 5, detection 557 nm ± 5) and FAM labelled Target genes were detected using the green channel (excitation 470 nm ± 10, detection 510 nm ± 5). Fluorescence was detected with a gain of 5. Rotor-Gene Q software version 2.3.1.49 was used. QPCR values were converted to fold changes using the 2^−(ΔΔCT) method (Livak and Schmittgen 2001). Briefly, samples were run in triplicate with Δ Cycle threshold (CT) calculated by subtracting the mean housekeeping gene (B2M) CT from the mean target gene CT. Cycle threshold was set to 0.040 (normalised fluorescence). Next ΔΔCT was calculated by

subtracting the mean ΔCT for the normalization or comparison group (normalization gene given in each figure) from the means of all other experimental groups. Finally, the ΔΔCT values were converted to fold changes using the equation 2^−(ΔΔCT). Graphs display converted mean ΔΔCT values and standard deviation error bars calculated from each individually converted repeat. TaqMan qPCR does not require melt-curve type validation as results are generated by the amplification of the target sequence, not from non-specific double-stranded DNA binding as used in the SYBR green qPCR assay. (https://www.thermofisher.com/uk/en/home/life-science/pcr/real-time-pcr/real-time-pcr-assays/why-choose-taqman-assays.html.)

Table 3.3. The Gene Targets and Associated TaqMan Gene Expression Assays Used in qPCR.

Gene Symbol (Aliases)	TaqMan Assay
ACTA2 (α-SMA)	Hs00426835_g1
CDKN1A (P21)	Hs00355782_m1
CDKN2A (P16)	Hs00923894_m1
COL1A1 (collagen type I alpha 1 chain)	Hs00164004_m1
COL3A1 (collagen type III alpha 1 chain)	Hs00943809_m1
FAP (Fibroblast Activation Protein Alpha)	Hs00990806_m1
FN1 (Fibronectin 1)	Hs01549976_m1
IL6 (interleukin 6)	Hs00985639_m1
PDGFRβ (platelet derived growth factor receptor beta)	Hs01019589_m1
S100A4 (FSP1)	Hs00243202_m1
TNC (Tenascin C)	Hs01115665_m1
VCAN V1 (Versican V1)	Hs01007937_m1
VIM (Vimentin)	Hs00958111_m1

3.14 Western Blotting

3.14.1. Protein Isolation and Lysis with RIPA Buffer

TCP grown NOF were detached using trypsin EDTA (0.5 g/l porcine trypsin and 0.2 g/l EDTA:4Na in Hanks Balanced Salt Solution with phenol red) (Sigma Aldrich, UK) and cells were resuspended in PBS. After centrifuging the cells at 192 RCF for 4 minutes the supernatant was removed and 100 µl of radioimmunoprecipitation assay (RIPA) buffer (Merck KGaA, DE) (0.5M Tris-HCl, pH 7.4, 1.5M NaCl, 2.5% deoxycholic acid, 10% NP-40, 10mM EDTA) with phosphatase inhibitor (PI) (Sodium Fluoride, Sodium Orthovanadate, Sodium Pyrophosphate, Beta-Glycerophosphate) was added to the pellet. One Pierce™ Phosphatase Inhibitor Mini Tablet (Thermo Fisher Scientific, US) was dissolved in 10 ml of RIPA buffer. The pellet was resuspended and incubated on ice for 30 minutes. Scaffolds containing NOF were washed in PBS and then placed in a 1.5 ml eppendorf tube and covered with 100 ml of RIPA Buffer and the tube was vortexed and then incubated on ice for 30 minutes. After incubation the tubes were centrifuged for 10 minutes at 16.3 x gravity and the supernatant was transferred to a 0.5 ml eppendorf tube and stored at −20 °C.

3.14.2. Protein Isolation with TRI Reagent®

Protein was isolated from samples lysed in TRI Reagent® (Zymo Research, US). After complete lysis of scaffold or TCP NOF in 400 µl of TRI Reagent®, 400 µl of EtOH was added. After mixing the solution it was added to a Zymo-Spin IICR Column (Zymo Research, US) with an attached collection tube and centrifuged in an GenFuge 24D microcentrifuge for 30 seconds at 16.3 x gravity. The flow-through was transferred to a Corning™ Falcon™ 15 ml conical centrifuge tube (Fisher Scientific, UK) and 3.2 ml of acetone, pre-cooled to −20 °C, was added and mixed. The mix was incubated on ice for 30 minutes after which it was spun at 16.3 x gravity in a refrigerated (4 °C) Heraeus Fresco 17 centrifuge (Thermo Fisher Scientific, US) for 10 minutes. The supernatant was discarded and the pellet was washed with 400 µl of 100% EtOH and centrifuged for 1 minute. After removing the EtOH the pellet was dried for 10 minutes at room temperature. Hereafter, the pellet was resuspended in 100 µl of

RIPA buffer and vortexed then incubated on ice for 30 minutes. After incubation the samples were centrifuged for 10 minutes at 16.3 x gravity and the supernatant was transferred to a 0.5 ml eppendorf tube and stored at −20 °C.

3.14.3. BCA Protein Assay

A bicinchoninic acid (BCA) assay was used to estimate protein concentrations in lysed NOF samples. A bovine serum albumin standard (Pierce™ Bovine Serum Albumin Standard Ampules, 2 mg/ml) was used to generate a standard curve with concentrations of 2, 1.5, 1, 0.75, 0.5, 0.25 and 0.125 (µg/µl) in RIPA buffer. The working reagent was prepared at a ratio of 50:1 BCA reagent A: BCA reagent B (Thermo Fisher Scientific, US). 200 µl of working reagent was pipetted into the wells of a 96 well plate. 10 µl of each albumin standard and each sample lysate was added in triplicate to the wells filled with working reagent and mixed by pipette aspiration. The plates were kept dark and incubated at 37 °C on a rocker plate for 30 minutes. The plate was cooled for 15 minutes at room temperature before it was read on Tecan M200 plate reader using Magellan software (Version V7.2) with an excitation wavelength of 480 nm and an emission wavelength of 520 nm.

3.14.4. Gel Electrophoresis and Electroblotting

Any kD™ Mini-PROTEAN® TGX Stain-Free™ Protein Gels, 10 well, 50 µl (Bio-Rad, UK) were used for gel electrophoresis. Gels were loaded into a Mini-PROTEAN Tetra Vertical Electrophoresis Cell (Bio-Rad, UK) attached to a PowerPac™ Basic Power Supply (Bio-Rad, UK). The electrophoresis cell was filled with sodium dodecyl sulphate (SDS) buffer (distilled water, Tris base (Merck KGaA, DE), Glycine (Thermo Fisher Scientific, US), NuPAGE™ 3-(N-morpholino)propane sulfonic acid (MOPS) SDS Running Buffer (Thermo Fisher Scientific, US)) inside and outside of the gel loading cassette. Up to 40 µl of protein from each NOF sample was added to Western-Ready™ Protein Sample Loading Buffer (5x) (Biolegend, UK) and heated to 95 °C for 5 minutes. Up to 50 µl of sample and SDS was added to the wells alongside control wells containing 50 µl of SDS buffer diluted in RIPA buffer and wells containing 5 µl of Prime-Step™ prestained broad range protein ladder (Thermo Fisher

Scientific, US). Samples were run on the gel at a voltage of 70 v for 20 minutes before the voltage was increased to 100 v for 1 hour.

After the gel was removed from the electrophoresis cell the comb was separated and the gel was placed on top of the bottom ion reservoir stack from a Trans-Blot Turbo Mini Nitrocellulose Transfer Pack (Bio-Rad, UK) and the top ion stack was placed on top of the gel. The gel stack was loaded into the Trans-Blot Turbo Blotting Instrument (Bio-Rad, UK) cassette and any bubbles were rolled out of the top ion reservoir stack. The cassette was sealed and placed into the blotting instrument and the 'Mixed MW' protocol was selected (1.3 A, 25 V for 7 minutes). The cassette was disassembled and protein transfer was confirmed with Ponceau S staining Solution (Thermo Fisher Scientific, US). Membranes were covered with ponceau solution for 5 minutes and then rinsed 3 times for 2 minutes.

3.14.5 Immunodetection and Development

Membranes were blocked in a blocking buffer (5% BSA in Tris-Buffered Saline with Tween) (TBST) - (20 mM Tris (Thermo Fisher Scientific, US), 150 mM Sodium Chloride (Thermo Fisher Scientific, US), 0.1% w/v Tween-20 (Sigma Aldrich, UK)) for 1 hour at room temperature. All western blot membrane incubations detailed below were carried out on a rocker plate. Membranes were rinsed with TBST for 5 minutes. Next, rabbit monoclonal antibodies raised to phosphorylated-p44/42 (P-p44/42) mitogen-activated protein kinase (MAPK) or p44/42 MAPK (Cell Signalling Technology, US) were diluted in blocking buffer and incubated overnight at 4 °C. Primary antibody was then removed and membranes were washed 3 times for 5 minutes in TBST. The secondary antibody, anti-rabbit HRP-linked antibody (Cell Signalling Technology, US) was diluted 1:3000 in blocking buffer and added to the membrane for 30 minutes at room temperature. The secondary antibody was removed and the membrane was washed 3 times for 5 minutes in TBST.

Excess TBS was removed from the membrane and the protein ladder was marked with an Azure ChemiWriter Enhanced Chemiluminescence (ECL) pen (Azure Biosystems, US). It was

then covered with 1 ml of ECL reagent containing 0.5 ml of SuperSignal™ West Pico PLUS Luminol/Enhancer (Thermo Fisher Scientific, US) and 0.5 ml of SuperSignal™ West Pico PLUS stable peroxide (Thermo Fisher Scientific, US). After 5 minutes the ECL reagent was removed and the membrane was read using a C-Digit Blot Scanner connected to Image Studio software (Version 5.2, LI-COR, Inc, US).

3.14.6 Blot Strip and Reprobe with GAPDH

Membranes were washed with TBST to remove the chemiluminescent substrate before being covered in western blot stripping buffer (Thermo Fisher Scientific, US) for 30 minutes at room temperature. Afterwards the membrane was rinsed in TBST for 5 minutes. The membrane was then re-blocked in a blocking buffer (5% BSA in TBST) for 30 minutes at room temperature. The membrane was then re-probed with glyceraldehyde 3-phosphate dehydrogenase (GAPDH) mouse monoclonal antibody (Proteintech Group, US) diluted 1:5000 in blocking buffer. After overnight incubation at 4 °C the membrane was rinsed 3 times for 5 minutes in TBST. Afterwards the membrane was incubated with Anti-mouse HRP (Cell Signalling Technology, US) diluted 1:3000 in blocking buffer for 30 minutes at room temperature. After 3 final washes in TBST for 5 minutes, each membrane was stained using ECL reagent (as described in 3.14.5) and imaged using a C-Digit Blot Scanner connected to Image Studio software (Version 5.2, LI-COR, Inc, US).

3.15 RNA sequencing

3.15.1 RNA Extraction and Quality Control

RNA was isolated from NOF using Tri-reagent as described in section 3.13.2 where RNA was isolated for qPCR. RNA was extracted from ES scaffold and TCP cultured NOF after 4 days. This time point was selected as contact inhibition thereafter would alter gene expression, influencing the RNA sequencing data. RNA quality control was conducted by Genewiz, an Azenta Life Sciences Company.

3.15.2. RNA Sequencing Outputs

After sequencing, sample similarity assessments were performed by Genewiz. This included the generation of a heatmap to show the euclidean distance between RNA samples and principal component analysis (PCA) plotting. These plots were based on the normalised hit counts for genes detected during RNA sequencing.

Using the DEseq2 method (Love, Huber et al. 2014) significantly differentially expressed (DE) genes were extracted from the hit count data by Genewiz to produce a volcano plot visualising global transcriptional changes. Finally using the RNA sequencing data provided by Genewiz, WebGestalt (Wang, Vasaikar et al. 2017) was used to interrogate the list of differentially expressed genes (https://www.webgestalt.org). First the protein analysis through evolutionary relationships (PANTHER) classification system (Mi, Muruganujan et al. 2013) was used in an over representation analysis (ORA) of biological process gene ontology terms that contained DE genes. This data was presented as a volcano plot and table. Next, the Kyoto encyclopaedia of genes and genomes (KEGG) (Kanehisa and Goto 2000) was used in a gene set enrichment analysis (GSEA) of pathways that contained DE genes. This data was presented as a bar chart with the top 20 most enriched pathways containing upregulated genes and the top 20 most enriched pathways containing downregulated genes.

3.16 Statistics

GraphPad Prism version 9.1.1 (GraphPad Software LLC, US) was used for all statistical analysis unless otherwise stated. *P*-value ranges and the number of biological and technical replicates are included in figure legends where relevant. A Gaussian non-linear regression was used alongside the D'Agostino and Pearson normality test when quantifying fibre diameter distribution data. The Games-Howell's multiple comparisons test was used to test for inter-batch consistency in fibre diameter, angle and surface porosity between scaffolds. The *P*-values provided for this data are adjusted to allow for multiple comparisons (*P*-adjusted). Multiple unpaired t-tests with Welch's correction were used to compare results between culture conditions unless otherwise stated. For Ki67 data pie charts were used to represent the

proportion of cells that were proliferative, with actual values provided in the text. The 2^−(ΔΔCT) method (Livak and Schmittgen 2001) was used for qPCR results, with values converted to fold change and control conditions provided with each graph. qPCR graphs show converted mean ΔΔCT values and standard deviation error bars. Dunnett's T3 multiple comparisons test was used to compare qPCR results between culture conditions with adjusted *P*-value ranges displayed on graphs and in the text.

Chapter 4: Fabrication and Characterisation of ES Scaffolds for Cell Viability Assessments

4.1. Introduction

Previous observations in Dr. Ortega's group indicated limited proliferation in live and metabolically active 3T3 fibroblasts grown on ES PCL scaffolds. This research project began with attempts to validate and quantify this observation. To achieve this, equivalent scaffolds were fabricated using a new medical grade PCL polymer that bore the advantage of easy clinical translation for potential future work. PCL has been favoured within the Ortega group due to its inert surface, slow rates of degradation and reproducible manufacturing qualities. Whilst the hydrophobic nature of PCL has previously decreased enthusiasm for the polymer, sterilisation with Ethanol and pre-wetting with media increased the surface hydrophilicity. Many of these PCL characteristics were explored within the thesis of Dr Santocildes Romero (Santocildes Romero, 2014). A variety of techniques were used to ensure inter-batch consistency and to characterise scaffold fibre diameter and angle, porosity and mechanical properties, with the aim of generating a 3D scaffold that mimicked collagen fibres of the ECM. Thereafter, cell viability was investigated using PrestoBlue and Live/Dead staining. Picogreen was used to determine the amount of DNA in each sample and therefore track changes in cell number. This data could be used to quantify any changes to the growth rate of cells cultured on the ES scaffold. In addition, they could be used to examine whether cell death contributed to changes in cell number. Furthermore, these assays provided an opportunity to optimise cell seeding methodology before progressing to work with more appropriate human primary NOF. As with the preliminary observations made by the Ortega group, we compared our scaffold culture environment with a TCP control.

4.2. Aims

- To produce ES scaffolds using a polymer and methodology previously optimised within our group and to fabricate a comparable scaffold using medical grade PCL.
- To characterise the physical and mechanical properties of the PCL scaffold and to evaluate inter-batch variability.
- To quantify fibroblast growth rates and viability on the PCL scaffold.

4.3. Specific Experimental Objectives

- To fabricate a 10% (w/v) Sigma PCL scaffold to provide a reference for appearance and handling qualities in culture.
- To fabricate an equivalent scaffold by optimising Purasorb PCL concentration.
- To characterise the selected scaffold using SEM image analysis to measure fibre diameter and angle as well as surface pore sizes.
- To prepare a sample for Mercury Intrusion Porosimetry (MIP) and to analyse the data collected.
- To characterise the macro-mechanical properties of the PCL membranes using the Lloyd LRX universal testing machine.
- To test the wettability of scaffolds using a water contact angle test.
- To complete PrestoBlue and PicoGreen assays for 3T3 fibroblasts grown on ES scaffolds and TCP controls.
- To complete PrestoBlue, PicoGreen and Live/Dead assays for NOF grown on ES scaffolds and TCP controls.

4.4. Results

4.4.1. Scaffold Fabrication Using Sigma PCL

Parameters for the fabrication of microfibrous scaffolds using Sigma Aldrich PCL M_n 80,000 were optimised previously within our group. Replicating those conditions to produce an ES scaffold (Figure 4.1) provided an opportunity to train with the custom rig at the University of Sheffield, School of Clinical Dentistry. Furthermore, it provided a point of reference to produce scaffolds from Purasorb PCL. Sigma PCL scaffolds (10% (w/v)) maintained integrity and were stiff enough to handle with ease once wetted in culture media. SEM imaging revealed that fibres were of similar diameters and were randomly orientated.

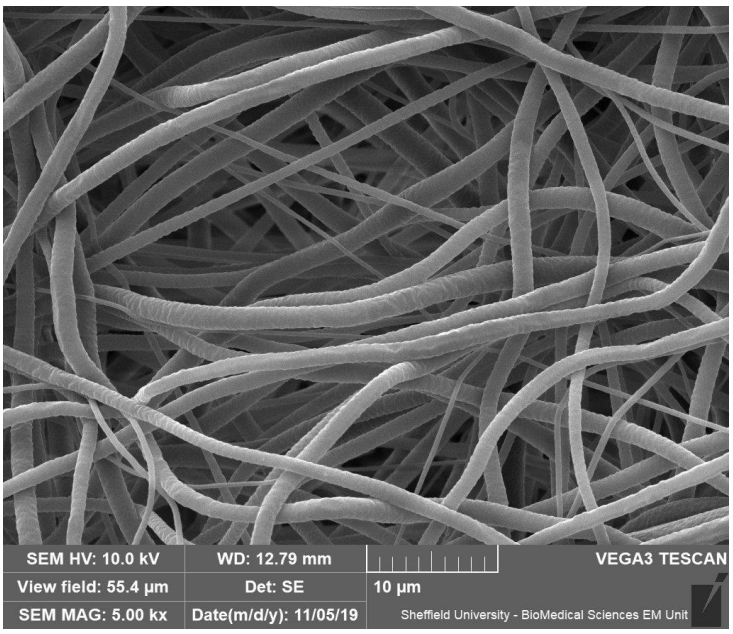

Figure 4.1. *A representative image of a 10% (w/v) Sigma PCL scaffold magnified 5000 times using a Tescan Vega 3 SEM.*

4.4.2. Scaffold Fabrication Using Purasorb PCL 12

To enhance the translatability of the work conducted during this project towards future therapeutic applications we began to use medical-grade Purasorb PCL. Upon initial tests in culture media, it became clear that at 10% PCL (w/v), scaffolds did not handle in the same manner as Sigma PCL scaffolds. Therefore 3 different solutions with weight percentages of 10%, 12% and 15% were produced and the resultant scaffolds imaged (Figure 4.2). At both 10% and 12% beading is visible and in culture media scaffolds would fold once wetted, becoming self-adhesive and difficult to handle. 15% scaffolds displayed randomly oriented fibres which had a high degree of homogeneity in diameter and surface appearance. They also handled in the same manner as Sigma PCL scaffolds, maintaining shape and stiffness in culture media.

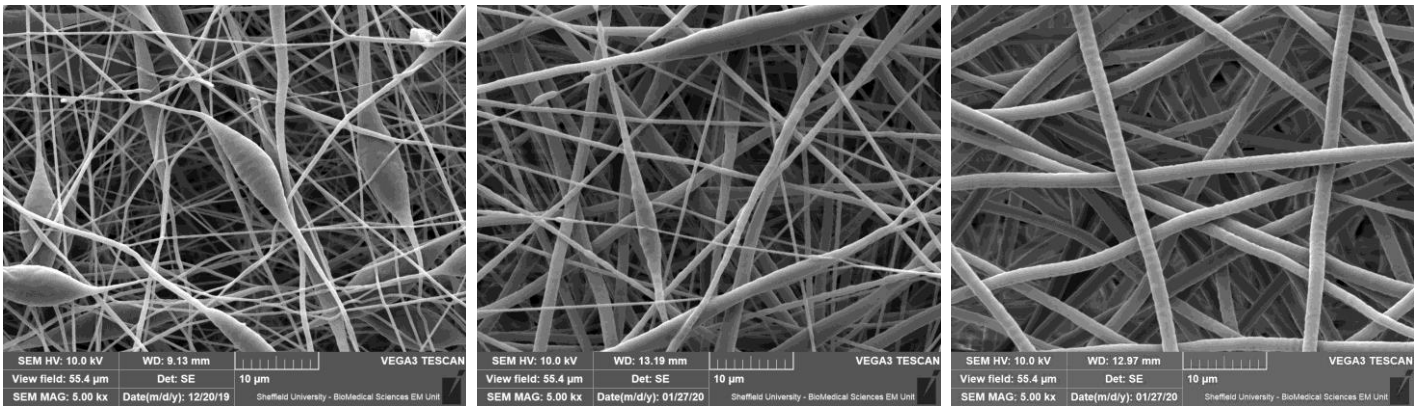

Figure 4.2. *Representative images of 10%, 12% and 15% (w/v) PCL 12 scaffolds. Large diameter beading is present in 10% and 12% but not in 15% (w/v) scaffolds.*

4.4.3. Characterization of 15% PCL Scaffolds

Having identified the optimum polymer concentration, three 15% PCL scaffolds were produced and fully characterised to ensure inter-batch consistency and to record the properties of our scaffold. Parameters that have been previously demonstrated to influence cellular behaviour such as fibre diameter and angle, porosity and mechanical profile were all characterised.

4.4.3.1. Fibre Diameter

ImageJ (v1.52p) was used to measure fibre diameters from SEM images. Average fibre diameter was 1.56 μm and the fibres measured were normally distributed according to the D'Agostino and Pearson test (P=0.065) (Figure 4.3). Fibre widths from each scaffold were not significantly different from each other according to Games-Howell's multiple comparisons test. Scaffold A vs B (P=0.119), A vs C (P=0.772), B vs C (P=0.662).

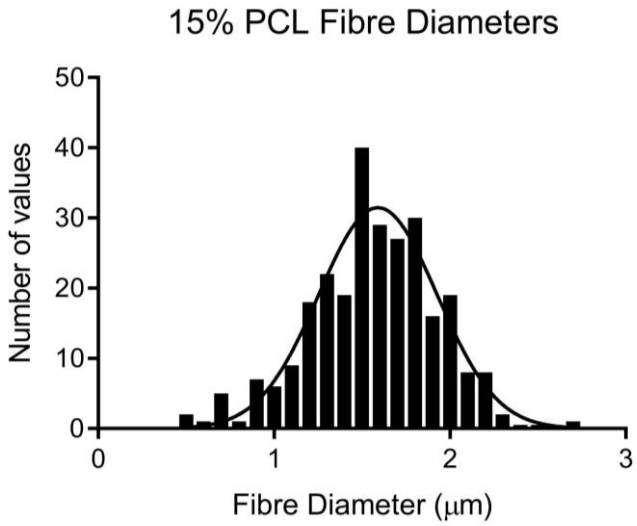

Figure 4.3. *Fibre diameter distribution with a Gaussian non-linear regression plotted. A total of 270 fibre diameters were measured with 10 fibres measured in each of 27 images taken from 9 samples which were cut from 3 scaffolds fabricated on different days.*

4.4.3.2. Fibre Orientation

Fibre orientation was characterised by measuring fibre angle distribution from SEM images using ImageJ. Fibres were spread across the full range of possible angles once normalised. Fibres were not normally distributed according to the D'Agostino and Pearson test ($P < 0.0001$), indicating that they are randomly orientated (Figure 4.4). Fibre angles from each scaffold were not significantly different from each other according to Games-Howell's multiple comparisons test. Scaffold A vs B (P=0.962), A vs C (P=0.710), B vs C (P=0.861).

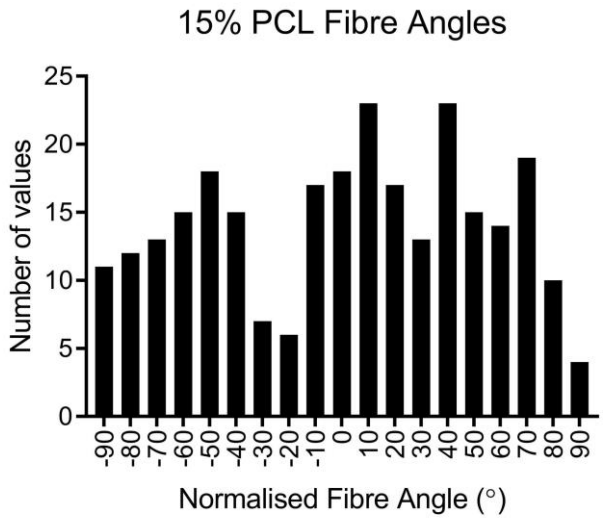

Figure 4.4. *Fibre angle distribution. A total of 270 fibre angles were measured with 10 fibres measured in each of 27 images taken from 9 samples which were cut from 3 scaffolds fabricated on different days.*

4.4.3.3. Scaffold Porosity

Mercury Intrusion Porosimetry (MIP) was used to calculate scaffold porosity. Bulk density was 0.113 g/ml and the apparent (skeletal) density was 0.442 g/ml with total porosity at 74.5%. By plotting dV/dlogD against logD we can visualise the pore size distribution (Figure 4.5). The smallest pores begin in the region of 0.8 μm diameter and most pores fall between 1 μm and 10 μm.

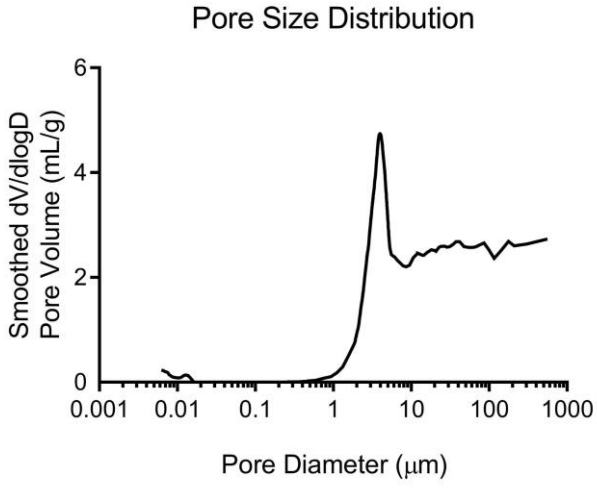

Figure 4.5. *Mercury Intrusion Porosimetry data plotted to show pore diameter distribution for one 15% PCL Scaffold.*

4.4.3.4. Scaffold Surface Porosity

Whilst MIP was able to provide whole scaffold porosity data, it was important to gain a better understanding of the surface topography of the scaffold with which fibroblasts would primarily interact. Using SEM images, average surface porosity was measured at 46%. Pores ranged from 0.1 μm^2 to 150 μm^2 with most pores falling between 1 μm^2 and 25 μm^2 (Figure 4.6). Surface pore sizes from each scaffold were not significantly different from each other according to Games-Howell's multiple comparisons test. Scaffold A vs B (P=0.897), A vs C (P=0.840), B vs C (P=0.993).

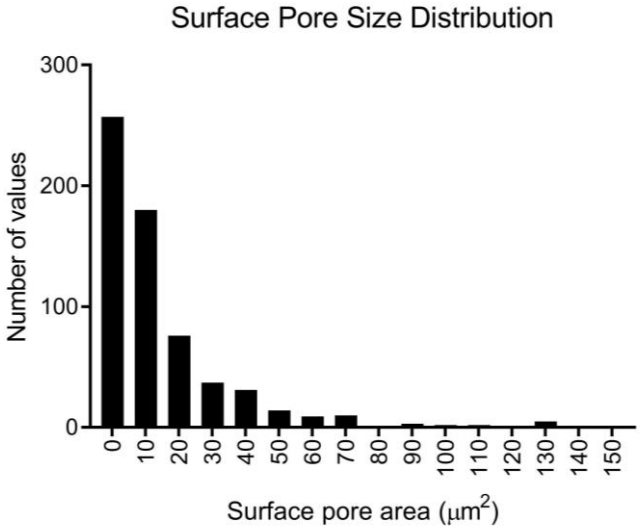

Figure 4.6. *Surface pore size distribution. A total of 628 pores were measured from 9 samples with 3 samples taken from 3 scaffolds.*

4.4.3.5. Mechanical Properties

Mechanical testing revealed that 15% PCL scaffolds have an average elastic modulus (ε) of 4.07 ± 0.71 MPa and an average ultimate tensile strength of 0.82 ± 0.17 MPa. Average elongation at break was 190.9% ± 77.1. Figure 4.7 shows the stress strain curves of each of the 6 samples characterised on the mechanical tester with the elastic region used to calculate the elastic modulus indicated using open circles.

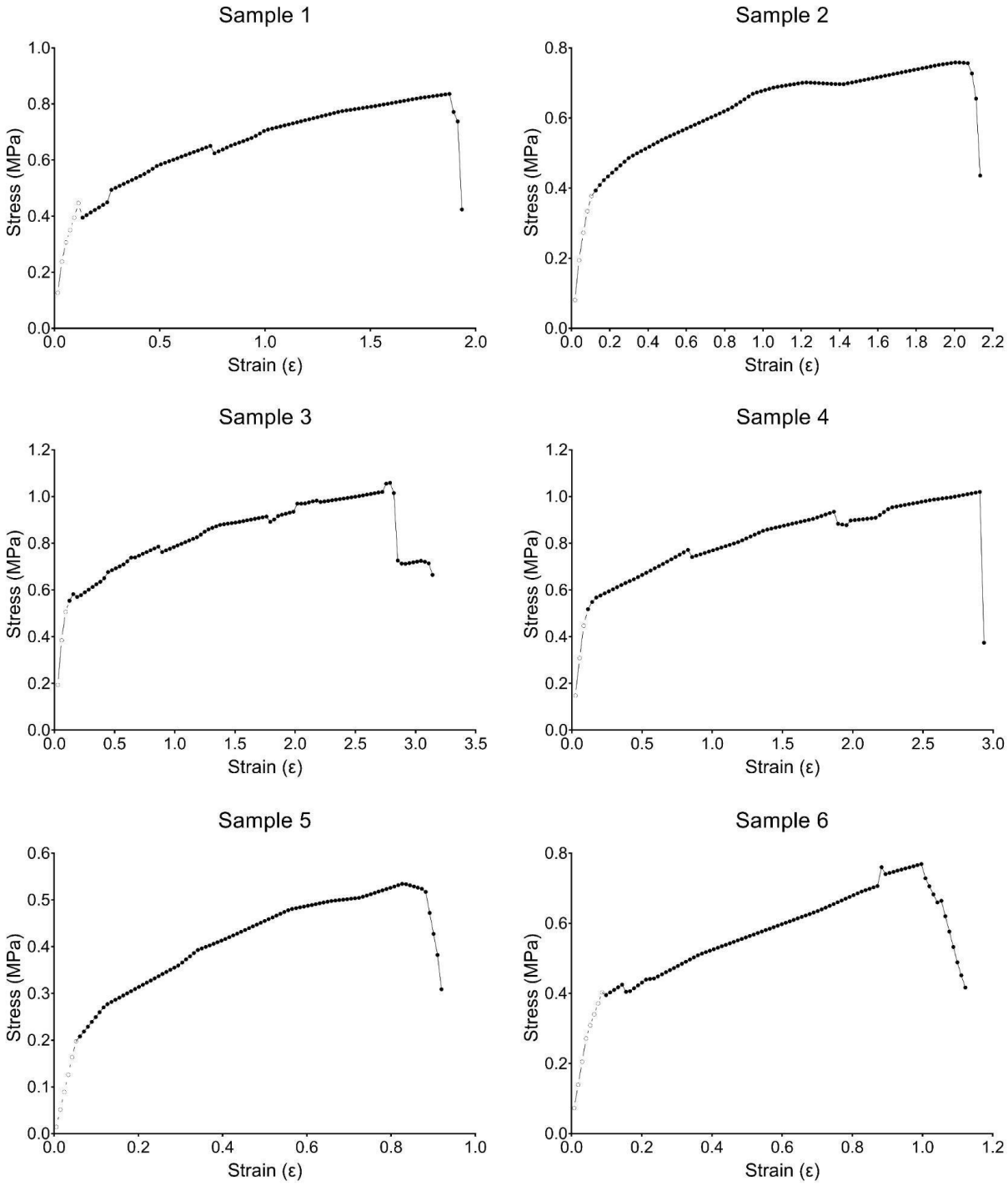

Figure 4.7. *The stress strain curves obtained from 6 samples tested from three 15% PCL scaffolds. Open circles indicate the elastic region that was used to calculate elastic modulus for each sample.*

4.4.4. Water Contact Angle

Another scaffold property measured was the surface wettability. A water contact angle drop test was performed on 15% PCL scaffolds alongside scaffolds treated with EtOH and culture media. Treated scaffolds were soaked in 100% EtOH for 5 minutes before they were rinsed in PBS 3 times. Treated scaffolds were then left in culture media for 5 minutes and finally they were dried before testing. The test was also performed on TCP polystyrene. Average water contact angles for untreated scaffolds and TCP were 148 ° ± 1.7 and 80 ° ± 4.6 respectively. In treated scaffolds water droplets spread within seconds making measurement impossible. Rapid spreading indicates high wettability. Figure 4.8 shows representative images of the water droplets that formed on TCP and scaffold samples.

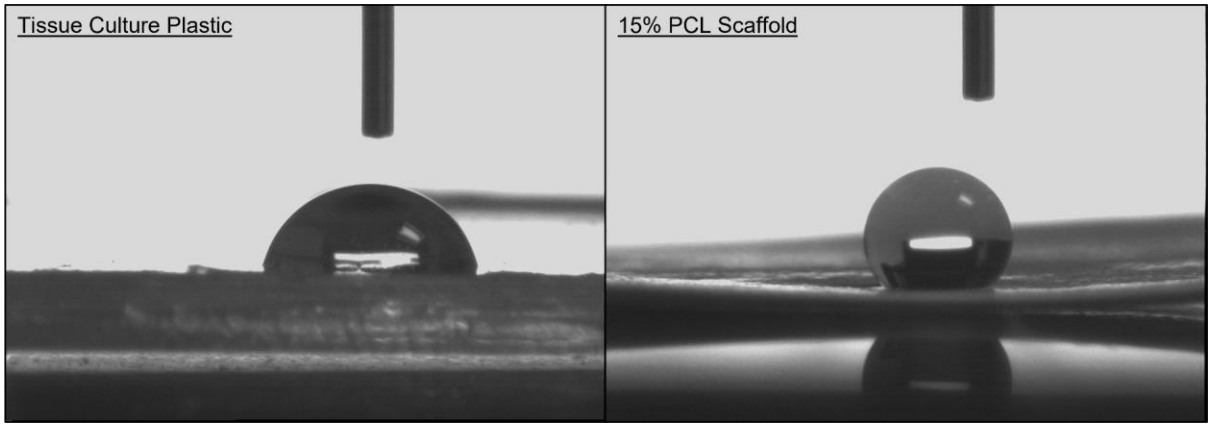

Figure 4.8. *Representative images of water droplets on tissue culture plastic and 15% PCL electrospun scaffolds.*

4.4.5. Assessment of 3T3 Viability on ES Scaffolds

Once the 15% PCL scaffold had been thoroughly characterised it was used to assess the viability of 3T3 cells cultured upon it. The PrestoBlue assay relies on cellular metabolism to determine whether cells are alive and the PicoGreen assay provides a method for quantifying cell numbers by binding to dsDNA. These assays also provide an opportunity to compare scaffold seeding methods.

4.4.5.1. PrestoBlue and PicoGreen Assays

There were significantly more metabolically active 3T3 present on the TCP than the scaffold after 4 and 7 days in culture (Figure 4.9 A). Similarly, there were higher dsDNA concentrations on the TCP control than the scaffold at day 4 and day 7 (Figure 4.9 B). 3T3 grown on the TCP showed a significant increase in viability (P = 0.009) and dsDNA levels (P = 0.004) between day 1 and day 7. The modest increase in viability and dsDNA levels from day 1 to day 7 in scaffold grown and bead seeded 3T3 cells was not significant. However, the increase in viability for diffusion seeded scaffolds was significant (P = 0.025), indicating that population growth was occurring, albeit at a reduced rate.

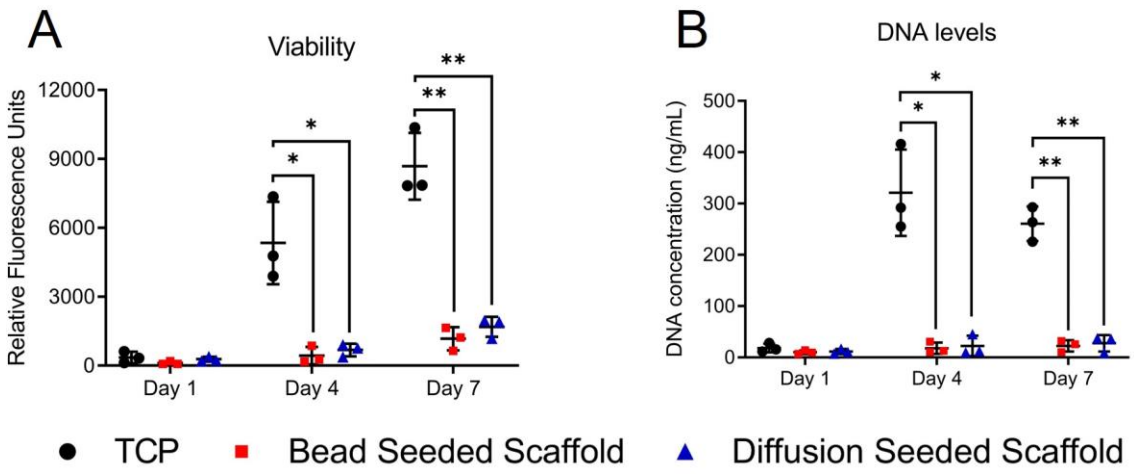

Figure 4.9. *(A) PrestoBlue and (B) PicoGreen assay data for 3T3 fibroblasts cultured on TCP and ES PCL scaffolds. GraphPad Prism software was used to generate graphs. *** p < 0.001, ** p < 0.01, * p < 0.05. Error bars represent standard deviation, n=3.*

4.4.6. Assessment of NOF Viability on ES Scaffolds

Our preliminary results using 3T3 fibroblasts supported observations previously made within the group that fibroblast populations were expanding at a reduced rate on the microfibrous ES scaffold. PrestoBlue and PicoGreen assays showed no significant difference in growth rates between the seeding methods. For our next phase of experiments, we aimed to confirm if the reduction in viability and cell number would also occur in another fibroblast population.

Transitioning to human primary NOF, Live/Dead staining would be used to understand whether the reduction in cell numbers was the result of excess cell death on the ES scaffold.

4.4.6.1. PrestoBlue and PicoGreen Assays

As with 3T3 cells greatly reduced NOF viability and dsDNA levels after 4 and 7 days in culture were observed (Figure 4.10). Viability was also significantly reduced after 1 day in culture. NOF grown on TCP showed significant increases in viability (P = 0.038) and dsDNA levels (P = 0.014) between day 1 and day 7. The increases seen in scaffold cultured NOF were not significant.

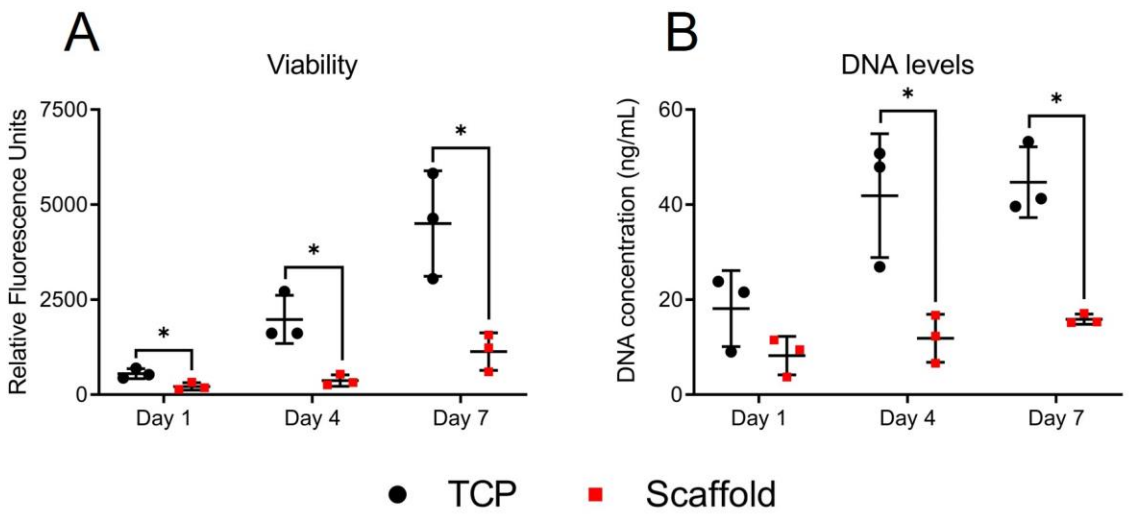

Figure 4.10. *(A) PrestoBlue and (B) PicoGreen assay data for NOF cultured on TCP and ES PCL scaffolds. GraphPad Prism software was used to generate graphs. ** p < 0.01, * p < 0.05. Error bars represent standard deviation, n=3.*

4.4.6.2. Live/Dead Assay

To assess whether the reduction in viability and cell number (dsDNA) was due to cell death, a Live/Dead assay was employed. Calcein AM stains live NOF green whilst ethidium homodimer 1 stains dead cells red. There was no observable change in the number of dead cells present on the ES scaffold compared to those on the glass coverslip control (Figure 4.11). This suggested that a fall in proliferation rate is responsible for the reduced cell number rather than excess cell death on the ES scaffold.

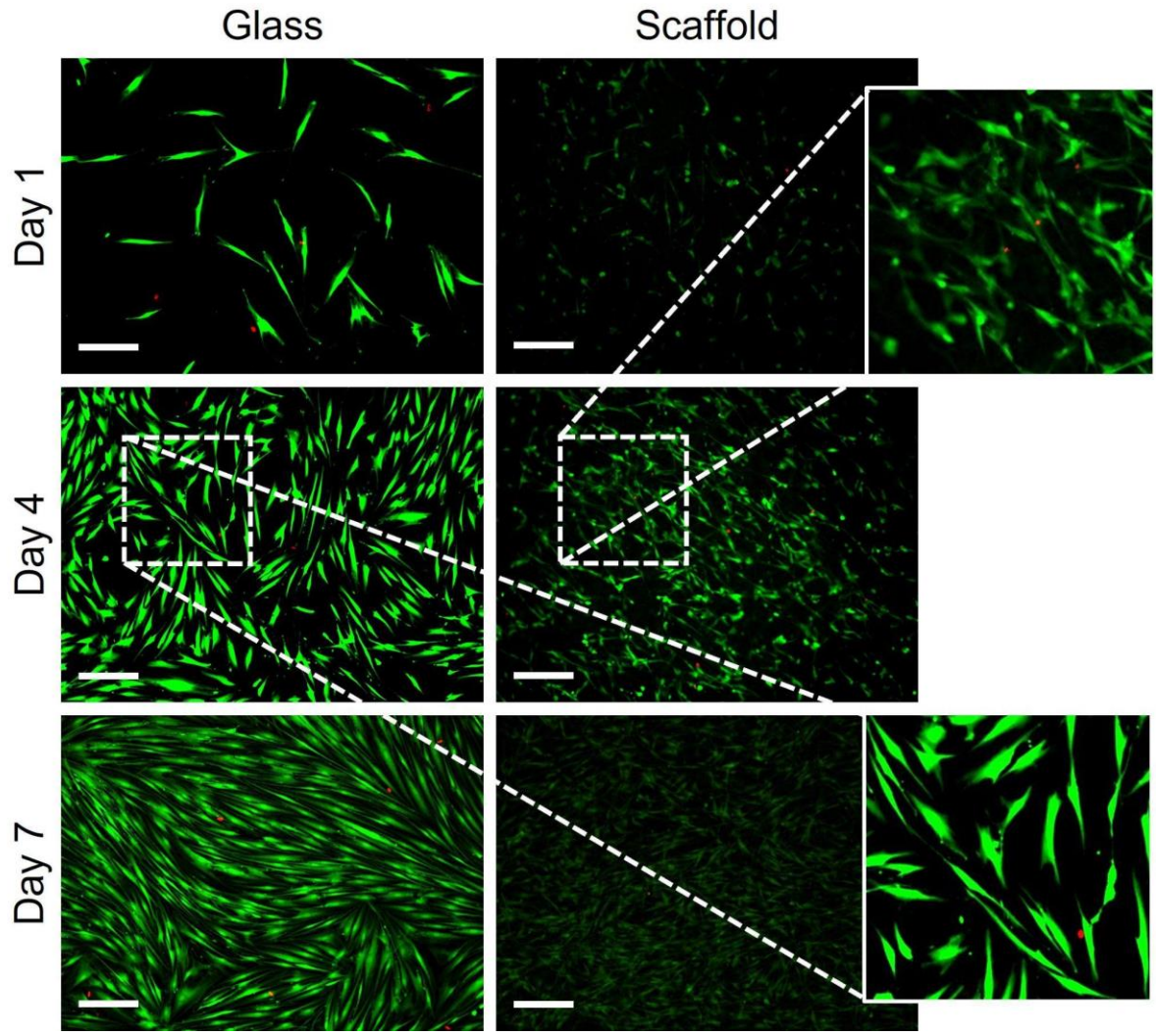

Figure 4.11. *Representative Live/Dead staining of NOF grown on TCP and scaffolds. Images were taken 1, 4 and 7 days post seeding. ImageJ was used to enhance all images equally using the 'subtract background' function and brightness increase tool. Live cells are stained green (cytoplasm) and dead cells are stained red (nucleus). The white scale bar is equal to 200 µm.*

The Live/Dead imaging also provided an opportunity to capture fibroblast morphology (Figure 4.10 - cutouts). On the ES scaffolds fibroblasts appear smaller and are either rounded or have elongated spindle-like projections. Fewer rounded cells can be seen on day 7. NOF grown on the glass coverslip display classic fibroblast morphology with a broader and more spread cytoplasm.

4.5. Discussion

Having fabricated an ES scaffold using 10% Sigma PCL (w/v) in a dichloromethane dimethylformamide solvent solution, Purasorb PCL (Corbion) scaffolds were produced using the same 10% (w/v) dilution. Use of the medical grade polymer from the outset of the project could enhance the relevance of the results in the case of clinical translation. However, it soon became apparent that the Purasorb PCL scaffold did not handle in the same manner and upon SEM imaging the fibre beading phenomenon was observed (Fong, Chun et al. 1999). In response, purasorb PCL scaffolds were fabricated with higher polymer concentrations of 12% and 15% PCL (w/v). The 15% PCL scaffold was selected due to its ease of handling once wetted and high degree of fibre homogeneity. This change in our polymer supplier highlighted how sensitive the electrospinning process is. The Sigma Aldrich PCL has an average M_n of 80,000. Corbion does not provide an average molecular weight for its PCL, only giving the polymers inherent viscosity of 1.2 dL/g. Polymer M_n, amongst other factors, influences viscosity (Balani, Verma et al. 2015). It is likely that the Purasorb PCL has a lower M_n and therefore forms a less viscous solution than solutions with the same concentration of Sigma PCL, increasing the probability of beading (Fong, Chun et al. 1999). Solution viscosity, surface tension and net charge density are all factors that influence beading characteristics (Fong, Chun et al. 1999). Recognising the importance of polymer molecular weight and its significance in the electrospinning process, our group has previously used gel permeation chromatography to measure Purasorb PC 12 M_n, returning a value of just over 61,000. This data, which supports our hypothesis that Purasorb PCL has a lower M_n, is due to be published in the coming months.

Aside from improving handling qualities, it was important to reduce the presence of beading in our scaffolds. When Chen et al. tried to produce a PCL scaffold with ultra small 117 nm fibres, beading occurred and the attachment and proliferation of 3T3 fibroblasts was greatly reduced (Chen, Patra et al. 2007). Beading reduces the surface area for cellular attachment compared to pure fibres and may lead to non-uniform growth and reduced global proliferation

(Chen, Patra et al. 2007). Furthermore, fibre diameter was shown to influence fibroblast behaviour, with fibroblasts attaching and proliferating best on fibres with an average diameter of 428 nm. As fibre widths were increased to 1051 nm proliferation and attachment fell. However, once fibres were generated with an average diameter of 1.647 μm adhesion and proliferation increased (Chen, Patra et al. 2007). For this reason, we sought to generate a scaffold with highly homogenous fibres with normally distributed diameters. Identifying which fibres were responsible for fibroblast behaviour on a scaffold with bimodal fibre populations would be challenging. The impact of altering spinning parameters on scaffold fibre diameter was explored in the thesis of Dr Martin-Eduardo Santocildes Romero (Santocildes Romero, 2014). This work demonstrated how altering fibre size reduced homogeneity, a feature that we aimed to maintain. It was interesting that, at an average diameter of 1.647 μm Chen et al. observed bimodal fibre distribution. This may provide an explanation for the increased attachment and proliferation rates compared to fibres of 1051 nm average. At a similar average diameter of 1.56 μm our fibres were of a single mode. This could be due to the use of a different polymer manufacturer, different M_n or different solvent system. The average fibre diameter of 1.56 μm falls within the range of observed collagen fibre diameters in the extracellular matrix (Ushiki 2002).

We chose to work with randomly aligned fibres to mimic the random orientation of collagen in the buccal tissue from which our primary cell line (NOF) were derived (Smitha and Donoghue 2011). Fibre alignment has been shown to influence cellular alignment and gene expression (Hughes, Gaston et al. 2015). Aligned fibres may lead to the deposition of aligned ECM proteins and could have clinical applications in tissue engineering and wound healing (Chen, Lui et al. 2019). It is possible that by mimicking certain aspects of the native buccal tissue like collagen arrangement, NOF will be encouraged to retain their in vivo quiescent phenotype (Plikus, Wang et al. 2021). This would include reduced growth rates.

Another important feature of a 3D culture platform is porosity. Many techniques including SEM image analysis, capillary flow porometry, liquid extrusion and MIP have been used to assess

ES scaffold porosity (Rutledge, Lowery et al. 2009). Capillary flow porometry can gives values for mean flow pore diameter whilst liquid extrusion and MIP are able to provide more data including total porosity and pore size distribution. MIP is the more accurate technique and is therefore favoured (Rutledge, Lowery et al. 2009). ES fibres are pliant however and the high pressures used during MIP can lead to scaffold deformation (Rutledge, Lowery et al. 2009). Rutledge et al. suggested that without correction when plotting pore size distribution, graphs will feature a tail which corresponds to large pores of between 100 and 300 μm diameter, caused by fibre deformation. This tail is present in our MIP data and consistent with the observations of Rutledge et al., our SEM images do not show any such large pores. Lowery et al. corrected MIP porosity values of three PCL scaffolds using different solvent systems and weight percentages of polymer, the pores sizes fell between 76% and 87% (Lowery, Datta et al. 2010). Without using identical spinning parameters and polymer concentrations it is impossible to tell how accurate our MIP porosity value is or how accurate the proposed correction methodology may be. Although at 75% our porosity value falls close to the corrected values proposed by Lowery et al. We also measured surface pore areas to provide an insight into the surface onto which NOF are seeded and interact. The pore areas of between 0 and 130 μm^2 indicate that fibroblasts should be able to attach to multiple fibrous struts. In this way NOF will form attachments to fibres in multiple planes as well as being forced to bridge certain pore areas or send projections to deeper fibre layers. Significantly larger pores would force NOF to align along single fibres. In this case fibroblasts would be growing with similar apical basolateral polarity and attachments to those which form in 2D culture. Porosity also controls the ability of fibroblast cells to penetrate the scaffold. Increasing pore size significantly would have resulted in cells passing through the scaffold and adhering to the TCP well beneath whilst reducing pore size would have blocked cells from spreading between struts and penetrating the scaffold in a 3D manner.

Finally, we have reported on whole-scaffold macro-mechanical properties. Whilst this data is useful for comparison between scaffolds, especially in terms of handling properties, it would

be inappropriate to evaluate the impact of scaffold stiffness on fibroblast behaviour. This is because fibroblasts interact with a relatively small area of the scaffold and the stiffness of individual fibres would provide a more appropriate measure. Atomic force microscopy (AFM) is a technique that has been used to measure the properties of fibres approaching the nanometer scale (Stachewicz, Bailey et al. 2012). Upon consultation with AFM experts based at the University of Sheffield it was decided that attempting to measure individual fibres represented a significant challenge. Not only is it difficult to probe individual fibres, but one must also consider the fibre length and the proximity of any adjacent or underlying fibres. Given the scope and timeline of this project it was decided that pursuing AFM microfibre characterisation would not be possible.

Water contact angle was used as a method to quantify scaffold and plastic surface wettability. The slightly uneven nature or the scaffold surface made recording contact angle more challenging. However, as a general measure to determine between hydrophilic surfaces with contact angles of less than 90° and hydrophobic surfaces with contact angles greater than 90° and given the large difference between scaffolds and TCP the method was appropriate. Prior to treatment with EtOH and the application of culture media the scaffold was found to be a hydrophobic, non-wetting material due to its contact angle of greater than 90° (Law 2014). This data highlights that the important step of scaffold sterilisation and pre-wetting with media increased the scaffold's surface hydrophilicity. Ultimately this will encourage cellular attachment during seeding (Ferrari, Cirisano et al. 2019).

Having thoroughly characterised the 15% PCL ES scaffold, fibroblast viability and growth rates were investigated. Preliminary studies used the bead technique to seed scaffolds causing concern that this technique could lead to contact inhibition, especially if cell spreading was limited by the scaffold. This could have explained the observed reduction in growth rates on the ES scaffold. For this reason, the diffusion seeding technique was introduced to test this hypothesis. To facilitate comparison between the preliminary data and our own, the same number of cells (10,000) were applied to the scaffold as were used in both studies. The

diffusion seeding technique did not outperform the bead seeding technique to a statistically significant level, and there was still a significant reduction in viability and dsDNA levels in the ES scaffold grown fibroblasts. The trend was the same for both 3T3 fibroblasts and NOF. As contact inhibition was not responsible for the reduction in fibroblast growth rates and 10,000 cells proved an adequate number to maintain proliferation in plastic cultures for up to 7 days the same number of cells were seeded for subsequent experimentation. Despite the similarities in performance between 3T3 and NOF, NOF were selected for future work as they represent a more relevant cell when considering activation behaviour and its role in human disease, especially when compared with immortalised non-human cell lines such as 3T3 or L929 mouse fibroblasts (Thonemann, Schmalz et al. 2002). Whilst working with primary human cells increases the relevance of our model, it is important when working with fibroblasts to acknowledge the high degree of heterogeneity present in populations throughout the body. Fibroblasts derive from unique embryonic tissues and serve a variety of tissue specific functions (Driskell and Watt 2015, Sriram, Bigliardi et al. 2015). Even within different regions of the same tissue, dermal fibroblasts have displayed different morphology, physiology and function (Tracy, Minasian et al. 2016). Explanted papillary fibroblasts had greater proliferation rates (Harper and Grove 1979), were subject to less contact inhibition at confluence (Schafer, Pandy et al. 1985) and contracted collagen gels quicker than reticular fibroblasts (Sorrell, Baber et al. 1996). The two populations of dermal fibroblasts even had different impacts on co-cultured keratinocytes (Sorrell, Baber et al. 2004). Interestingly far less is known about heterogeneity within buccal fibroblast populations.

Having established a reduction in the number of cells present on the ES scaffold through viability and dsDNA content assays, we used live dead staining to evaluate whether this was the result of cell death on the scaffold. There was no evidence of an increase in the number of dead cells on the scaffold compared to the TCP control. This indicated that a reduction in the proliferative capacity of NOF may be responsible for the fall in cell numbers.

4.6. Conclusion

This chapter began by introducing the background to the study, referring to observations made by the Ortega group of reduced fibroblast proliferation on an ES PCL scaffold. To begin investigating this observation scaffolds were produced and characterised using several methods. Characterisation not only allowed for comparisons to other ES scaffolds in the literature but confirmed inter-batch consistency between scaffolds produced on different days. This data and the supporting literature highlighted the broad range of scaffold characteristics that can be modified through subtle changes to the electrospinning parameters and materials. Furthermore, the diameter and alignment of electrospun fibres mimic collagen fibres in the ECM. PrestoBlue and PicoGreen assays with both 3T3 fibroblasts and human NOF were used to validate the previously observed reduced growth rates on ES scaffolds. Scaffold seeding methodology was optimised and contact inhibition after bead seeding was ruled out as the reason for reduced growth rates. Finally, using Live/Dead staining excessive cell death on the scaffold was ruled out as the cause of reduced growth. These results have led to the hypothesis that proliferation rates have fallen in NOF grown on the ES scaffold. In the next chapter to investigate this hypothesis, Ki67 immunolabeling will be used to determine the proportion of proliferative cells on the ES scaffolds.

Chapter 5: Fibroblast Activation Traits

5.1. Introduction

In chapter 4, ES scaffolds produced from 15% Purasorb PCL were characterised and used to grow 3T3 fibroblasts and NOF. When compared with TCP, PrestoBlue and PicoGreen assays revealed a fall in the growth rates of both cell types. LiveDead staining was used to rule out cell death as the reason for this fall in growth rate.

In this chapter fluorescent staining of the Ki67 nuclear protein was used as a method to identify if the reduced growth rate was the result of a reduction in proliferation. Ki67 is expressed in all proliferative cells but not by cells in cell cycle phase G0 (Scholzen and Gerdes 2000). To further investigate any changes to Ki67 expression qPCR was selected as a method to distinguish between senescent and quiescent phenotypes. Proliferation is one hallmark of fibroblast activation and so alongside proliferation assays, qPCR was used to quantify the expression of characteristic activation markers and genes coding for ECM proteins deposited by activated fibroblasts.

Cell spreading, cell to cell connections and cell morphology are all features that are regularly reported in studies concerned with fibroblast behaviour in 3D culture environments (Woodley, Lambert et al. 2022). For this reason, SEM imaging was used to gain a better understanding of how normal oral fibroblasts (NOF) interact with the ES scaffold and adjacent cells. SEM images were used in conjunction with immunofluorescence images to better visualise cell margins, attachments and protein expression.

5.2. Aims

- To identify whether changes to growth rates are due to a fall in the number of proliferative cells and if senescence or quiescence is responsible for those changes.
- To quantify the expression of activation associated genes including those encoding both cytoskeletal and extracellular proteins.
- To observe fibroblast morphology and attachments.

5.3. Specific Experimental Objectives

- Use immunohistochemistry to fluorescently label Ki67 positive cells.
- Induce senescence in NOF using hydrogen peroxide.
- Use contact inhibition to model quiescence in NOF.
- Use qPCR to quantify the expression of senescence associated markers.
- Use qPCR to quantify the expression of cytoskeletal activation markers.
- Use qPCR to quantify the expression of genes coding for extracellular proteins.
- Image NOF using a scanning electron microscope (SEM).
- Fluorescently label focal adhesion proteins, filamentous-actin (F-actin) and vinculin.

5.4. Results

5.4.1. Ki67 Expression

Ki67 is expressed in all cells that are proliferating but not in those cells in cell cycle phase G0. Figure 5.1 shows representative fluorescent images of scaffold and glass grown NOF taken after 1, 4 and 7 days of culture. Cell nuclei were counted and the proportion of Ki67 positive nuclei has been indicated in the superimposed pie-charts. At day 1 there were significantly ($p < 0.0001$) fewer proliferative cells on the ES scaffolds (36%) than on the glass control (83%). By day 4 the proportion of proliferative cells had increased on the scaffold to 54% and reduced on the glass to 70% as some areas of the control began to reach confluence. There were still significantly ($p = 0.0002$) fewer proliferative cells on day 4. By day 7 both the glass and scaffold grown NOF had reached confluence and the proportion of proliferating cells was 13% and 17% respectively.

The total number of cell nuclei in each image of 727 x 543 μm were counted and reflected the changes in proliferative population. On glass the average cell number rose from 16 cells on day 1 to 99 on day 4. There was no increase in cell numbers from day 4 to 7 with a day 7 average of 94. On ES scaffolds a higher density of cells was recorded with 45 on day 1 rising to 87 on day 4 and 123 on day 7.

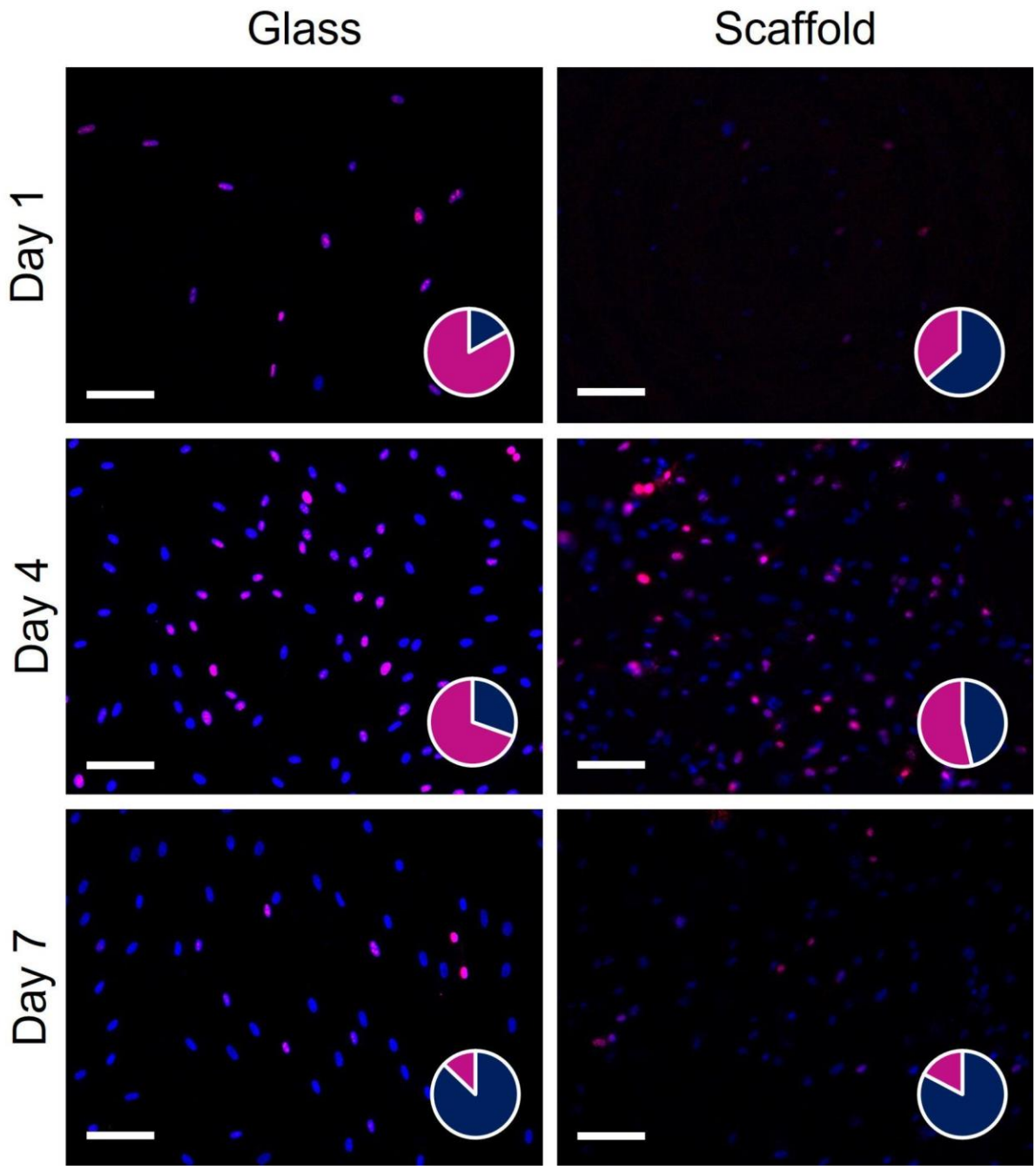

Figure 5.1. *Representative Ki67 immunofluorescence images. Ki67 positive nuclei appear purple whilst Ki67 negative nuclei appear blue due to DAPI counterstaining of all nuclei. All images had the same enhancement using ImageJ software to subtract background fluorescence and increase brightness. Superimposed pie-charts show the proportion of proliferative (Ki67+) cells in purple and non-proliferative (Ki67−) cells in blue. The nuclei in a total of 27 images were counted for each pie-chart with 3 images taken from each of 3 technical replicates cut from 3 biological replicates. The white scale bar is equal to 100 μm.*

5.4.2. Testing NOF for Senescence and Quiescence

Both senescent and quiescent cells exit the cell cycle and do not express Ki67. To test whether ES scaffold grown NOF were senescent or quiescent the expression of several senescence associated genes were compared to TCP grown, induced senescent and quiescent NOF.

5.4.2.1 Senescence and Quiescence Induction

White arrows indicate some of the areas of blue β-gal staining in senescent NOF after H_2O_2 was used to induce DNA damage (Figure 5.2 A). NOF were grown to confluence to be used as a model for quiescence, after cells had been at confluence for 7 days. A representative image of confluent NOF after 1 week in culture shows the entire surface area is covered by cells (Figure 5.2 B).

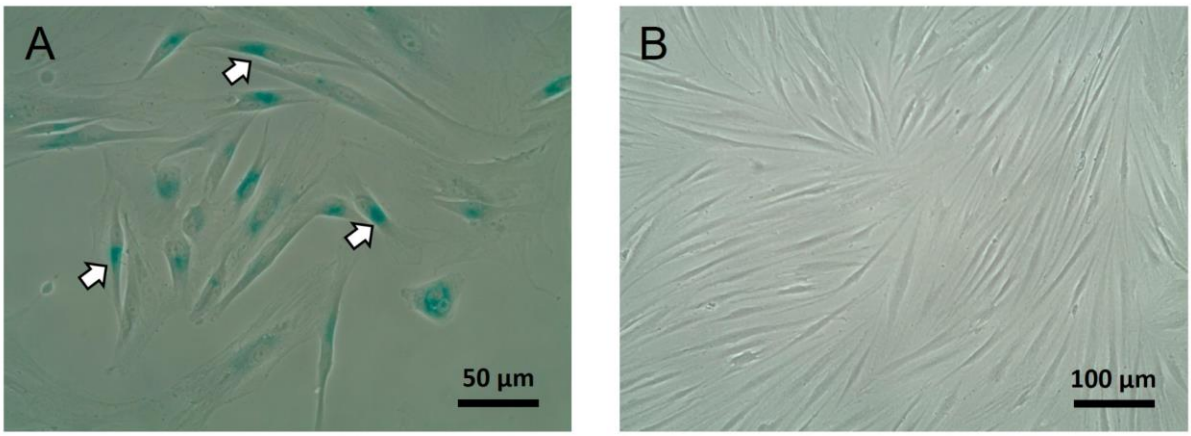

Figure 5.2 *(A). Representative β-gal staining in NOF after senescence induction using 500 µM H_2O_2. White arrows point to some of the areas of blue β-gal staining. (B) Confluent cells used as a model of quiescence.*

5.4.2.2 Senescence-Associated Gene Expression

Having prepared quiescent and senescent NOF populations, qPCR was used to compare the expression levels of P16, P21 and IL6 mRNA. There was no significant difference in the expression levels of any of the senescence associated genes between NOF grown on the TCP control and ES scaffold (Figure 5.3). There were no significant differences in IL6 expression between any of the NOF groups, including the senescent and quiescent populations (Figure 5.3). By contrast, there was a significant increase in P21 expression in the induced senescent NOF (Figure 5.3).

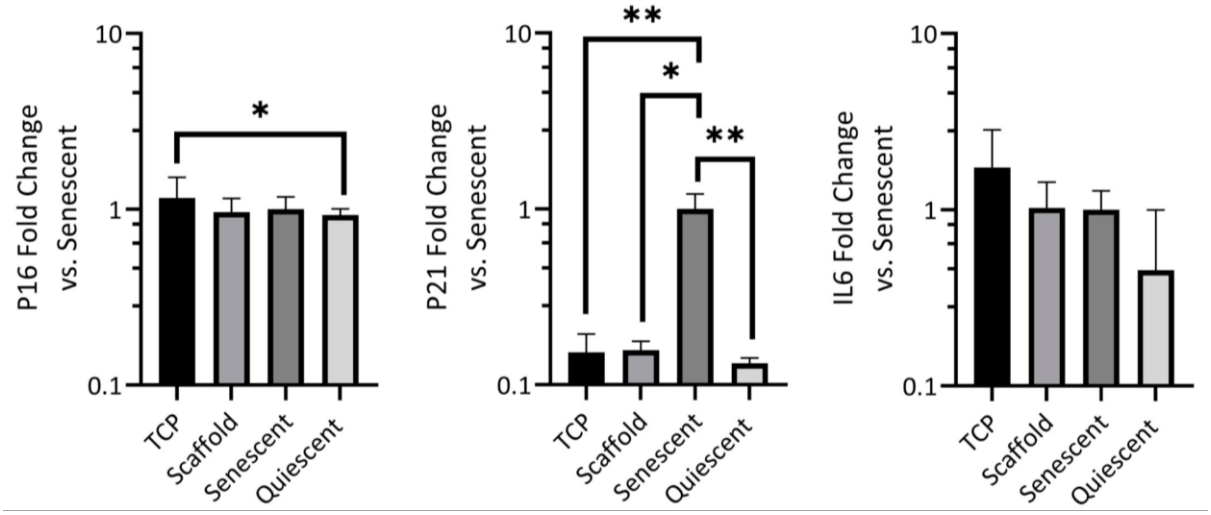

Figure 5.3. *Fold changes in expression of senescence-associated genes versus senescent NOF. Error bars represent standard deviation. * p < 0.05, ** p < 0.01, *** p < 0.001. TCP and scaffold biological replicates = 9, technical replicates = 3. Senescent and quiescent biological replicates = 3, technical replicates = 3.*

5.4.3. Quantifying the Expression of Fibroblast Activation Markers

With NOF exhibiting reduced proliferation rates, other markers of fibroblast activation were investigated. Alongside reduced proliferation, expression of the ACTA2 (α-SMA) gene is a hallmark of fibroblast activation and the transition to the myofibroblast phenotype. Like α-SMA, vimentin is a cytoskeletal protein, however it is expressed in both fibroblasts and myofibroblasts. Aside from cytoskeletal changes, activated fibroblasts are also known to upregulate the production of several extracellular proteins including members of the collagen family, fibronectin and versican.

5.4.3.1. The Expression of Cytoskeletal Genes and Activation Markers

ACTA2 and VIM encode α-SMA and vimentin cytoskeletal proteins, respectively. TGF-β1 was used to stimulate fibroblast activation in NOF grown on TCP and Scaffolds. TGF- β1 is known to trigger fibroblast to myofibroblast differentiation (Wynn and Ramalingam 2012) and was therefore used to create activated fibroblasts as a positive control and also to investigate the impact of TGF-β1 stimulation on fibroblasts grown on the electrospun scaffold. ACTA2 expression was significantly reduced ($p = 0.0046$) in scaffold grown NOF compared with those grown on TCP (Figure 5.4 A). TGF-β1 stimulation led to a significant increase in ACTA2 expression for both scaffold and TCP NOF. TGF-β1 stimulated scaffold NOF had levels of ACTA2 that were not significantly different to unstimulated TCP grown NOF. TGF-β stimulated TCP NOF exhibited ACTA2 levels that were significantly higher than all other culture conditions including TGF-β stimulated scaffold NOF. QPCR results for vimentin gene expression are displayed in Figure 5.4 B. VIM is expressed by both fibroblasts and activated myofibroblasts and there was no significant difference in its expression between TCP and scaffold NOF. TGF-β stimulation led to a modest increase in VIM expression in scaffold grown NOF.

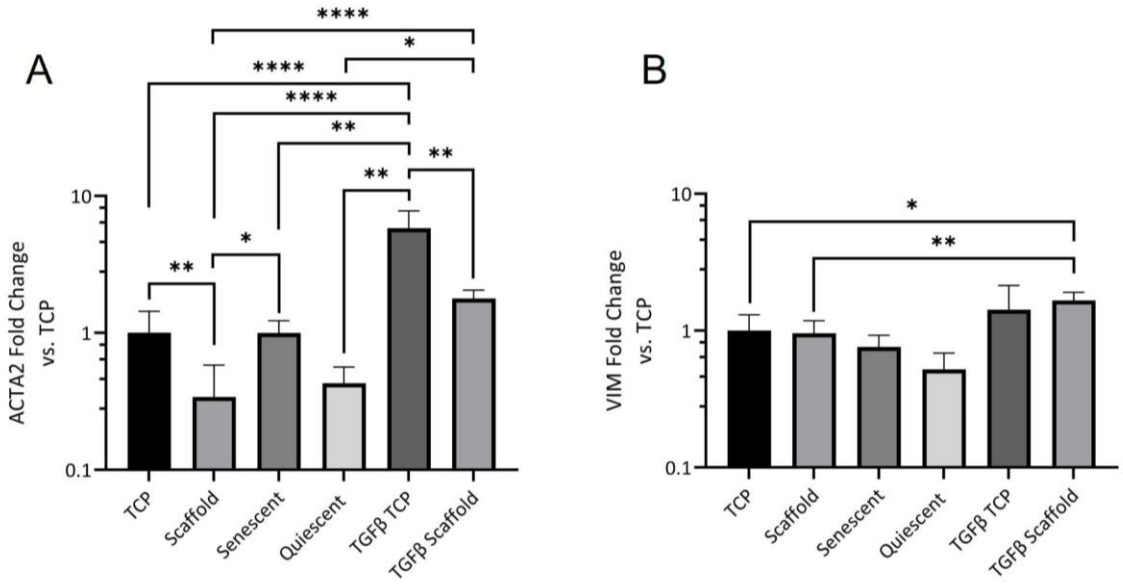

Figure 5.4. *QPCR results for cytoskeletal gene expression of (A) ACTA2 and (B) VIM, versus TCP grown NOF. * p < 0.05, ** p < 0.01, *** p < 0.001, **** p < 0.0001. Error bars show standard deviation. TCP and Scaffold biological replicates = 9, technical replicates = 3. Senescent and Quiescent biological replicates = 3, technical replicates = 3. TGF-β TCP and Scaffold biological replicates = 6, technical replicates = 3.*

5.4.3.2. ECM Gene Expression

QPCR was used to investigate the expression of several ECM protein coding genes that are expressed at elevated levels in activated fibroblasts. Versican is a large proteoglycan secreted by fibroblasts and encoded by the VCAN gene. VCAN (V1) expression was significantly lower in scaffold NOF than TCP and quiescent NOF (Figure 5.5 A). COL1A expression was significantly lower in scaffold NOF than TCP and senescent NOF (Figure 5.5 B). There was no significant difference in COL1A expression between scaffold and quiescent NOF (Figure 5.5 B). COL3A was significantly elevated in senescent NOF but remained unchanged in all other culture conditions (Figure 5.5 C).

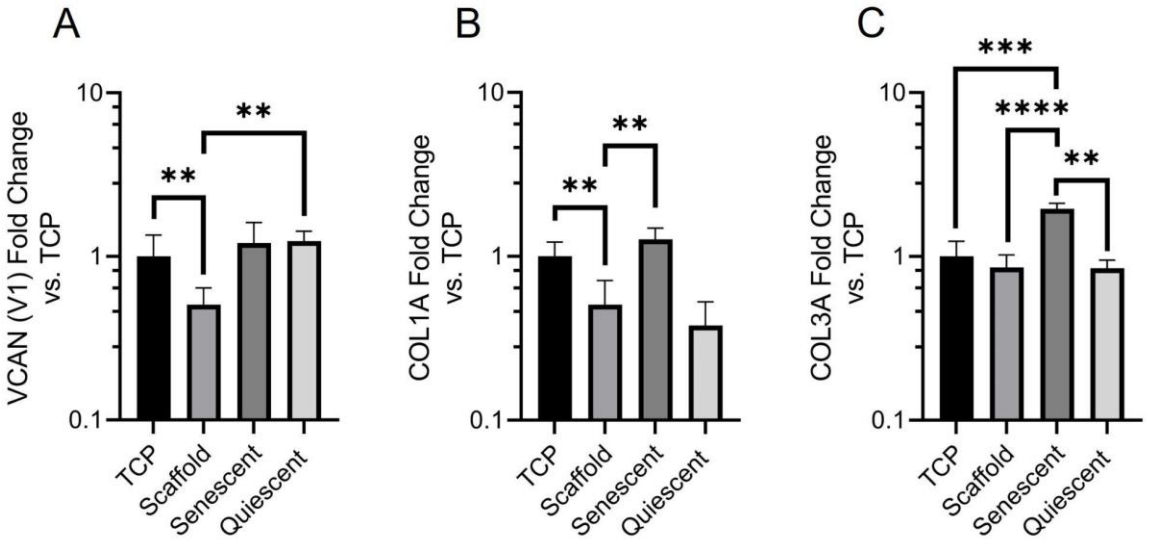

Figure 5.5. *QPCR results for ECM gene expression of (A) VCAN (V1), (B) COL1A, (C) COL3A, versus TCP grown NOF. * p < 0.05, ** p < 0.01, *** p < 0.001, **** p < 0.0001. Error bars show standard deviation. TCP and Scaffold biological replicates = 9, technical replicates = 3. Senescent and Quiescent biological replicates = 3.*

FN1 encodes the ECM protein fibronectin. Unlike VCAN, COL1A and COL3A the expression of gene FN1 was time dependent. Figure 5.6 shows a decline in the expression of FN1 from day 1 to day 7 in both Scaffold and TCP NOF. On day 1 significantly more FN1 was expressed by TCP NOF than scaffold NOF.

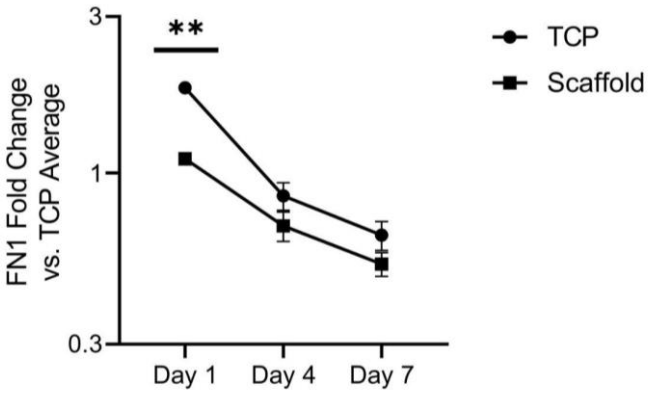

Figure 5.6. *QPCR results for ECM gene FN1 expression, versus the average TCP expression. * p < 0.05, ** p < 0.01, *** p < 0.001. Error bars show standard deviation. Per day, biological replicates = 3, technical replicates = 3.*

5.4.4. NOF Spreading and Morphology

Having reported on several aspects of fibroblast activation using different techniques, SEM imaging was used to gain a better understanding of NOF morphology and how cells interacted with the electrospun scaffold. Figure 5.7 shows how NOF are well spread across the surface of the scaffold. NOF make attachments to fibres above, below and on the same plane as themselves. They penetrate the first few layers of fibres allowing some degree of cellular overlap. There is no obvious change to morphology from day 1 to day 7. Fibroblasts grown on glass coverslips exist in only one plane assuming an apical-basolateral polarity. By day 7 cells and deposited protein coated almost the entire coverslip whilst large areas of the scaffold were still visible.

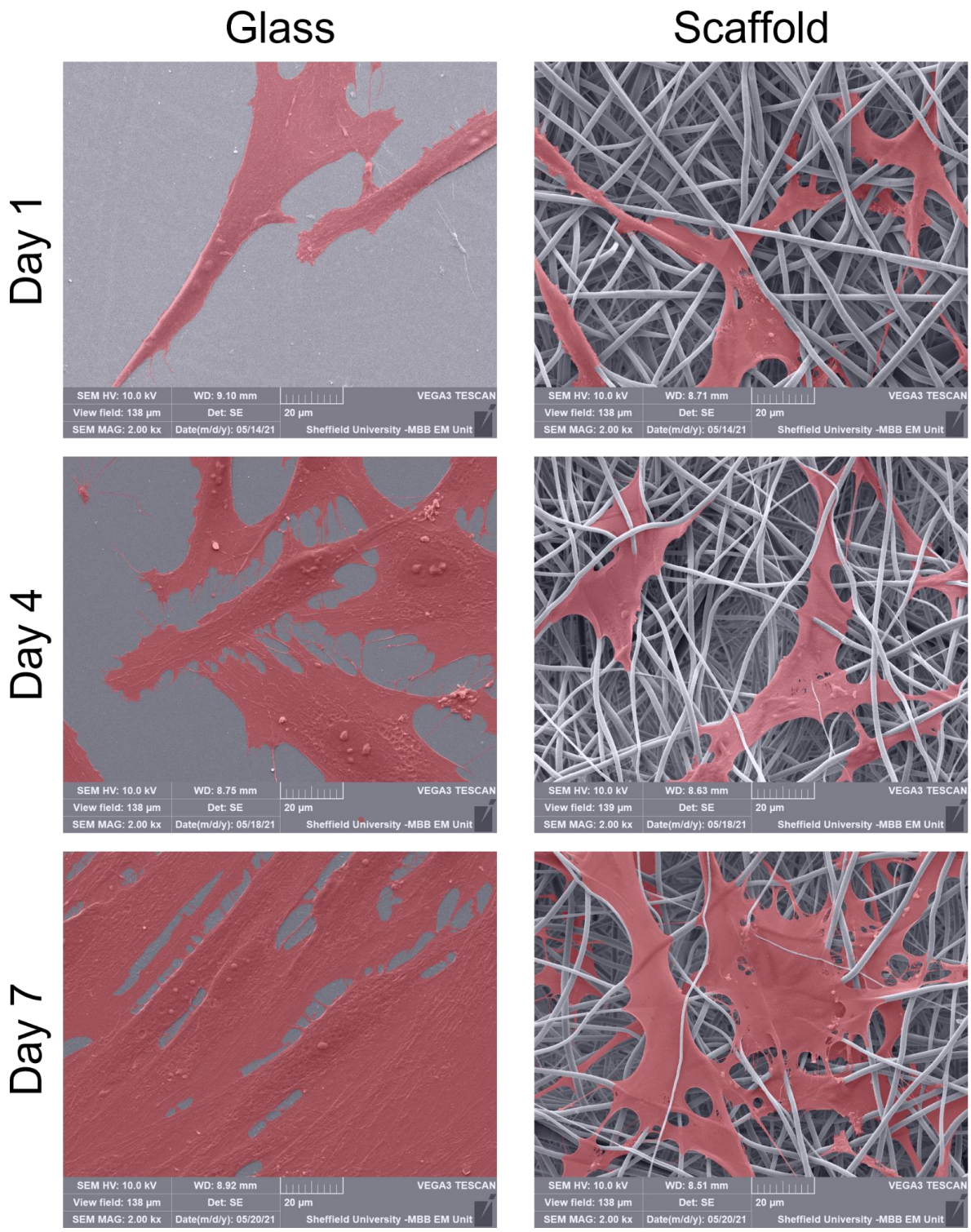

Figure 5.7. *Representative SEM Images taken after 1, 4 and 7 days of culture. Images have been magnified 2000x and each image contains a scale bar. Adobe Photoshop 2021 was used to artificially colour NOF red.*

5.4.5. NOF Cytoskeleton Organisation and Attachments

As distinguishing between cell and extracellular protein deposits was not possible in greyscale SEM images, immunofluorescent images were used to show cell margins. Furthermore, by staining F-actin and vinculin it was possible to look for stress-fibres and focal adhesions in NOF. Figure 5.8 shows how prominent F-actin stress fibres formed in glass NOF populations. F-actin staining was also visible in scaffold cultures although this was less clearly aggregated into filamentous stress fibres. Vinculin staining was accompanied by a high degree of background fluorescence giving pale green staining across the entire cell. In some images of glass NOF, more intense vinculin staining was seen at focal adhesion sites (white arrows). In scaffold culture no points of vinculin concentration were observed. Whether this was the result of a higher degree of background staining and scaffold autofluorescence or a reduction in the number of focal adhesions is not clear. For this experiment flat spin coated PCL membranes were also used to grow NOF. Cell morphologies appeared closer to those observed on glass with broader cytoplasmic spreading. Some stress fibres were observed and some vinculin aggregation at focal adhesions were visible (white arrows).

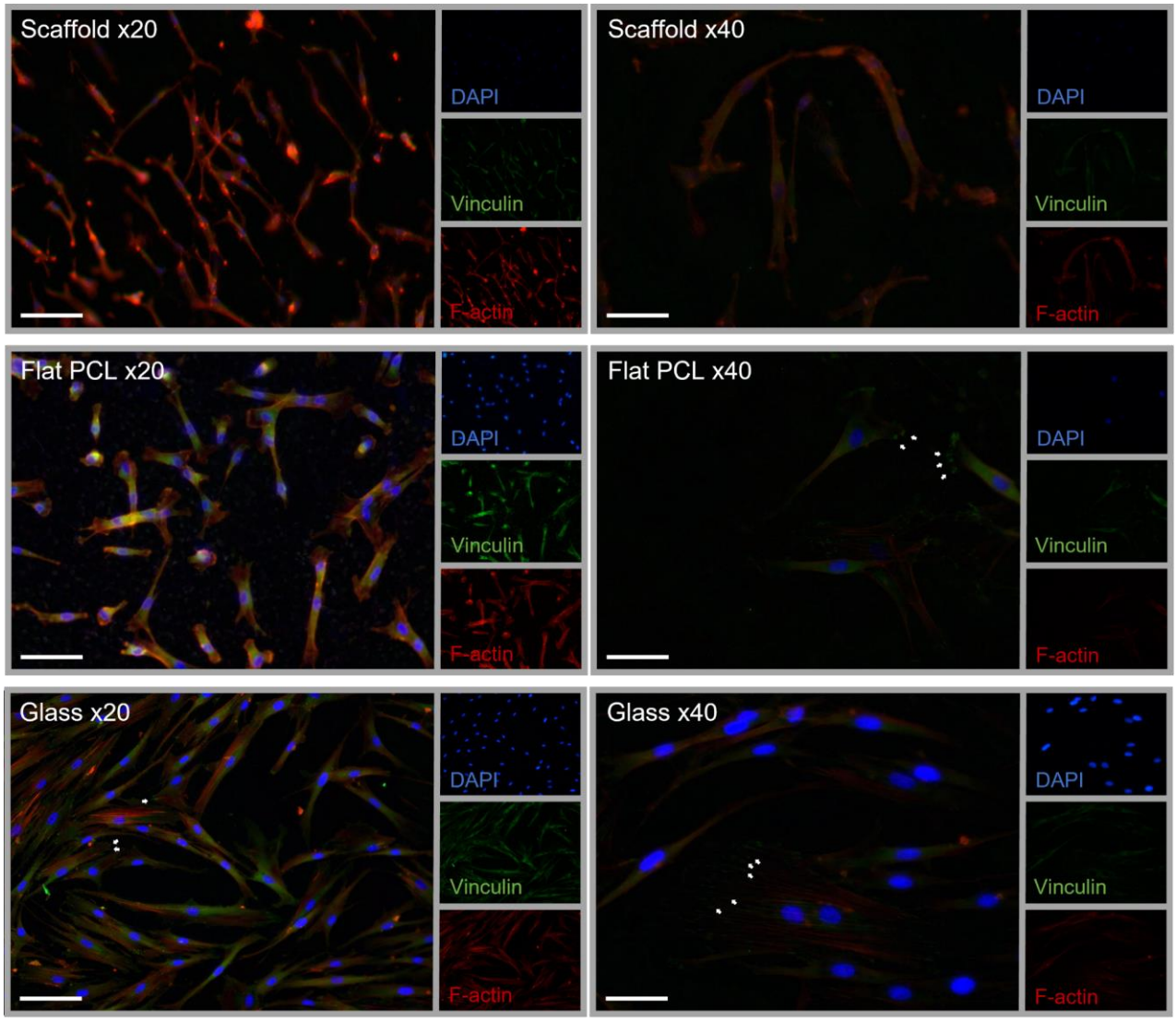

Figure 5.8. *Representative immunofluorescent images of NOF grown on scaffolds, glass and flat PCL membranes. White arrows point to examples of focal adhesion sites. White scale bars are 100 μm long in x20 magnification images and 50 μm long in x40 magnification images. The same image enhancement has been performed in all images, using ImageJ to subtract background fluorescence and increase brightness.*

5.5. Discussion

Counting the proportion of Ki67 positive nuclei was used as a method to quantify the proliferative capacity of NOF grown on ES scaffolds and glass coverslips. Ki67 is a nuclear protein expressed in all proliferating cells except those in cell cycle phase G0 (Muniyandi, Palaninathan et al. 2020). Therefore, those cells that expressed Ki67 were proliferative whilst those that did not, were not. In this experiment glass was used as the control surface rather than TCP due to the ease of staining and imaging the coverslips. It is important to acknowledge that the surface chemistries of TCP and glass are not identical, however they remain comparable in their 2D structure. Despite the reduction in proliferative cells, scaffold NOF were able to grow to a higher degree of confluence after 7 days, with an average cell number per image of 123, higher than the 96 recorded on glass. As indicated in SEM images this is likely the result of some overlapping of cells facilitated by the 3D nature of the scaffold.

Ki67 downregulation has been observed in non-cycling cells of both a senescent and quiescent nature (Alessio, Aprile et al. 2021). Therefore, a qPCR screen for senescence-associated genes p21 and p16 (Campisi and di Fagagna 2007) was completed, alongside quantification of the inflammatory cytokine IL6. IL6 has been associated with the senescence-associated secretory phenotype (SASP) (Coppe, Desprez et al. 2010). IL6, p21 and p16 were shown to be expressed in elevated amounts in NOF after H_2O_2 treatment (Kabir, Leigh et al. 2016). Used at sub-lethal concentrations, H_2O_2 can induce cellular senescence by causing oxidative DNA damage (Chen and Ames 1994). Here, H_2O_2 application was used to generate senescent NOF in tissue culture flasks. Alongside the senescent cells, NOF were grown to confluence for use as a model of quiescence (Coller, Sang et al. 2006). Senescent NOF were β-gal positive and expressed high levels of p21, however p16 expression was not elevated. p21 is a target of p53 signalling and therefore it is responsible for the initial linking of DNA damage with cell cycle arrest (Bunz, Dutriaux et al. 1998). The phased activation of cyclin-dependent kinase inhibitors has been observed before, in human diploid fibroblasts approaching replicative senescence. High levels of p21 expression declined as cells moved

from a pre-senescent state to become fully senescent, at which point high levels of p16 expression took over (Alcorta, Xiong et al. 1996). This suggests that the H_2O_2 treated NOF were in an early phase of senescence. As with p16, IL6 expression remained unchanged in senescent cells. This may support the hypothesis that H_2O_2 treated NOF were in a pre-senescent state, as previous studies cultured NOF for 15 days after H_2O_2 treatment, longer than the 7 days used in this study. Despite using NOF in an early phase of senescence, it is important to note that there was no significant difference in the levels of any of the senescence-associated genes between scaffold and TCP NOF. Furthermore, there was no significant difference between scaffold NOF and confluent quiescent NOF. This indicates that the low proliferation rates in scaffold NOF are due to cellular quiescence and not senescence.

With scaffolds supporting viable NOF that exhibited reduced proliferation rates, it was important to investigate whether other aspects of fibroblast activation were diminished. Alpha-SMA is part of the contractile apparatus in myofibroblast cells where it is recognized as an indicator of fibroblast activation and differentiation (Desmouliere, Geinoz et al. 1993, Tomasek, Gabbiani et al. 2002). The expression of ACTA2 (α-SMA) was significantly reduced in scaffold NOF, although its expression was restored by TGF-β stimulation. Even when stimulated with TGF-β, scaffold NOF still expressed significantly less ACTA2 than NOF that were stimulated with TGF-β on TCP. The TGF-β pathway is therefore modulated by the scaffold microenvironment to some extent.

The next aspect of fibroblast activation investigated was the expression of genes responsible for the production of extracellular matrix proteins including versican (VCAN), collagen 1 (COL1A), collagen 3 (COL3A) and fibronectin (FN1). Versican is a large proteoglycan and the V1 isoform has been shown to modulate cell cycle progression and enhance proliferation (Sheng, Wang et al. 2005). Furthermore, it has been shown to be upregulated in activated NOF (Melling, Flannery et al. 2018). Versican binds to several cell surface receptors, including integrins and the epidermal growth factor receptor, which are both known to regulate proliferation (Wu, La Pierre et al. 2005). VCAN expression was significantly reduced in scaffold

NOF compared to TCP NOF. Interestingly, confluent quiescent NOF expressed significantly more VCAN than scaffold NOF. This showed that there is a difference in the mechanisms of proliferation control in the scaffold NOF compared to the contact-inhibited quiescent NOF. Collagen deposition is another hallmark of fibroblast activation (Hinz 2007). COL1A expression was significantly reduced in scaffold NOF, whilst COL3A expression remained equal for all culture conditions, apart from senescent NOF where it was significantly elevated. The involvement of several collagen subtypes in senescence has been established, however there is little substantiated evidence of a role for collagen 3 in cellular senescence (Blokland, Pouwels et al. 2020). FN1 was the only ECM protein coding gene that displayed a time dependence in its expression levels. FN1 expression fell from day 1 to day 7 in both TCP and scaffold NOF. There was significantly more FN1 expression in TCP NOF 1 day after seeding. Lower levels of fibronectin deposition may offer one explanation for the lower proportion of proliferative NOF at day 1 in scaffold culture, given that fibronectin binding by integrins is a mechanism by which cells may proceed through cell-cycle growth phase 1 (Danen and Yamada 2001). Although it is important to recognize that changes to fibronectin conformation on different substrates has also been shown to control the proliferation and differentiation of C2C12 myoblasts (Garcia, Vega et al. 1999). Furthermore, matrix mechanical properties are also communicated through integrins and influence cellular behaviour (Geiger, Bershadsky et al. 2001). The fall in FN1 expression could be the result of cellular confluence increasing, as the confluent quiescent cells had a ΔΔCT value of 0.43 (data not shown in Figure 5.6). That is less than half of the average ΔΔCT value for TCP NOF and close to the values recorded for TCP and scaffold NOF at day 7 - 0.65 and 0.53, respectively.

Finally, SEM and immunofluorescent images were taken to observe cell morphology and how NOF interact with the scaffold. SEM images showed the degree to which NOF can penetrate the scaffold, how they spread and form attachments to multiple fibres. However, the greyscale images fail to distinguish between extracellular protein deposits and cell bodies making comparing NOF morphology between SEM and previous live/dead images difficult. During

live/dead staining, calcein AM is converted into fluorescent calcein by intracellular esterase activity (Somodi and Guthoff 1995) and only the cell body fluoresces. Cytoskeletal proteins F-actin and vinculin were stained to gain a better understanding of cell morphology and the type of attachments that were made between NOF and the scaffold. These images revealed a morphology similar to that observed in live/dead images, with many bipolar cells with long slender projections. Vinculin is a key component of focal adhesions where it links the actin cytoskeleton to integrins attaching to the ECM (Geiger, Bershadsky et al. 2001). Areas of high vinculin fluorescence that co-localise with F-actin stress fibres indicate focal adhesion sites and appear to be less prevalent in scaffold grown NOF. This could have been the result of imaging challenges associated with 3D culture and scaffold autofluorescence.

5.6 Conclusion

This chapter has described how several aspects of fibroblast activation are diminished in ES scaffold culture. Fluorescent staining indicated that F-actin stress fibres were retained in these in vivo-like low activity fibroblasts. After Ki67 quantification revealed a reduction in the proportion of proliferative NOF, qPCR was used to rule out cellular senescence as the root cause. Subsequent qPCR studies revealed that activation marker ACTA2 expression was reduced, as were ECM proteins VCAN, COL1A and FN1. FN1 expression also displayed a time dependence, which could be linked to the slow initial growth rates on the scaffold. Based on SEM images fibroblasts can penetrate within the first few layers of the scaffold and form attachments to multiple fibres. Vinculin immunofluorescence was inconclusive in revealing whether these attachments were focal adhesions, though given the presence of stress fibres, vinculin positive focal adhesions might be expected. In the next chapter several different opportunities to exploit this scaffold and the low-activity NOF phenotype it induces will be explored. This includes investigating the mechanism of fibroblast activation through western blotting and whole genome RNA sequencing. The value of this scaffold as a model to investigate disease states is also considered through the study of pathogenic CAF.

Chapter 6: Applications for Electrospun Scaffolds in the Study of Fibroblast Activation and Disease Modelling

6.1. Introduction

In chapter 5, fibroblast behaviour was thoroughly characterised on the electrospun scaffold. Key fibroblast activation traits were found to be diminished in electrospun scaffolds when compared with TCP cultures. Immunofluorescent staining of Ki67 revealed a reduction in the proportion of proliferative NOF and qPCR suggested that this was not caused by cellular senescence. QPCR indicated that the expression levels of the activation marker α-SMA were reduced alongside several extracellular matrix protein coding genes that also fell when compared to TCP grown NOF. Finally, SEM images and immunofluorescent labelling of F-actin and vinculin revealed that fibroblasts attach to multiple fibres within the first few layers of the scaffold.

Based on these results, it was concluded that the scaffold represents a valuable platform for the study of fibroblast behaviour, with a particular focus on the influence of the culture environment on fibroblast activation. De-regulated activation is a prerequisite of fibrotic disease and so understanding which features of the scaffold microenvironment control activation behaviour could help to combat fibrotic diseases. Fibrosis is not the only disease in which fibroblasts play a significant role. Cancer associated fibroblasts (CAF) represent a unique population of activated cells that may also be studied in the 3D microfibrous scaffold. CAF are highly heterogeneous stromal cells with both tumour suppressive and tumour promoting roles (Chen and Song 2019). They therefore represent a complex therapeutic target. ECM stiffness and matrix degradation, features regulated by CAF, contribute to cancer progression, CAF in turn are subject to ECM and tumour derived cues (Nelson and Bissell 2006, Colombo and Cattaneo 2021). For this reason, finding appropriate ECM models in which to study CAF has great therapeutic potential.

This chapter presents attempts to develop our understanding of fibroblast activation and to identify potential applications for the scaffold in the modelling of disease states. Western-blotting was used to investigate MAPK/ERK pathway activation and next-generation RNA sequencing was used to gain an insight into the impact of scaffold culture on NOF gene expression. Finally, the scaffold was used to culture CAF to understand how the electrospun scaffold may control the phenotype of an activated oral fibroblast population.

6.2. Aims

- To investigate the molecular pathways involved in fibroblast activation on the electrospun scaffold using western blotting.
- To use next-generation RNA-sequencing to gain an appreciation of any changes to the transcriptome of NOF grown on the scaffold.
- To culture cancer associated fibroblasts (CAF) on the electrospun scaffold and use qPCR to characterise any changes to the expression of traditional CAF markers.

6.3. Specific Experimental Objectives

- Extract protein from NOF and confirm its presence using gel electrophoresis.
- Western blot for MAPK and phospho-MAPK.
- Extract RNA from NOF for RNA-sequencing.
- Interpret RNA sequencing data.
- Culture CAF on electrospun scaffolds.
- Use qPCR to quantify the expression of specific CAF markers.

6.4. Results

6.4.1. Quantifying MAPK Phosphorylation Using Western Blotting

Activation of the p44/p42 MAPK (ERK 2/1) pathway is required for proliferation in monolayer cultures and is dependent on integrin attachments to extracellular structures (Rosenfeldt and Grinnell 2000). Reduced phosphorylation of p44/p42 MAPK was observed in relaxed collagen hydrogels and this observation led to the hypothesis that matrix mechanical properties may act via the MAPK pathway to reduce proliferation rates in fibroblasts (Rosenfeldt and Grinnell 2000). With reduced proliferation rates also observed in NOF grown on the electrospun polycaprolactone scaffold, whether MAPK activation (p44/p42 phosphorylation) was altered in scaffold cultures was investigated. Western blotting was selected as the technique to quantify any changes in p44/p42 phosphorylation. The first experimental step was protein isolation.

6.4.1.2. Protein Isolation and Lysis

Protein extraction was attempted using a radioimmunoprecipitation assay (RIPA) buffer. A bicinchoninic acid (BCA) assay was used to determine protein concentration. A low protein concentration of 14 ng/µl was extracted when using the RIPA buffer to lyse cells on the scaffold (Table 6.1). For this reason, it was not possible to load equal amounts of protein into wells for gel-electrophoresis. Ponceau staining revealed successful protein separation with staining visible across a range of molecular weights in TCP NOF (Figure 6.1). Almost no visible ponceau staining was observed in protein extracted from the scaffold (Figure 6.1). When traditional RNA extraction procedures failed to isolate RNA from cells attached to the electrospun scaffold, Tri Reagent was used to dissolve the scaffolds and lyse the NOF. For this reason, the same Tri Reagent based cell and scaffold lysis was used to extract protein from the scaffold. Following extraction, protein concentration was again determined using a BCA assay. With extracted protein concentrations of 95 ng/µl from NOF grown on scaffolds and 683 ng/µl from the TCP, it was possible to load equal amounts of protein into an SDS-polyacrylamide gel (Table 6.1). Ponceau staining revealed thick protein bands of approximately 66 kDa for both TCP and scaffold grown NOF (Figure 6.1). The band at 66 kDa

was visibly smaller for protein extracted from the scaffold. RIPA extraction produced a low protein yield from scaffold grown NOF with almost no detectable protein transferred to the nitrocellulose membrane. Therefore, protein extracted using TRI reagent was used for western blotting. Antibodies directed towards p44/p42 MAPK produced thick bands that co-localised with the 66 kDa band seen in ponceau staining (Figure 6.1). GAPDH was used as an endogenous control and produced a band in the same location as the MAPK band (Figure 6.1).

Table 6.1. BCA Assay Results for Whole Cell Lysates Extracted from NOF.

RFU	Extraction	Condition	Concentration (ng/µl)	Volume (µl)	Protein (µg)
0.1661	TRI	Scaffold only	60.583	40	2.4
0.1545	TRI	Scaffold media	31.417	40	1.3
0.1800	TRI	Scaffold media NOF	95.250	40	3.8
0.1544	TRI	Scaffold serum-free media NOF	31.333	40	1.3
0.2474	TRI	TCP media NOF	263.750	40	10.6
0.2101	TRI	TCP serum-free media NOF	170.583	40	6.8
0.4152	RIPA	TCP media NOF	683.250	40	27.3
0.1163	RIPA	TCP serum-free media NOF	-63.917	40	-2.6
0.1476	RIPA	Scaffold media NOF	14.167	40	0.6
0.1121	RIPA	Scaffold only	-74.417	40	-3.0

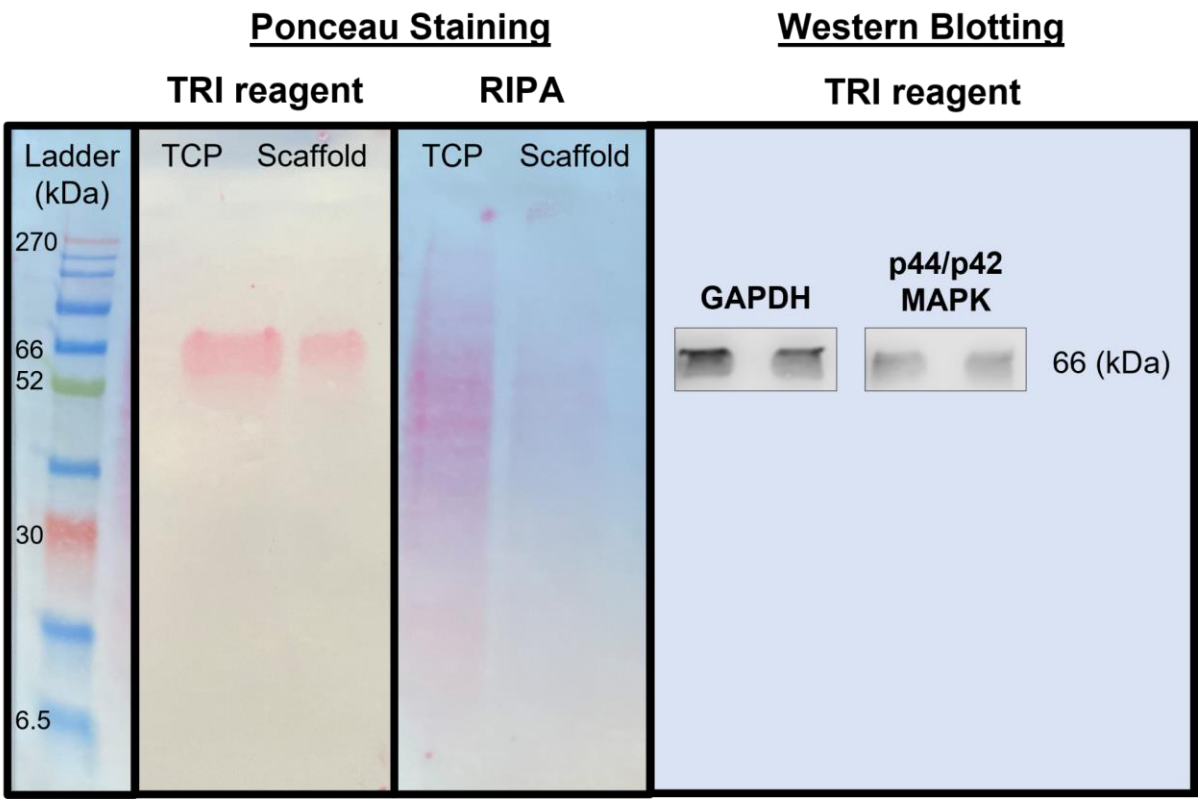

Figure 6.1. *Ponceau staining (pink) identifies protein transferred from a polyacrylamide electrophoresis gel to a nitrocellulose membrane by electroblotting. Cells were lysed using TRI reagent or RIPA buffer. Western blotting was conducted using antibodies directed towards GAPDH and p44/p42 MAPK.*

6.4.2. Next Generation RNA-Sequencing

Due to challenges in the isolation and lysis of protein for western blotting, an alternative approach to gain an insight into the mechanisms controlling the quiescent fibroblast phenotype was explored. As RNA was successfully isolated from scaffold grown NOF for qPCR, next generation RNA-sequencing (NGS) was used to explore the fibroblast phenotype further. After isolation in our laboratory, RNA samples were sequenced by Genewiz, an Azenta Life Sciences Company.

6.4.2.1. RNA Sample Quality Control

Four RNA samples (biological replicates) were submitted from NOF grown on tissue culture plastic (TCP 1 - 4). Four RNA samples were submitted from NOF grown on ES scaffolds (Scaffold 1 - 4). Quality control of the submitted samples included analysis of the 28S/18S ratio and calculation of the RNA Quality Number (RQN), using capillary electrophoresis to perform RNA fragment analysis. The 28s/18s ratio relates to the large 28s and small 18s ribosomal subunits and the expected ratio for complete RNA samples is > 2. For each sample, RQN and 28S/18S ratio were reported in Table 6.2, alongside RNA concentrations that were measured using a Qubit device.

Table 6.2. RNA Quality Control and Concentration Values for TCP and Scaffold Biological Replicates.

Sample Name	Sample Quality Control					
	General			RNA Qubit	Fragment Analyzer	
	Sample Type	Volume (µl)	Quantity (ng)	Concentration (ng/µl)	RQN	28S/18S
TCP 1	Total RNA	16	1534	95.9	10.0	2.5
TCP 2	Total RNA	17	1130	66.5	10.0	2.5
TCP 3	Total RNA	16	1936	121	10.0	2.3
TCP 4	Total RNA	16	534	33.4	10.0	2.4
Scaffold 1	Total RNA	16	550	34.4	10.0	2.5
Scaffold 2	Total RNA	16	491	30.7	10.0	2.2
Scaffold 3	Total RNA	16	502	31.4	10.0	2.1
Scaffold 4	Total RNA	16	690	43.1	10.0	2.2

RNA, Ribonucleic acid; RQN, RNA Quality Number.

RNA samples were extracted after NOF had been cultured for 4 days as thereafter NOF would become contact inhibited. The electropherogram for RNA sample TCP 1 is provided and is representative of all the samples (Figure 6.2). Characteristic 28S (blue) and 18S (pink) ribosomal subunit RNA peaks are visible alongside the lower marker (LM) peak used for calibration. No significant peak was detected below 200 nucleotides (nt) in size.

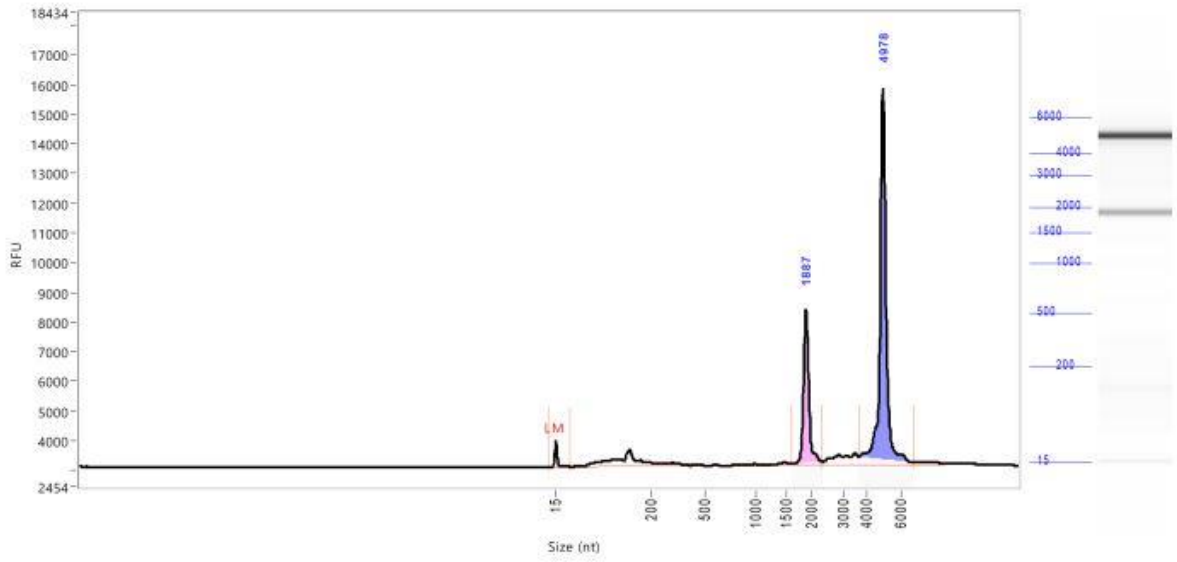

Figure 6.2. *A representative electropherogram taken from sample TCP 1. RNA samples submitted for RNA sequencing were analysed by Genewiz using a capillary fragment analyzer.*

6.4.2.2. Sample Similarity Assessment

Sample similarity tests were performed by Genewiz to identify any samples that were not representative of the population. All sample similarity figures are based on the gene hit count data which has been normalised to the log2 scale. As such, we can visualise how similar samples are from within each group, to identify outliers and to compare the similarity of samples between the culture environments. A heatmap was used to show the euclidean distance between samples (Figure 6.3). Samples from each culture condition are related more closely to one-another than they are to samples from the other culture condition. The darker blue colours indicate that samples TCP 1 - 4 (TCP RNA) are more closely related than samples Scaffold 1 - 4 (scaffold RNA).

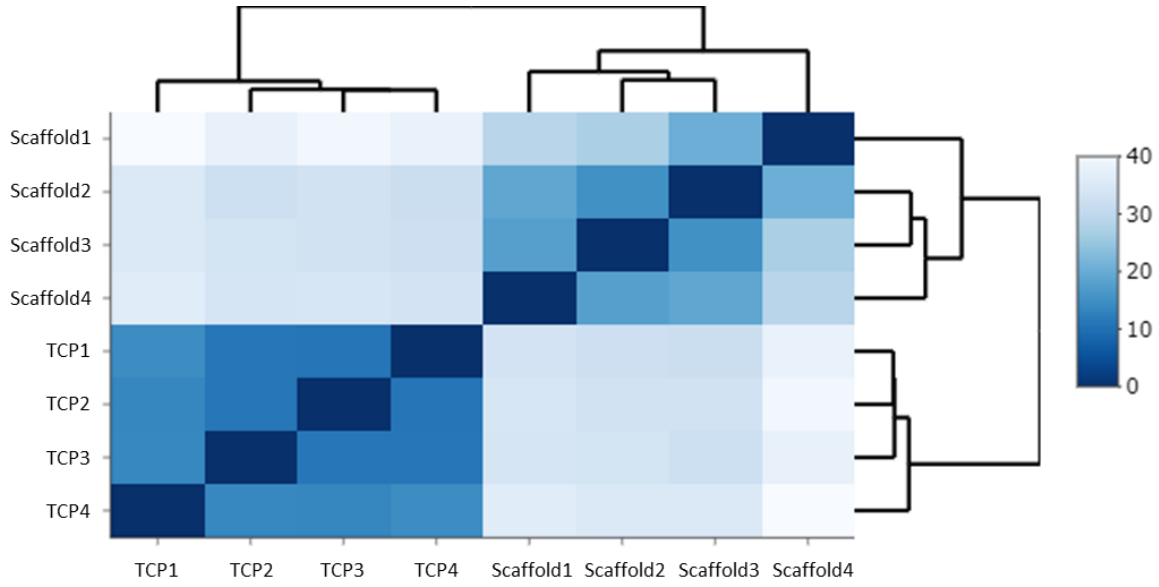

Figure 6.3. *A heatmap showing the Euclidean distance between RNA samples, based on the normalised hit counts for genes detected during RNA sequencing.*

A principal component analysis (PCA) plot was used to visually represent the difference between samples in a 2D matrix (Figure 6.4). The high degree of variance indicated by principal component (PC) 1 of 91.84% shows that the culture conditions are responsible for the greatest difference in gene hit count data. The PCA plot presents the same picture as the heatmap in Figure 6.3, indicating a greater variance between scaffold RNA replicates (1 - 4) than TCP RNA replicates (1 - 4).

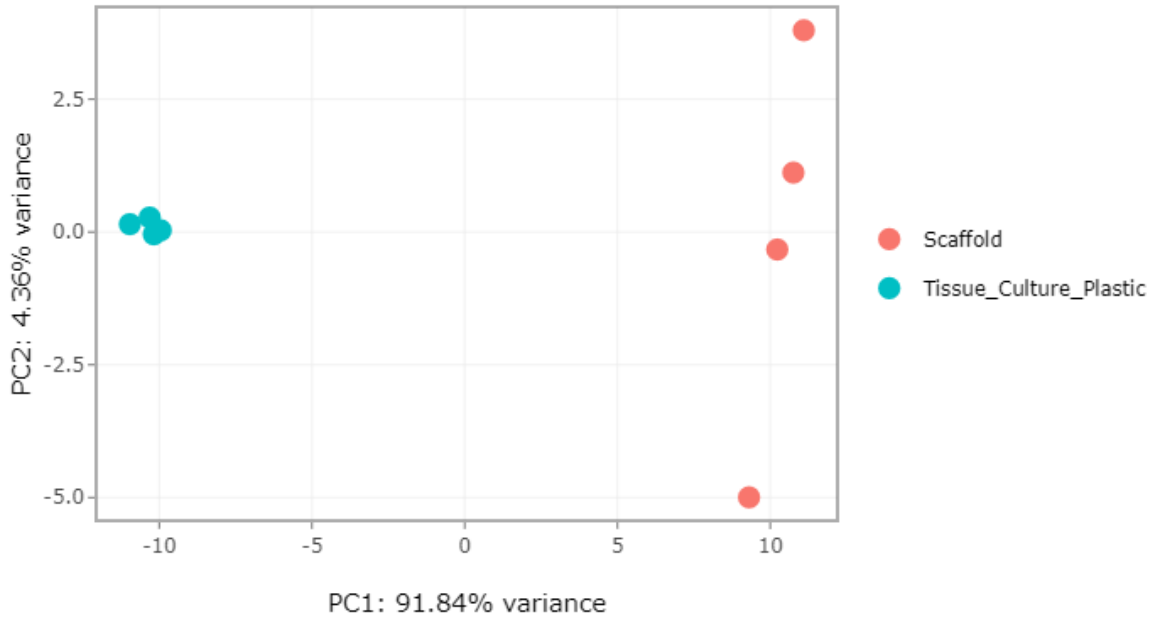

Figure 6.4. *A PCA plot describing the variance in the number of normalised hit counts per gene for each RNA sample. PC1 and PC2 relate to the greatest two sources of variance in the data set.*

6.4.2.3. Differential Gene Expression

With sample variance checks completed the next step was to look at which genes were significantly differentially expressed (DE). Using the DEseq2 method, genes which exhibited an absolute log2 fold change > 1 and had an adjusted p value of < 0.05 were considered differentially expressed. A total of 983 genes were differentially expressed in the scaffold grown NOF compared to the TCP grown NOF, with 585 of them downregulated and 398 upregulated. The volcano plot shows the distribution of DE genes (Figure 6.5). Each dot represents a gene and its relative expression level in scaffold grown NOF 'vs' TCP NOF. Green dots show the downregulated genes (fold change (log2) < −1) and red dots show the upregulated genes (fold change (log2) > 1). Grey dots are the genes that did not meet the expression or significance level threshold in the scaffold NOF compared to TCP NOF.

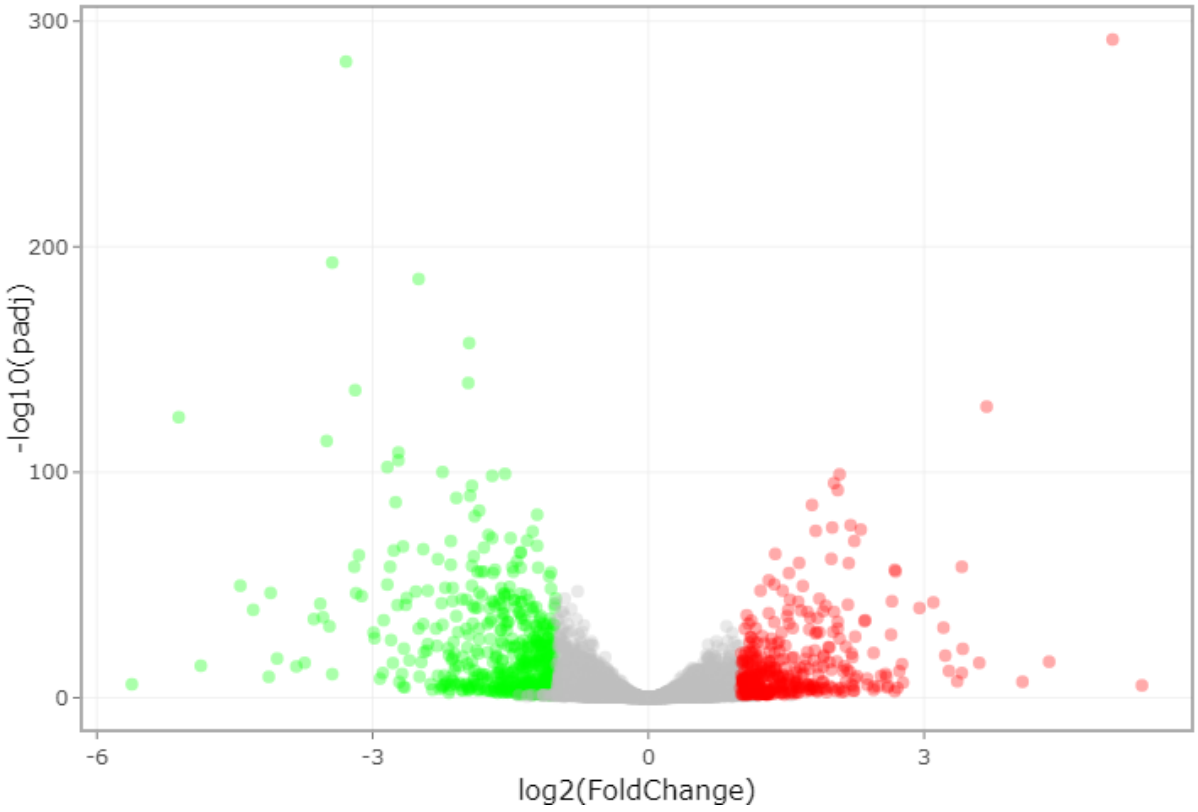

Figure 6.5. *Global transcriptional changes visualised as a volcano plot. Green dots represent genes which were downregulated and red dots represent genes which were upregulated in the scaffold cultured NOF compared to TCP cultured NOF.*

6.4.2.4. Over-representation Analysis and Gene Ontology

With a list of 983 DE genes, techniques such as gene ontology (GO) analysis or over-representation analysis (ORA) can be employed to identify biological processes that are significantly enriched in the DE genes. ORA considers the total number of DE genes and calculates whether the number of DE genes appearing in any given GO group is more than would be expected to appear by chance. In this way ORA filters out GO terms that appear due to the size of the GO group and the high number of DE genes present in many RNA sequencing experiments. Of the top 10 most significantly enriched GO groups (with the smallest false discovery rate (FDR)) (Figure 6.6), the two most enriched terms were extracellular matrix organisation (GO:0030198) and extracellular structure organisation (GO:0043062). The DE genes in these enriched GO terms were members of the ADAM metallopeptidase family and matrix metallopeptidase (MMP) family. There were also many DE ECM genes including several collagen subtypes, aggrecan, elastin, fibrillin, vitrin and vitronectin amongst others. Integrin subunits were also part of the DE genes within these GO terms. Other terms in the top 10 most significantly enriched processes were biological adhesion (GO:0022610), cell adhesion (GO:0007155) and cell migration (GO:0016477). Once again, the terms contained many overlapping DE genes including ADAMs, MMPs, collagens and integrins. These terms also included DE genes involved in cellular signalling, such as cellular receptors, growth factors and intracellular signalling molecules. These included G protein-coupled receptors, fibroblast growth factors and TGF-β receptors. The other most significantly enriched GO terms were all related to the circulatory system. Once more, a large proportion of the DE genes within these terms were collagen, integrin and ADAMs family genes. Outside of the top 10 other significantly (FDR < 0.05) enriched GO terms of interest included MAPK and ERK regulation, features investigated during western blotting (section 6.4.1.) and other terms related to fibroblast behaviour including wound healing (GO:0042060) and collagen fibril organisation (GO:0030199). The top 10 most significantly enriched GO terms are listed in Table 6.3 alongside other GO terms of interest.

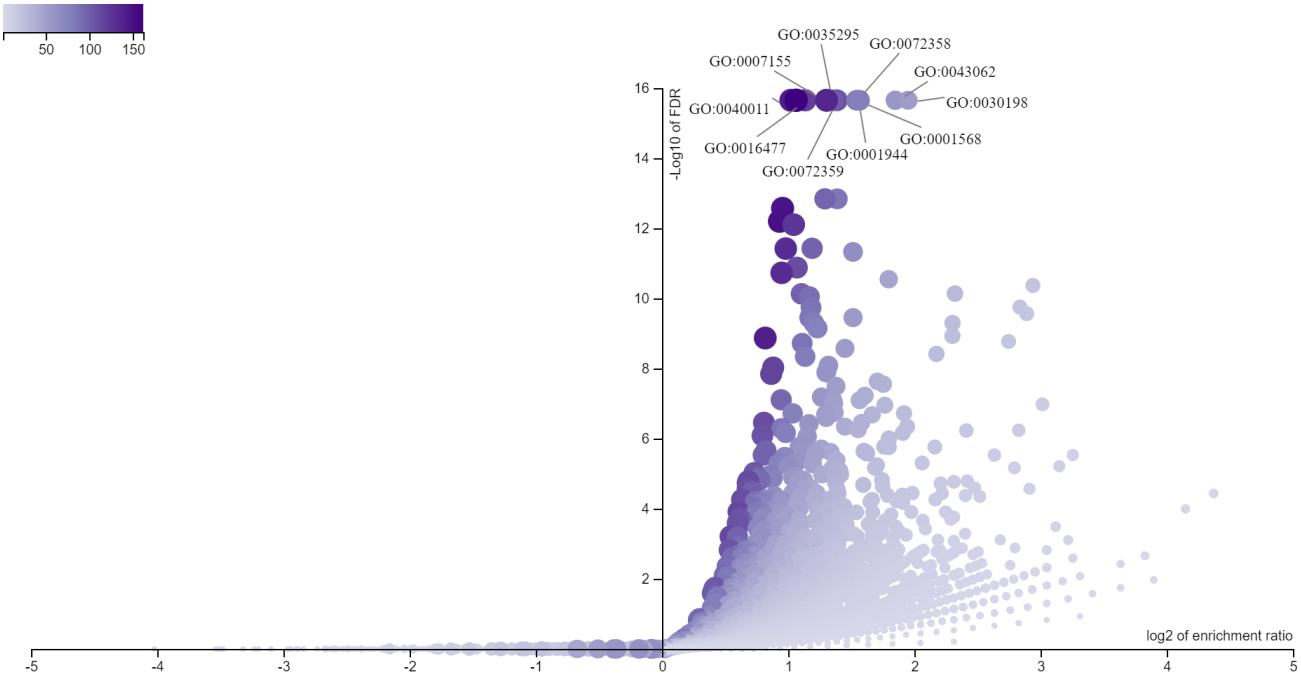

Figure 6.6. *A volcano plot showing all the enriched GO terms from the ORA. The top 10 most significant GO groups are labelled. Purple colouring and circle size relate to the number of DE genes within a term.*

Table 6.3. Selected ORA Terms.

Gene Set	Description	Size	Overlap	Expect	Enrichment Ratio	FDR
GO:0090269	fibroblast growth factor production	7	4	0.3	14.191	2.18E-03
GO:0030199	collagen fibril organization	49	14	2.0	7.096	5.78E-07
GO:0007229	integrin-mediated signaling pathway	101	16	4.1	3.934	1.24E-04
GO:0030198	extracellular matrix organization	347	54	14.0	3.865	0
GO:0043062	extracellular structure organization	400	58	16.1	3.601	0
GO:0001568	blood vessel development	654	78	26.3	2.962	0
GO:0001944	vasculature development	682	81	27.5	2.950	0
GO:0072358	cardiovascular system development	691	81	27.8	2.911	0
GO:0072359	circulatory system development	1026	108	41.3	2.614	0
GO:0035295	tube development	992	102	39.9	2.554	0
GO:0022610	biological adhesion	1377	137	55.4	2.471	0
GO:0007155	cell adhesion	1369	136	55.1	2.467	0
GO:0042060	wound healing	532	49	21.4	2.287	5.24E-06
GO:0016477	cell migration	1368	121	55.1	2.197	0
GO:0070848	response to growth factor	690	60	27.8	2.160	1.69E-06
GO:0048870	cell motility	1518	126	61.1	2.061	7.85E-13
GO:0070372	regulation of ERK1 and ERK2 cascade	308	24	12.4	1.935	2.27E-02
GO:0008283	cell proliferation	1986	141	80.0	1.763	1.35E-09
GO:0007267	cell-cell signaling	1575	111	63.4	1.750	3.50E-07
GO:0000165	MAPK cascade	896	63	36.1	1.746	4.22E-04

Size: the total number of genes in each GO term; Overlap: the number of scaffold NOF DE genes that also feature in the GO term; Expect: the number of terms that would overlap by chance; Enrichment Ratio: overlap/expect; FDR: False Discovery Rate. ERK, Extracellular Signal-Regulated Kinase; FDR, False Discovery Rate; GO, Gene Ontology.

Whilst ORA is a useful technique, each enriched GO term consists of multiple DE genes that are both up and downregulated. Looking for GO terms that are enriched in groups of only up or downregulated genes is one method for identifying groups of associated genes that may be acting in tandem to produce effects. WebGestalt was used to generate Figure 6.7. Rather than GO terms, biological pathways stored in the Kyoto Encyclopedia of Genes and Genomes (KEGG) database were investigated. As GO terms and KEGG pathway groups contain antagonistic genes such as pathway activators and inhibitors and this analysis only considers over or under expressed genes, the number of significant (FDR < 0.05) results is low.

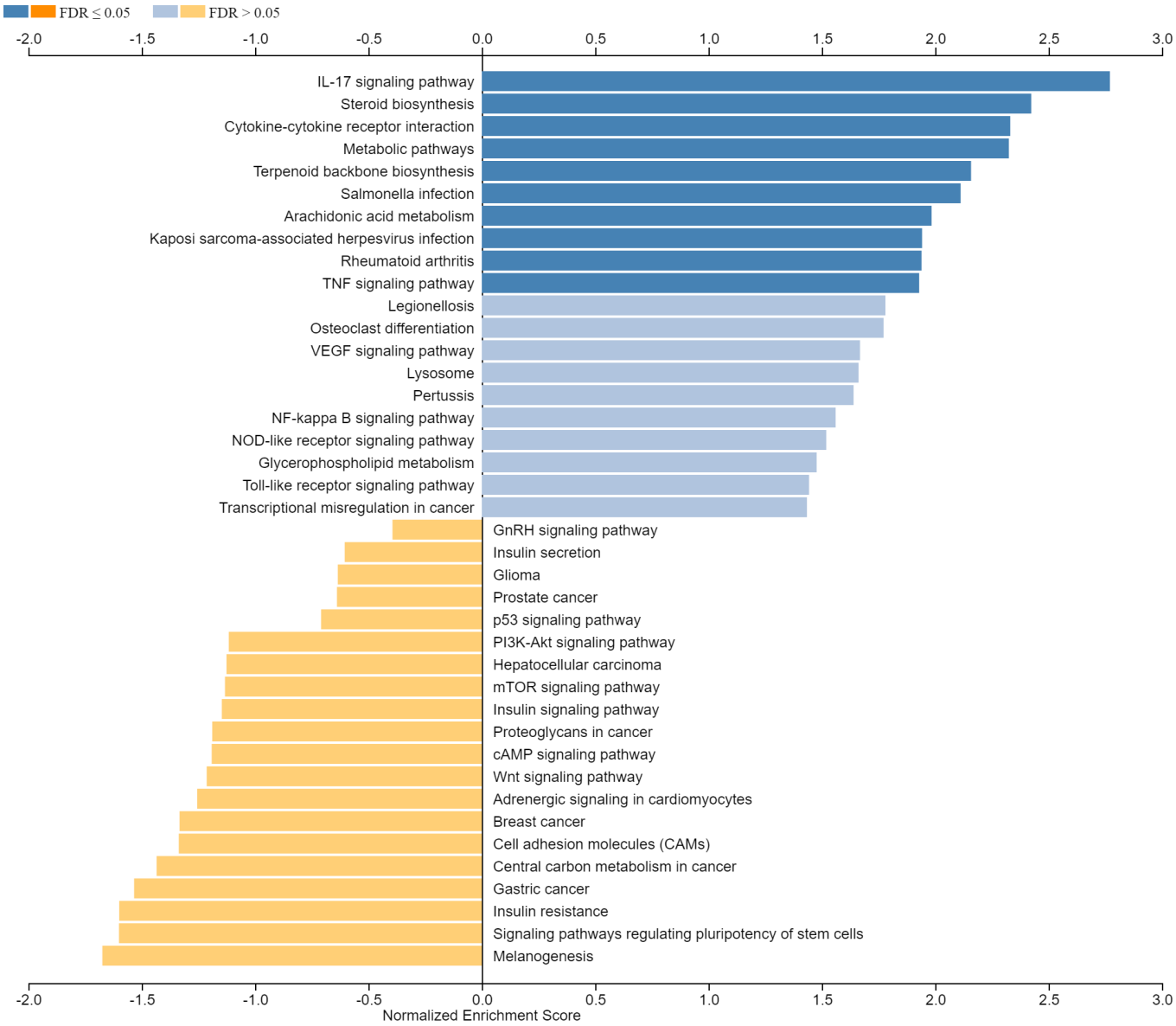

Figure 6.7. *Pathways from the KEGG database that were enriched with DE expressed genes that were all upregulated or all downregulated.*

Many of the pathways that were significantly enriched (FDR < 0.05) contain members of the C-X-C motif chemokine ligand family that were upregulated in unison in NOF grown on the electrospun scaffold. An alternative approach is to take each GO from the ORA and look at the DE genes within it. One example would be the differentially expressed collagens in GO:0007155 - cell adhesion, which were almost all downregulated except for Col13A1 and Col23A1 which were upregulated.

6.4.3. Electrospun Scaffolds as Platform to Study CAF

Cancer associated fibroblasts (CAF) are activated fibroblasts and are the most abundant cellular component of cancerous stroma (Kalluri 2016). Matrix remodelling through the secretion of MMPs and modulation of the chemical and physical composition of the ECM allow CAF to regulate cancer initiation and progression (Kalluri 2016). After observing a reduction in the activation traits of normal oral fibroblasts it was of interest to see if the scaffold culture environment would regulate the phenotype of pre-activated CAF and limit the expression of classical CAF markers. As key mediators of cancer initiation and progression reducing CAF activation has great therapeutic potential. CAF were seeded onto ES scaffolds and TCP using the same methodology used with NOF and outlined in the materials and methods section 3.3 - 3.5. QPCR was then used to quantify the expression of different CAF and fibroblast markers after 1, 4 and 7 days of culture. ACTA2 was one of the first recognized clinical markers for CAF (Lazard, Sastre et al. 1993). The expression of FAP, FSP1, PDGFRβ, TNC, IL6 and VCAN have since been identified in CAF (Han, Liu et al. 2020, Nurmik, Ullmann et al. 2020).

6.4.3.1. Expression of CAF Markers

ACTA2 (α-SMA) expression followed the same pattern in CAF as was observed in NOF with significantly lower expression in scaffold grown cells and no time dependence (Figure 6.8). FAP expression fell in scaffold grown CAF, becoming significantly lower from day 1 to day 7 and from day 4 to day 7. On day 1 there was no difference between FAP expression in TCP and scaffold CAF, however as the level of FAP fell in scaffold CAF, levels became significantly lower than TCP grown CAF on day 4 (Figure 6.8). Fibronectin (FN1) expression showed a time dependence in scaffold CAF, falling significantly from day 1 to day 7. The average FN1 expression across all time points was significantly lower in scaffold CAF than in TCP CAF ($P = 0.031$) ($N = 9$). FSP1 expression remained unchanged during 7 days of culture on plastic or scaffolds (Figure 6.8).

On day 4 and 7 in culture IL6 expression was significantly lower in scaffold grown CAF than in TCP CAF (Figure 6.9). There was no significant difference in PDGFRβ expression between

TCP and scaffold cultured CAF at any stage over seven days (Figure 6.9). However, a T-test with Welch's correction revealed that average PDGFRβ expression across days 1, 4 and 7 was significantly lower in Scaffold CAF (P = 0.049) (N = 9). Tenascin C (TNC) expression was significantly lower at day 4 and day 7 in CAF grown on ES scaffolds than at day 1. TCP CAF TNC expression was also significantly lower at day 7 (Figure 6.9). There was no significant difference in VCAN (V1) expression (Figure 6.9). However, a T-test with Welch's correction revealed that average VCAN expression across days 1, 4 and 7 was significantly lower in Scaffold CAF (P = 0.0006) (N = 9).

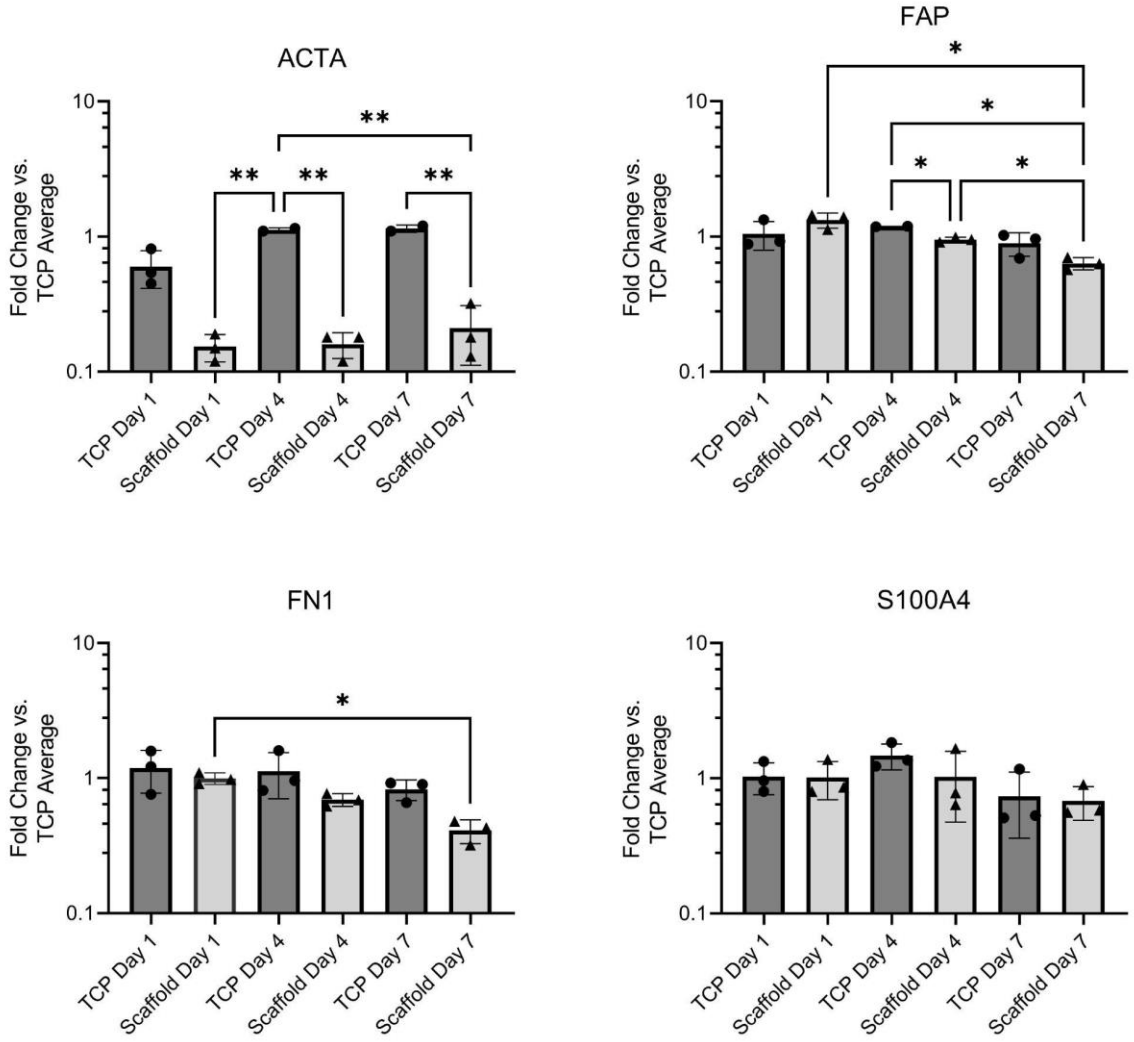

Figure 6.8. *QPCR results showing fold expression levels for ACTA2, FAP, FN1 and FSP1 versus the average expression in TCP grown NOF. * p < 0.05, ** p < 0.01, *** p < 0.001. Error bars show standard deviation. Biological replicates = 3, technical replicates = 3 (per day).*

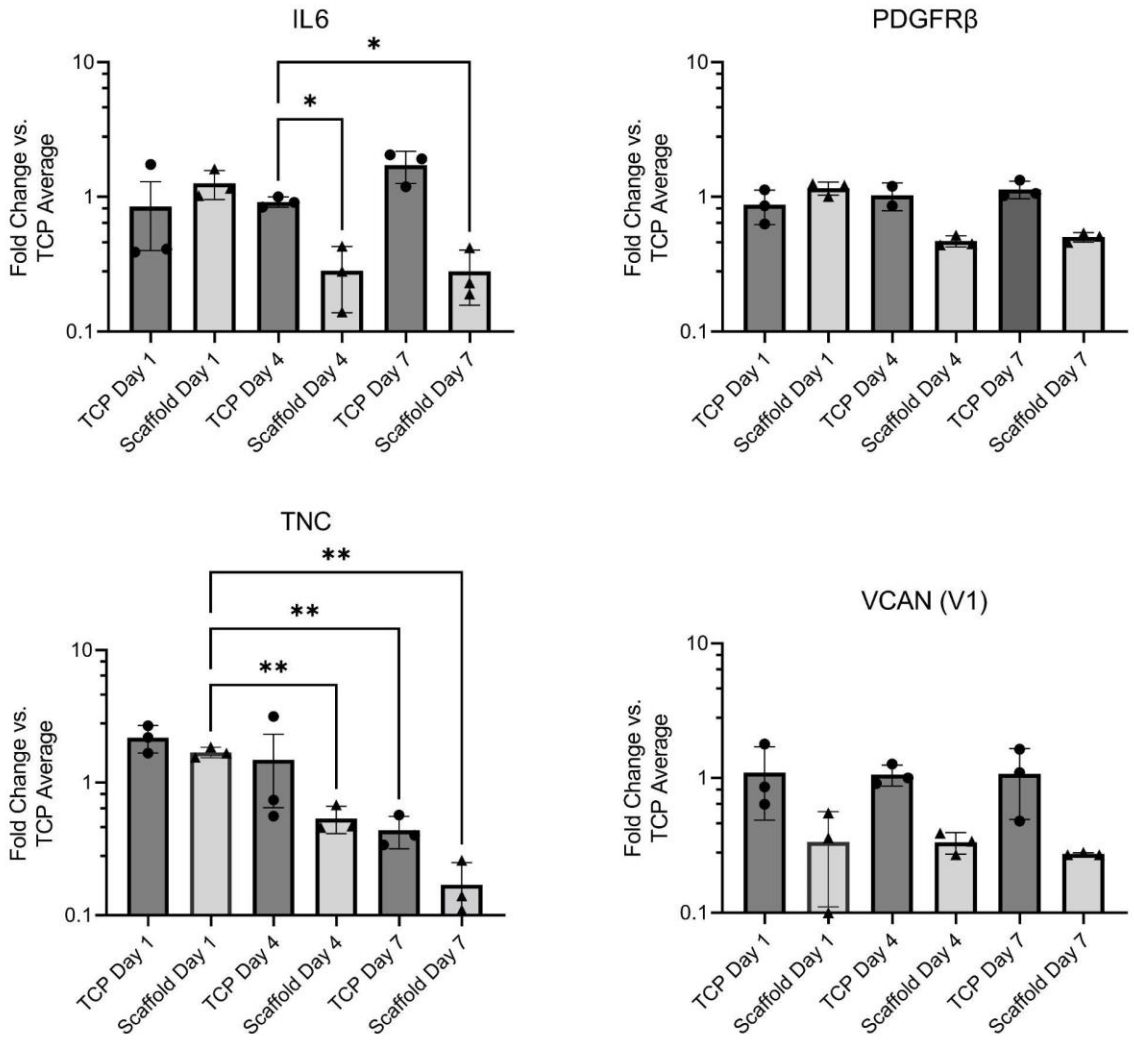

Figure 6.9. *QPCR results showing fold expression levels for IL6, PDGFRβ, TNC and VCAN (V1) versus the average expression in TCP grown NOF. * p < 0.05, ** p < 0.01, *** p < 0.001. Error bars show standard deviation. Biological replicates = 3, technical replicates = 3 (per day).*

6.5. Discussion

Research presented in this chapter was conducted with the aim of investigating the molecular mechanisms that control the low activity fibroblast phenotype characterised in chapter 5. This is important in the context of finding new ways to target fibroblast activation, a major driver of disease in fibrosis and cancer (Plikus, Wang et al. 2021). In a recent example, Mascharack et al. found that mechanical tension in collagen hydrogels drove Engrailed-1 activation in fibroblasts, a process which leads to scarring. By blocking mechanotransduction pathways it was possible to curtail engrailed-1 activation leading to scar free healing (Mascharak, DesJardins-Park et al. 2021). CAF have also been studied in 3D environments, most often in co-cultures with tumour cells. Some research has begun to investigate CAF phenotype control in 3D biomaterials (Cao, Cheng et al. 2021) and to the best of our knowledge our research is the first to show a reduction in CAF traits as a function of their culture environment.

Many aspects of fibroblast activation behaviour have been investigated in an array of 3D biomaterials (Woodley, Lambert et al. 2022). The ability to control individual aspects of the electrospun scaffold microarchitecture and mechanical properties provides the opportunity to build upon previous studies (Woodley, Lambert et al. 2022). One pathway that had been previously hypothesised to control fibroblast proliferation in collagen gels was the MAPK/ERK pathway (Rosenfeldt and Grinnell 2000). Reduced phosphorylation of p44 and p42 MAPK, also referred to as extracellular signal-regulated kinase (ERK) 2 and 1 respectively, was identified in relaxed collagen gel cultures (Rosenfeldt and Grinnell 2000). As proliferation in monolayer cultures is anchorage-dependent and acts via the MAPK pathway, it was hypothesised that reduced MAPK phosphorylation was responsible for the fall in proliferation in relaxed collagen gel cultures. As the study compared both relaxed gels and gels under tension, it was suggested that mechanical stimuli may be integrated into the MAPK pathway. It was proposed that disruption to integrin association with Src homology 2 domain containing adapter protein regulated the MAPK pathway (Rosenfeldt and Grinnell 2000). Our work in this

chapter began with attempts to understand whether the MAPK pathway was involved in regulating the fibroblast phenotype in the ES scaffolds.

Western blotting was used as a technique to quantify MAPK phosphorylation. Issues surrounding cell lysis and protein separation limited the scope of this work. When cell free scaffolds were lysed using TRI reagent, a BCA assay indicated that protein was present, despite the absence of both cells and media. This led to an overestimation of the protein concentration isolated from scaffold NOF. Furthermore, ponceau staining indicated that proteins were aggregating in one dense band at 66 kDa, the weight of bovine serum albumin. Protein extraction using RIPA buffer produced a normal ponceau staining pattern, indicating successful protein isolation and separation for TCP NOF. However, it was not possible to extract enough protein from NOF grown on electrospun scaffolds using the RIPA buffer.

Having struggled to successfully isolate proteins from NOF grown on the ES scaffolds, another method was required to investigate the molecular changes driving the fibroblast phenotype. Having successfully isolated RNA from the scaffolds for qPCR, it was logical to continue this work, looking for transcriptional changes on a larger scale. To do so RNA was extracted and whole genome sequencing was conducted. The first phase of the RNA sequencing was quality control. The 28s/18s ratio has been shown to produce inconsistent results (Schroeder, Mueller et al. 2006) and therefore it is important to combine with data collected from a fragment analyzer. An RQN of 10 was calculated for all our samples. Small peaks and an elevated baseline below 200 nt on an electropherogram trace are indicative of small RNA, usually tRNA and degraded RNA. A significant peak in this region would indicate the presence of a large amount of degraded RNA and would lower a sample's RQN. Assured that RNA quality was high, sample similarity assessments were conducted. Sample similarity analysis is based on hit count data and the sample similarity heatmap indicated that RNA samples from TCP were closely related. There was more variation in RNA samples from Scaffold grown NOF although total variation was still low. Electrospun scaffolds are likely to introduce more variance than tissue culture plastic surfaces which are entirely uniform and have almost no inter-batch

variability. RNA sequencing produces a highly dimensional matrix of transcriptome profiles with rows of genes and columns for each experimental sample (Marini and Binder 2019). Principal component analysis (PCA) is a method for reducing the dimensionality of large datasets to enable a better interpretation of its variance (Jolliffe and Cadima 2016). PCA analysis showed that TCP and scaffold samples formed separate groups with principal component 1 (PC1) showing a large variance of 91.84%. This indicates that gene expression differences exist between the groups (Conesa, Madrigal et al. 2016). Any outliers could be identified at this stage of NGS analysis. Sample similarity assessments indicated that the experimental conditions were responsible for the largest variance in data, with TCP and scaffold samples grouping.

Next the DEseq2 method was used to generate fold changes in gene expression based on hit count data (Love, Huber et al. 2014). An over representation analysis (ORA) volcano plot was used to identify the top 10 most significantly enriched (FDR) gene ontology groups. The analysis appears to favour smaller GO groups. Larger groups which overlapped with more DE genes had lower enrichment ratios than smaller groups which overlapped with fewer genes. Whilst it was not possible to quantify MAPK phosphorylation using western blotting, GO:0070372 - regulation of ERK1 and ERK2 cascade, was significantly enriched in the ORA analysis. The DE genes that overlapped with the GO term all acted to suppress activation of the pathway. DE receptor tyrosine kinase (RTK) genes were universally downregulated in the scaffold cultured NOF including FLT1, EPHA5, IGF1R, KIT, LTK and PDGFRβ. FGFR is the gene which encodes the fibroblast growth factor receptor, a receptor which has tyrosine kinase activity and stimulates the MAPK pathway. FGFR was downregulated along with mitogens FGF2 and FGF18. Alongside a reduction in cell surface receptor expression and activation, MAPK pathway inhibitors were upregulated including SPRY1, SPRY2, DUSP6 and PTPN22. When activated sprouty (SPRY) 1 and 2 bind to Grb2 and inhibit the recruitment of the Grb2-SOS complex to the FGFR associated docking protein FRS2 or Shp6, to regulate the MAPK cascade (Hanafusa, Torii et al. 2002). DUSP6, also known as MKP3 is a dual specificity

phosphatase that dephosphorylates P44/P42 MAPK (ERK 2/1) (Muda, Boschert et al. 1996, Kim, Rice et al. 2003). Taken together this RNA sequencing data shows that at multiple levels the MAPK pathway is subject to transcriptional regulation which reduces pathway activation in scaffold culture. It also supports the hypothesis that the MAPK pathway could be a therapeutic target in diseases with fibroblast activation.

There has been a great deal of research aimed at targeting the MAPK pathway therapeutically, particularly in cancer research (Braicu, Buse et al. 2019). However, most pathway inhibitors have been shown to trigger drug resistance in tumour cells due to compensatory methods of activation within tumour cells and the tumour microenvironment (Braicu, Buse et al. 2019). The importance of using appropriate 3D culture environments to study cancer therapeutics and drug resistance was highlighted in a 2010 study by Weigelt et al. Human epidermal growth factor receptor type 2 (HER2) amplification and overexpression is present in up to 20% of all breast cancers and is associated with a poor prognosis (Weigelt, Lo et al. 2010). HER2 promotes proliferation through both the MAPK and AKT signalling pathways (Yarden and Sliwkowski 2001). When breast cancer cell lines with HER2 amplification were cultured in 2D and 3D their responses to HER2 targeted therapeutics Trastuzumab, Pertuzumab and Lapatinib varied (Weigelt, Lo et al. 2010). The variation in drug sensitivity appeared to be the result of a switch from PI3K-AKT signalling in monolayer cultures to RAS-MAPK signalling in 3D reconstituted ECM gels (Weigelt, Lo et al. 2010). Furthermore, β1 integrin inhibition magnified the cellular response to HER2 therapies in 3D cultures but not in 2D (Weigelt, Lo et al. 2010). Whether such mechanisms also exist in fibroblasts remains to be seen.

The final section of this chapter focuses on the culture of cancer associated fibroblasts (CAF) on the electrospun scaffold. As for normal fibroblasts, CAF can be difficult to define. Elongated cells that lack markers for epithelial or endothelial cells and contain mesenchymal markers such as vimentin are generally considered CAF (Sahai, Astsaturov et al. 2020). There has also been some concern within the field that culturing CAF in vitro may diminish certain CAF traits as passage number increases (Sahai, Astsaturov et al. 2020). As CAF play a crucial role

in cancer progression, understanding how matrix conditions control cellular behaviour using the electrospun scaffold could ultimately help us target CAF therapeutically. Furthermore, understanding how the electrospun scaffold influences CAF behaviour may also enable the selection of ECM targeting therapies to modify CAF and tumour cell behaviour in vivo (Belhabib, Zaghdoudi et al. 2021).

A selection of fibroblast and CAF biomarkers were used for qPCR including ACTA2 (α-SMA), FAP (fibroblast activation protein α), S100A4 (FSP1), TNC (tenascin-C), PDGFRβ (platelet-derived growth factor receptor β), FN1 (fibronectin), VCAN (V1) (versican) and IL6 (interleukin 6) (Han, Liu et al. 2020, Nurmik, Ullmann et al. 2020). None of the markers are entirely specific to CAF (Han, Liu et al. 2020). There is significant overlap with the markers of fibroblast activation and several of these genes were used during NOF qPCR in chapter 5 allowing for comparison. Sample variance within the experimental groups was larger in CAF qPCR than during previous qPCR with NOF, this led to fewer statistically significant differences. ACTA2 expression was significantly lower in electrospun scaffold grown CAF, mirroring the observations with NOF and TGFβ activated NOF. FAP is regularly used alongside ACTA2 as a CAF marker. In contrast to the dramatic and instant reduction in ACTA2 expression levels, FAP expression gradually diminished in scaffold grown CAF. This would suggest that the regulation of FAP and ACTA2 does not occur in the same manner in the scaffold. FAP was initially considered a therapeutic target in cancer treatment, however FAP has been shown to be differentially expressed in CAF sub-populations taken from colorectal cancers (Li, Courtois et al. 2017). It is also expressed in cancer associated cells of epithelial original that have undergone epithelial to mesenchymal transition (EMT) (Kahounova, Kurfurstova et al. 2018) reducing its value as it is not a specific marker (Nurmik, Ullmann et al. 2020).

S100A4 (FSP1) is a generic fibroblast marker (Nurmik, Ullmann et al. 2020) and as with the generic marker vimentin's expression in NOF, scaffold culture did not alter its expression levels. IL6 is an inflammatory cytokine expressed by some CAF subpopulations with tumour promoting qualities (Ohlund, Handly-Santana et al. 2017, Han, Liu et al. 2020). IL6 expression

was significantly lower in the scaffold after 4 and 7 days in culture compared with TCP expression on day 4. The time dependent reduction of IL6 expression was not observed in NOF qPCR. PDGFRβ is a RTK which has been associated with many tumour types (Heldin 2013), however it is not upregulated in CAF populations (Gascard and Tlsty 2016, Nurmik, Ullmann et al. 2020). TNC is an ECM glycoprotein that is highly expressed in the tumour microenvironment (Xia, Lal et al. 2016). Alongside ACTA2 and S100A4, TNC was shown to be a poor prognostic marker in cervical cancers (Xia, Lal et al. 2016). Whilst TNC expression was reduced at day 4 and day 7 of scaffold culture, there was no significant difference when compared with TCP expression at equivalent timepoints. VCAN is another extracellular glycoprotein that has been associated with the inflammatory stage of several diseases including cancer (Wight, Kang et al. 2020). Average VCAN expression over the duration of the experiment was significantly reduced in scaffold culture, as it was in NOF.

Studies in which tumour cells are cultured in 3D are becoming increasingly common (Pape, Emberton et al. 2021). Most research focuses on tumour cells rather than stromal cells however some studies do focus on CAF. CAF have been used to generate ECM matrices with cancer stroma-like properties that can trigger the activation of normal fibroblasts (Amatangelo, Bassi et al. 2005). CAF have also been co-cultured with tumour cells in 3D models (Gaggioli, Hooper et al. 2007, Miki, Ono et al. 2012, Yamaguchi and Sakai 2015, Lugo-Cintron, Gong et al. 2020, Millet, Bollmann et al. 2022). However, there has been very little work conducted with a focus on CAF phenotype as a feature of 3D microenvironments such as the ES scaffold. One recent study reported that high fibre density and hydrogel stiffness in a collagen-alginate interpenetrating network generated distinct inflammatory CAF that had low ACTA2 expression and high IL6 expression (Cao, Cheng et al. 2021). Conversely lower collagen fibre density and a softer gel favoured myofibroblastic CAF with high ACTA2 and low IL6 expression (Cao, Cheng et al. 2021). With CAF markers such as ACTA2 and tumour promoting IL6 expression reduced in our ES scaffold, further work is required to elucidate the molecular control of CAF within the scaffold microenvironment. Further work could help to distinguish whether CAF

grown on the ES scaffold are closer in phenotype to the myofibroblast or inflammatory CAF described in the previous study. Whether the same pathways such as MAPK that are downregulated in NOF RNA sequencing are also downregulated in CAF remains to be seen.

6.6. Conclusion

The work in this chapter was completed with the aim of demonstrating future applications for the electrospun polycaprolactone scaffold in growing our understanding of how matrix conditions may contribute to disease states with fibroblast involvement. Our research began with attempts to identify whether the MAPK pathway was activated in electrospun scaffolds before progressing to next generation RNA sequencing. We demonstrated how differential gene expression can be used to probe for up and down regulated pathways in the low-activity NOF phenotype observed on this scaffold. In this chapter it was also demonstrated that oral CAF can be returned to a lower-activity state with reduced expression of key CAF markers, some of which have been associated with a poor disease prognosis. Understanding which pathways are involved may present therapeutic targets to reduce CAF activation. The next step for this research is to introduce scaffold modifications, to test how individual features of the scaffold micro-architecture and chemical composition combine to regulate this phenotype. This research is significant as targeting CAF in the tumour stroma via direct modulation of the ECM has been identified as a possible therapeutic target (Belhabib, Zaghdoudi et al. 2021).

Chapter 7: General Discussion

7.1. Chapter 4 - Major Findings and Experimental Limitations

In chapter 4 work began to validate the previous observations of an MSc student, Dr Amanpreet Kaur, who was working under the supervision of Dr Ortega Asencio. This involved creating electrospun scaffolds using parameters previously optimised by Dr Martin Eduardo Santocildes Romero. The decision was made to switch to a medical grade polymer, purasorb PC 12 polycaprolactone, as it would be easier to translate this research for clinical applications. Given that the use of different MW polymers led to variable scaffold properties, including the appearance of beading at higher polymer concentrations, the decision to stick to one polymer from the outset of the project was justified. Due to the sensitivity of fibroblasts to changes in scaffold fibre diameter (Chen, Patra et al. 2007), changing the polymer would have required experimental repetition.

The scaffolds produced were characterised to ensure inter-batch consistency and to establish scaffold microarchitectural properties. This work exposed one of the challenges in the field of biomaterial research, a consistent approach to characterisation parameters and methodology between studies. For example, electrospun scaffold porosity has been quantified using numerous techniques including SEM image analysis, capillary flow porometry, liquid extrusion and mercury intrusion porosimetry (MIP). For this reason, two characterization methods, SEM and MIP, were used in this study. Another limitation encountered was the difficulty of measuring scaffold micro-mechanical properties. Atomic force microscopy (AFM) can be used to measure the elastic modulus of individual fibres (Stachewicz, Bailey et al. 2012). However, the challenge of mathematically accounting for strut length and the proximity of adjacent fibres combined with the physical challenge of moving a highly sensitive AFM probe across the porous surface of an ES scaffold, put this work out of reach. Given our objectives and the timescale of this project we used a uniaxial tensile tester to quantify whole scaffold macro-mechanical properties.

Once inter-batch consistency was confirmed and scaffold properties were established, work began to validate the observation made by Dr Kaur, that 3T3 fibroblasts had reduced growth rates on electrospun scaffolds. Tissue culture plastic (TCP) was selected as a 2D control as it was used in the preliminary studies of Dr Kaur. The decision to continue to use TCP was taken as it provided a consistent baseline against which to measure the behaviour of fibroblasts grown on the scaffold. Glass coverslips were also used as 2D controls for several of the assays when imaging was required. The surface chemistries of glass and TCP are not identical however they are often used interchangeably to facilitate easier immunohistochemical staining and microscopy. There have been almost no published studies that compare the properties of both tissue culture plastic and glass. To progress towards a greater understanding of the cues controlling fibroblast behaviour it will be important to move beyond TCP and glass as 2D control surfaces. Potential alternatives are discussed in section 7.4, future perspectives. Using cell viability and dsDNA quantification assays it was possible to confirm that 3T3 fibroblast populations grew at a reduced rate over the course of 7 days in culture. Given the role of fibroblast activation behaviour in human disease the studies were repeated using human fibroblasts. As primary human cells, normal oral fibroblasts (NOF) were more appropriate for investigating human conditions than the immortalised 3T3 mouse fibroblasts (Thonemann, Schmalz et al. 2002). Live dead staining of NOF showed that cell death was not the cause of reduced fibroblast population growth on electrospun scaffolds.

7.2. Chapter 5 - Major Findings and Experimental Limitations

Chapter 4 established the 15% PCL electrospun scaffold as an ECM model upon which NOF grew at a reduced rate. In chapter 5 the scaffold NOF phenotype was evaluated with a focus on activation characteristics. Immunofluorescent detection of Ki67 indicated that a greater proportion of NOF accumulate in cell cycle phase G0 when grown on ES scaffolds than on 2D glass coverslips. Subsequent qPCR suggested that this was due to cellular quiescence and not senescence as there was no difference in the expression of senescence associated genes, CDKN1A (p21), CDKN2A (p16) or IL6 between the TCP and scaffold NOF. This was supported

through a comparison of gene expression with quiescent and senescent induced NOF. Work to establish whether there was a difference in genetic markers of fibroblast quiescence could also have supported the hypothesis that fibroblasts were quiescent. Whilst CD39 expression has been used to identify non-CAF tissue resident fibroblasts in mice (Agorku, Langhammer et al. 2019), it is not a commonly used marker of quiescence. CD39 has in fact been used as a marker of activation in B-lymphocytes (Dwyer, Deaglio et al. 2007). There are many studies that report on markers of stem cell quiescence like p21, p27 and p57 (Urban and Cheung 2021) and whilst the genetic regulation of quiescence is likely to be conserved, fibroblast quiescence is often overlooked (Agorku, Langhammer et al. 2019). Subsequent qPCR in chapter 5 examined the expression of fibroblast activation markers like α-SMA (Hinz 2007) and ECM proteins deposited by activated fibroblasts including collagen (Desmouliere, Geinoz et al. 1993, Tomasek, Gabbiani et al. 2002) and versican (Sheng, Wang et al. 2005). These genes could have also been detected as proteins, using immunofluorescence or western blotting to validate RNA expression levels. In section 7.3 attempts to adapt traditional protein isolation and lysis strategies used in western blotting for use in our electrospun scaffold are discussed.

Finally in chapter 5 fibroblast morphology was investigated. SEM images showed how fibroblasts attach to multiple fibres and are distributed within the first few layers of the scaffold. The grayscale images made it challenging to identify the shape of individual fibroblasts where cells overlapped and extracellular protein was deposited. Immunofluorescent images revealed that NOF were smaller when grown on the scaffold but were otherwise morphologically similar to TCP NOF with slender bipolar projections. More background fluorescence within cell bodies limited the ability to quantify the presence of smaller structures such as focal adhesions in scaffold grown NOF, although larger structures such as nuclei stained with Ki67 antibodies remained easy to quantify. One aspect of fibroblast activation behaviour that was not investigated was motility. Live cell microscopy and cell tracking or a modified scratch assay could have been used to quantify fibroblast motility on the electrospun scaffold. Similar work

has been conducted to quantify endothelial cell migration on electrospun scaffolds with aligned fibres (Ahmed, Ramos et al. 2018). Briefly, a bar placed perpendicularly to the electrospun fibres was used to cover a region of the scaffold surface during seeding. It was removed once cells had attached to the scaffold. Fibroblasts were imaged repeatedly over a period of 48 hours and movement into the space created by the bar was quantified using a Cell Profiler (Broad Institute) pipeline developed by the authors (Ramos, Ahmed et al. 2015). However, the challenge of accounting for a rougher topography that occurs due to the randomly oriented fibres in our scaffold and the lack of directional guidance that was present in the aligned scaffold used by Ahmed et al, adds to the complexity of this research.

7.3. Chapter 6 - Major Findings and Experimental Limitations

Having produced a scaffold in chapter 4 and in chapter 5 reported on the reduced activation traits of scaffold cultured NOF, chapter 6 documented attempts to explore how this culture environment could be used in disease modelling. This involved looking for the pathways that control fibroblast activation and culturing CAF on the scaffold. Limited by challenges encountered when isolating protein from the electrospun scaffold, investigations into activation of the MAPK pathway through p42/p44 MAPK phosphorylation were unsuccessful. With further optimisation it may be possible to improve the amount of protein isolated from the scaffold. Alternative approaches could include immunohistochemistry accompanied by quantification. This could also be used to support and enhance the qPCR results collected in chapter 5 by showing protein distribution across the scaffold surface.

Next generation sequencing was used as an alternative approach to investigate the genetic pathways that were altered in scaffold grown NOF. Our research revealed that the MAPK pathway was downregulated in scaffold NOF, with receptor tyrosine kinase genes downregulated and pathway inhibitors upregulated. The genes identified represent potential targets to curtail fibroblast activation therapeutically. Evidence of a differential resistance to HER2 targeted cancer therapies in 2D and 3D cultures (Weigelt, Lo et al. 2010) highlighted the importance of models such as the one described in this thesis for disease modelling and

drug screening. As such, the final area of research considered in this thesis was the application of the electrospun scaffold for CAF culture. To the best of our knowledge, we are the first to report on a reduction in the expression of several classical CAF markers in a 3D scaffold. This work once again establishes the electrospun scaffold as a valuable model for the study of diseases with fibroblast involvement.

7.4. Future Perspectives

Based on the results presented in chapters 4, 5 and 6 and the limitations detailed in chapter 7, there are several ways in which this research could progress.

1. Determine which aspects of the scaffold microarchitecture, chemical composition and mechanical properties control the low activity fibroblast phenotype.

At present it is impossible to say whether the elastic modulus of the scaffold, its fibrous 3D microarchitecture, the chemical composition of polycaprolactone, or a combination of all three features regulates fibroblast behaviour. Collagen gels revealed cellular mechanosensing is a key regulator of fibroblast fate (Grinnell 1994). Whilst our scaffolds are not as stiff as 2D TCP they are far stiffer than collagen gels and most soft tissues of the body (Liu, Zheng et al. 2015). As such, any future work would require accurate mechanical characterization of scaffold micromechanical properties. The scaffold's fibrous architecture does not give rise to large spread cells that have a high degree of apico-basolateral polarity as seen on planar surfaces. A reduction in polarisation did not significantly reduce α-SMA expression in hydrogel sandwich culture but did in 3D hydrogel culture (Smithmyer, Cassel et al. 2019). Like the sandwich culture, our scaffold reduces NOF polarity whilst enabling cell spreading and cell-cell contacts that are lost when cells are encapsulated in 3D hydrogels. As α-SMA expression is reduced in our electrospun scaffold but not in gel sandwich cultures, other features must contribute to fibroblast behaviour in the scaffold. Finally in terms of scaffold chemical properties, scaffold sterilisation and pre-wetting with culture media increases hydrophilicity, ultimately encouraging cellular attachment during seeding (Ferrari, Cirisano et al. 2019). However, the surface has

not been optimised for cellular attachment and protein adsorption in the same manner as the TCP controls used in our research. Air plasma treatment is one commonly used method to increase the hydrophilicity of electrospun scaffolds (Mozaffari and Gashti 2022). Focal adhesions were observed in NOF grown on 2D PCL films but not in the 3D electrospun scaffolds. Optimisation is required to test whether this was a result of imaging challenges like background fluorescence in scaffold grown NOF. Given what we already know about the scaffold properties outlined above, achieving objective 1 would require the production of multiple new control scaffolds and 2D polycaprolactone films. Comparing a 2D PCL film with an electrospun scaffold would decouple chemical properties from microarchitectural ones. Measuring and seeking to control the elastic modulus of scaffold fibres would decouple microarchitecture and chemical properties from mechanical ones. Through extensive comparisons of fibroblast behaviour and gene expression it is possible to develop our understanding of fibroblast activation cues in the electrospun scaffold. A greater understanding of the pathways involved in a relevant 3D model would provide fresh therapeutic targets and grow our knowledge of fibroblast biology.

2. Seek opportunities to develop clinically relevant models of tissue regeneration and cancer progression.

The electrospun PCL scaffold gives rise to more physiologically appropriate low-activity fibroblasts that better represent the quiescent tissue resident fibroblasts of the healthy adult stroma. There is a need for more appropriate 3D models for use in early-stage drug discovery and trials (Breslin and O'Driscoll 2013, Belfiore, Aghaei et al. 2021). This was evident in the research on differential drug efficacy in HER2 targeted cancer therapies presented in section 7.3. (Weigelt, Lo et al. 2010). Drug discovery and validation is a challenging and expensive process with only 3.4% of cancer trials progressing from phase 1 trials to regulatory approval between 2000 and 2015 (Wong, Siah et al. 2019). Many factors contribute to trial failure including funding depletion, poor trial design and patient recruitment, the presence of side effects or poor drug metabolism (Fogel 2018). However, in a study of 650 phase 3 clinical

trials, 57% failed during clinical development, with 54% of them failing due to inadequate drug efficacy (Hwang, Carpenter et al. 2016). These studies identify the need for higher quality target validation models, allowing for a 'fail-fast' system that reduces the number of poor pre-clinical candidates entering clinical trials (Belfiore, Aghaei et al. 2021). Appropriate in vitro models are one way to achieve this aim alongside animal studies. Animal studies are heavily relied upon for drug toxicity testing. However, recent evidence has suggested that animal models may not always accurately predict the toxicity of a drug in humans (Van Norman 2019). Tissue engineered models have been identified as one of the possible solutions to this problem (Van Norman 2020).

Beyond possible uses in preclinical drug testing, a model that maintains quiescent fibroblast populations could help to develop other tissue engineering aspirations. For example, the incorporation of stromal cells like fibroblasts, maintained in an in vivo-like state, will enhance the complexity and biomimicry of stem cell niche models. The stem cell niche is the physical microenvironment in which adult stem cells reside and where external cues converge to control stem cell fate (Ferraro, Lo Celso et al. 2010). Within the niche, cell-cell and cell-matrix interactions as well as biochemical cues influence stem cell gene regulation (Ferraro, Lo Celso et al. 2010). Harnessing adult stem cells that can self-renew and differentiate, could transform the treatment of both acute injuries and genetic conditions (Lutolf and Blau 2009). To do so requires an interdisciplinary approach that combines every aspect of the stem cell niche. In recent years there have been many attempts to mimic the microarchitectural features of stem cell niches (Ramos-Rodriguez, MacNeil et al. 2021) as well as to mimic biological and molecular features that govern the stem cell microenvironment (Lutolf and Blau 2009). However, introducing stromal support cells into artificial microenvironments has yet to become common practice.

Some characterisations of niche support cell-stem cell interactions have been carried out in invertebrate model organisms (Jones and Wagers 2008). Cadherin-mediated attachment anchors stem cells to niche support cells in the *Drosophila* ovary (Song and Xie 2002, Song,

Zhu et al. 2002) and such connections between niche hub cells and germline stem cells (GSC) may influence GSC asymmetric division (Yamashita, Jones et al. 2003). Mammalian stem cell niches are less well defined; however, they have been characterised in the intestinal crypt of the gut (Barker, van Es et al. 2007) in the skin (Levy, Lindon et al. 2005), muscle (Kuang, Kuroda et al. 2007), bone marrow (Calvi, Adams et al. 2003, Zhang, Niu et al. 2003) and the subventricular zone of the central nervous system (Doetsch, Caille et al. 1999). One stem cell niche where fibroblasts' roles have been explored is in the rete ridges of the skin, where epithelial stem cells (ESC) exist close to the dermis and the interlocking dermal papilla (Lawlor and Kaur 2015). In in vitro studies, fibroblasts were shown to play a vital role in the production and maintenance of the basal membrane to which ESCs attach (Marinkovich, Keene et al. 1993, Andriani, Margulis et al. 2003, El Ghalbzouri, Jonkman et al. 2005). Beyond generating the structures to which ESCs can anchor (Lawlor and Kaur 2015), fibroblasts were able to enhance keratinocyte outgrowth in collagen gels through the release of diffusible factors (Tuan, Keller et al. 1994).

The importance of incorporating stromal cells such as fibroblasts into tissue engineered skin constructs alongside keratinocytes has been recognised for several decades (Delvoye, Pierard et al. 1988, Konig and Brucknertuderman 1991). The goal is to produce thick, fully stratified skin constructs with an intact basement membrane (Bottcher-Haberzeth, Biedermann et al. 2010). Topographically controlled microfabricated scaffolds have been used to generate more appropriate models (Ramos-Rodriguez, MacNeil et al. 2021). However, in these constructs, little attention is paid to the complex behaviour of fibroblasts or their role in the creation of an artificial microenvironment which best mimics the ESC niche. Alongside models of regeneration such as tissue engineered skin, cancer models can also be enhanced through the incorporation of both quiescent fibroblasts and activated CAF (Cao, Cheng et al. 2021).

Covid-19 Impact Statement

In March 2020, The University of Sheffield closed in response to the coronavirus pandemic. The University was closed to postgraduate research students for four months. Upon our return to campus on the 22nd of July 2020, laboratory research was limited to just 10 hours per week for each student. These measures were in place for the next 12 months to ensure the safety of staff, students and the wider community of Sheffield.

Despite these restrictions I was able to adapt my research to mitigate their impact on my project. During the March-July lockdown, I set goals that could be achieved outside of the laboratory. I completed my first-year confirmation review based on the research I had completed during the first 6 months of my PhD. I then worked to adapt my literature review into a review paper which was subsequently published in the journal Tissue Engineering Part B: Reviews (Woodley, Lambert et al. 2022). I was also proud to share my work at two online conferences, presenting a poster at the World Biomaterials Congress and giving a podium presentation to the White Rose Biomaterials and Tissue Engineering Group (BiTEG).

Upon my return to the laboratory careful planning was required to ensure that maximum productivity was achieved during the limited experimental time allocated to me each week. Once again I was able to use the extra time outside of the laboratory to progress to towards the publication of my research in the journal Bioengineering (Woodley, Lambert et al. 2023). Finally, I used this time to successfully apply for a 3-month stipend extension, granted by the University and the Engineering and Physical Sciences Research Council (EPSRC).

I am proud of the work I completed during the pandemic period and the funding extension enabled me to spend an extra 3 months in the laboratory. However, it is important to acknowledge the impact that COVID-19 had on this research thesis. A significant amount of laboratory time was lost and the amount of experimental data collected was consequently reduced, despite our extensive steps towards mitigation.

License to Reproduce Published Content

MARY ANN LIEBERT, INC. LICENSE

TERMS AND CONDITIONS

Jul 04, 2023

This Agreement between The University of Sheffield -- Joe Woodley ("You") and Mary Ann Liebert, Inc. ("Mary Ann Liebert, Inc.") consists of your license details and the terms and conditions provided by Mary Ann Liebert, Inc. and Copyright Clearance Center.

License Number: 5581861491261

License date: Jul 04, 2023

Licensed Content Publisher: Mary Ann Liebert, Inc.

Licensed Content Publication: Tissue Engineering Part B: Reviews

Licensed Content Title: Understanding Fibroblast Behavior in 3D Biomaterials.

Licensed Content Author: Joe P. Woodley, Daniel W. Lambert, Ilida Ortega Asencio

Licensed Content Date: Jun 1, 2022

Licensed Content Volume: 28

Licensed Content Issue: 3

Type of Use: Dissertation/Thesis

Requestor type: author of the original work

Format: print and electronic

Portion: full article

Distribution quantity:10

Title: Mr. Joe P Woodley

Institution name: The University of Sheffield

Expected presentation date: Jul 2023

Licensed Content Title: Reduced Fibroblast Activation on Electrospun Polycaprolactone Scaffolds

References

Agorku, D. J., A. Langhammer, U. Heider, S. Wild, A. Bosio and O. Hardt (2019). "CD49b, CD87, and CD95 Are Markers for Activated Cancer-Associated Fibroblasts Whereas CD39 Marks Quiescent Normal Fibroblasts in Murine Tumor Models." *Frontiers in Oncology* 9: 13.

Ahmed, M., T. Ramos, P. Wieringa, C. van Blitterswijk, J. de Boer and L. Moroni (2018). "Geometric constraints of endothelial cell migration on electrospun fibres." *Scientific Reports* 8: 10.

Alcorta, D. A., Y. Xiong, D. Phelps, G. Hannon, D. Beach and J. C. Barrett (1996). "Involvement of the cyclin-dependent kinase inhibitor p16 (INK4a) in replicative senescence of normal human fibroblasts." *Proceedings of the National Academy of Sciences of the United States of America* 93(24): 13742-13747.

Alessio, N., D. Aprile, S. Cappabianca, G. Peluso, G. Di Bernardo and U. Galderisi (2021). "Different Stages of Quiescence, Senescence, and Cell Stress Identified by Molecular Algorithm Based on the Expression of Ki67, RPS6, and Beta-Galactosidase Activity." *International Journal of Molecular Sciences* 22(6): 3102.

Amatangelo, M. D., D. E. Bassi, A. J. P. Klein-Szanto and E. Cukierman (2005). "Stroma-derived three-dimensional matrices are necessary and sufficient to promote desmoplastic differentiation of normal fibroblasts." *American Journal of Pathology* 167(2): 475-488.

Andriani, F., A. Margulis, N. Lin, S. Griffey and J. A. Garlick (2003). "Analysis of microenvironmental factors contributing to basement membrane assembly and normalized epidermal phenotype." *Journal of Investigative Dermatology* 120(6): 923-931.

Badylak, S. F., D. O. Freytes and T. W. Gilbert (2009). "Extracellular matrix as a biological scaffold material: Structure and function." *Acta Biomaterialia* 5(1): 1-13.

Bae, W.-G., J. Kim, Y.-H. Choung, Y. Chung, K. Y. Suh, C. Pang, J. H. Chung and H. E. Jeong (2015). "Bio-inspired configurable multiscale extracellular matrix-like structures for functional alignment and guided orientation of cells." *Biomaterials* 69: 158-164.

Bahcecioglu, G., N. Hasirci and V. Hasirci (2018). "Effects of microarchitecture and mechanical properties of 3D microporous PLLA-PLGA scaffolds on fibrochondrocyte and L929 fibroblast behavior." *Biomedical Materials* 13(3): 12.

Bainbridge, P. (2013). "Wound healing and the role of fibroblasts." *Journal of Wound Care* 22(8): 407-412.

Balani, K., V. Verma, A. Agarwal and R. Narayan (2015). Physical, Thermal, And Mechanical Properties Of Polymers. Biosurfaces: a Materials Science and Engineering Perspective. K. Balani, V. Verma, A. Agarwal and R. Narayan. Westerville, Amer Ceramic Soc**:** 329-344.

Barker, N., J. H. van Es, J. Kuipers, P. Kujala, M. van den Born, M. Cozijnsen, A. Haegebarth, J. Korving, H. Begthel, P. J. Peters and H. Clevers (2007). "Identification of stem cells in small intestine and colon by marker gene Lgr5." *Nature* 449(7165): 1003-U1001.

Belfiore, L., B. Aghaei, A. M. K. Law, J. C. Dobrowolski, L. J. Raftery, A. D. Tjandra, C. Yee, A. Piloni, A. Volkerling, C. J. Ferris and M. Engel (2021). "Generation and analysis of 3D cell culture models for drug discovery." *European Journal of Pharmaceutical Sciences* 163: 10.

Belhabib, I., S. Zaghdoudi, C. Lac, C. Bousquet and C. Jean (2021). "Extracellular Matrices and Cancer-Associated Fibroblasts: Targets for Cancer Diagnosis and Therapy?" *Cancers* 13(14): 38.

Beningo, K. A., M. Dembo and Y. I. Wang (2004). "Responses of fibroblasts to anchorage of dorsal extracellular matrix receptors." *Proceedings of the National Academy of Sciences of the United States of America* 101(52): 18024-18029.

Blokland, K. E. C., S. D. Pouwels, M. Schuliga, D. A. Knight and J. K. Burgess (2020). "Regulation of cellular senescence by extracellular matrix during chronic fibrotic diseases." *Clinical Science* 134(20): 2681-2706.

Bottcher-Haberzeth, S., T. Biedermann and E. Reichmann (2010). "Tissue engineering of skin." *Burns* 36(4): 450-460.

Braicu, C., M. Buse, C. Busuioc, R. Drula, D. Gulei, L. Raduly, A. Rusu, A. Irimie, A. G. Atanasov, O. Slaby, C. Ionescu and I. Berindan-Neagoe (2019). "A Comprehensive Review on MAPK: A Promising Therapeutic Target in Cancer." *Cancers* 11(10): 25.

Breslin, S. and L. O'Driscoll (2013). "Three-dimensional cell culture: the missing link in drug discovery." *Drug Discovery Today* 18(5-6): 240-249.

Bucala, R., L. A. Spiegel, J. Chesney, M. Hogan and A. Cerami (1994). "Circulating fibrocytes define a new leukocyte subpopulation that mediates tissue-repair." *Molecular Medicine* 1(1): 71-81.

Bunz, F., A. Dutriaux, C. Lengauer, T. Waldman, S. Zhou, J. P. Brown, J. M. Sedivy, K. W. Kinzler and B. Vogelstein (1998). "Requirement for p53 and p21 to sustain G(2) arrest after DNA damage." *Science* 282(5393): 1497-1501.

Calvi, L. M., G. B. Adams, K. W. Weibrecht, J. M. Weber, D. P. Olson, M. C. Knight, R. P. Martin, E. Schipani, P. Divieti, F. R. Bringhurst, L. A. Milner, H. M. Kronenberg and D. T. Scadden (2003). "Osteoblastic cells regulate the haematopoietic stem cell niche." *Nature* 425(6960): 841-846.

Campisi, J. and F. D. di Fagagna (2007). "Cellular senescence: when bad things happen to good cells." *Nature Reviews Molecular Cell Biology* 8(9): 729-740.

Cao, H., H. S. Cheng, J. K. Wang, N. S. Tan and C. Y. Tay (2021). "A 3D physio-mimetic interpenetrating network-based platform to decode the pro and anti-tumorigenic properties of cancer-associated fibroblasts." *Acta Biomaterialia* 132: 448-460.

Cattaruzza, S. and R. Perris (2005). "Proteoglycan control of cell movement during wound healing and cancer spreading." *Matrix Biology* 24(6): 400-417.

Chang, H. Y., J. T. Chi, S. Dudoit, C. Bondre, M. van de Rijn, D. Botstein and P. O. Brown (2002). "Diversity, topographic differentiation, and positional memory in human fibroblasts." *Proceedings of the National Academy of Sciences of the United States of America* 99(20): 12877-12882.

Chen, H., Y. S. Lui, Z. W. Tan, J. Y. H. Lee, N. S. Tan and L. P. Tan (2019). "Migration and Phenotype Control of Human Dermal Fibroblasts by Electrospun Fibrous Substrates." *Advanced Healthcare Materials* 8(9): e1801378.

Chen, K. D., Y. S. Li, M. Kim, S. Li, S. Yuan, S. Chien and J. Y. J. Shyy (1999). "Mechanotransduction in response to shear stress - Roles of receptor tyrosine kinases, integrins, and Shc." *Journal of Biological Chemistry* 274(26): 18393-18400.

Chen, M., P. K. Patra, S. B. Warner and S. Bhowmick (2007). "Role of fiber diameter in adhesion and proliferation of NIH 3T3 fibroblast on electrospun polycaprolactone scaffolds." *Tissue Engineering* 13(3): 579-587.

Chen, Q. and B. N. Ames (1994). "Senescence-like Growth Arrest Induced by Hydrogen-Peroxide in Human-Diploid Fibroblast F65 Cells." *Proceedings of the National Academy of Sciences of the United States of America* 91(10): 4130-4134.

Chen, X. M. and E. W. Song (2019). "Turning foes to friends: targeting cancer-associated fibroblasts." *Nature Reviews Drug Discovery* 18(2): 99-115.

Cipitria, A., A. Skelton, T. R. Dargaville, P. D. Dalton and D. W. Hutmacher (2011). "Design, fabrication and characterization of PCL electrospun scaffolds-a review." *Journal of Materials Chemistry* 21(26): 9419-9453.

Coller, H. A., L. Y. Sang and J. M. Roberts (2006). "A new description of cellular quiescence." *Plos Biology* 4(3): 329-349.

Colley, H. E., V. Hearnden, A. V. Jones, P. H. Weinreb, S. M. Violette, S. MacNeil, M. H. Thornhill and C. Murdoch (2011). "Development of tissue-engineered models of oral dysplasia and early invasive oral squamous cell carcinoma." *British Journal of Cancer* 105(10): 1582-1592.

Colombo, E. and M. G. Cattaneo (2021). "Multicellular 3D Models to Study Tumour-Stroma Interactions." *International Journal of Molecular Sciences* 22(4): 19.

Colwell, A. S., M. T. Longaker and H. P. Lorenz (2003). "Fetal wound healing." *Frontiers in Bioscience* 8: 1240-1248.

Conesa, A., P. Madrigal, S. Tarazona, D. Gomez-Cabrero, A. Cervera, A. McPherson, M. W. Szczesniak, D. J. Gaffney, L. L. Elo, X. G. Zhang and A. Mortazavi (2016). "A survey of best practices for RNA-seq data analysis (vol 17, 13, 2016)." *Genome Biology* 17: 2.

Coppe, J. P., P. Y. Desprez, A. Krtolica and J. Campisi (2010). The Senescence-Associated Secretory Phenotype: The Dark Side of Tumor Suppression. Annual Review of Pathology-Mechanisms of Disease. Palo Alto, Annual Reviews. **5:** 99-118.

Costa, A., Y. Kieffer, A. Scholer-Dahirel, F. Pelon, B. Bourachot, M. Cardon, P. Sirven, I. Magagna, L. Fuhrmann, C. Bernard, C. Bonneau, M. Kondratova, I. Kuperstein, A. Zinovyev, A. M. Givel, M. C. Parrini, V. Soumelis, A. Vincent-Salomon and F. Mechta-Grigoriou (2018). "Fibroblast Heterogeneity and Immunosuppressive Environment in Human Breast Cancer." *Cancer Cell* 33(3): 463-+.

Cukierman, E., R. Pankov, D. R. Stevens and K. M. Yamada (2001). "Taking cell-matrix adhesions to the third dimension." *Science* 294(5547): 1708-1712.

Cukierman, E., R. Pankov and K. M. Yamada (2002). "Cell interactions with three-dimensional matrices." *Current Opinion in Cell Biology* 14(5): 633-639.

da Cunha, C. B., D. D. Klumpers, W. A. Li, S. T. Koshy, J. C. Weaver, O. Chaudhuri, P. L. Granja and D. J. Mooney (2014). "Influence of the stiffness of three-dimensional

alginate/collagen-I interpenetrating networks on fibroblast biology." *Biomaterials* 35(32): 8927-8936.

Danen, E. H. J. and K. M. Yamada (2001). "Fibronectin, integrins, and growth control." *Journal of Cellular Physiology* 189(1): 1-13.

Davidson, S., M. Coles, T. Thomas, G. Kollias, B. Ludewig, S. Turley, M. Brenner and C. D. Buckley (2021). "Fibroblasts as immune regulators in infection, inflammation and cancer." *Nature Reviews Immunology* 21(11): 704-717.

Delvoye, P., D. Pierard, A. Noel, B. Nusgens, J. M. Foidart and C. M. Lapiere (1988). "Fibroblasts induce the assembly of the macromolecules of the basement-membrane." *Journal of Investigative Dermatology* 90(3): 276-282.

Desmouliere, A., C. Chaponnier and G. Gabbiani (2005). "Tissue repair, contraction, and the myofibroblast." *Wound Repair and Regeneration* 13(1): 7-12.

Desmouliere, A., A. Geinoz, F. Gabbiani and G. Gabbiani (1993). "Transforming Growth-Factor-Beta-1 Induces Alpha-Smooth Muscle Actin Expression in Granulation-Tissue Myofibroblasts and in Quiescent and Growing Cultured Fibroblasts." *Journal of Cell Biology* 122(1): 103-111.

Desmouliere, A., C. Guyot and C. Gabbiani (2004). "The stroma reaction myofibroblast: a key player in the control of tumor cell behavior." *International Journal of Developmental Biology* 48(5-6): 509-517.

Dimancheboitrel, M. T., L. Vakaet, P. Pujuguet, B. Chauffert, M. S. Martin, A. Hammann, F. Vanroy, M. Mareel and F. Martin (1994). "In-vivo and in-vitro invasiveness of a rat colon-cancer cell-line maintaining E-cadherin expression - an enhancing role of tumor-associated myofibroblasts." *International Journal of Cancer* 56(4): 512-521.

Doetsch, F., I. Caille, D. A. Lim, J. M. Garcia-Verdugo and A. Alvarez-Buylla (1999). "Subventricular zone astrocytes are neural stem cells in the adult mammalian brain." *Cell* 97(6): 703-716.

Doshi, J. and D. H. Reneker (1995). "Electrospinning process and applications of electrospun fibers." *Journal of Electrostatics* 35(2-3): 151-160.

Driskell, R. R. and F. M. Watt (2015). "Understanding fibroblast heterogeneity in the skin." *Trends in Cell Biology* 25(2): 92-99.

Dwyer, K. M., S. Deaglio, W. Gao, D. Friedman, T. B. Strom and S. C. Robson (2007). "CD39 and control of cellular immune responses." *Purinergic Signalling* 3(1-2): 171-180.

Ehrmann, R. L. and G. O. Gey (1956). "The growth of cells on a transparent gel of reconstituted rat-tail collagen." *Journal of the National Cancer Institute* 16(6): 1375-&.

El Ghalbzouri, A., M. F. Jonkman, R. Dijkman and M. Ponec (2005). "Basement membrane reconstruction in human skin equivalents is regulated by fibroblasts and/or exogenously activated keratinocytes." *Journal of Investigative Dermatology* 124(1): 79-86.

Elango, J., C. Y. Hou, B. Bao, S. J. Wang, J. de Val and W. H. Wu (2022). "The Molecular Interaction of Collagen with Cell Receptors for Biological Function." *Polymers* 14(5): 25.

Elmusrati, A. A., A. E. Pilborough, S. A. Khurram and D. W. Lambert (2017). "Cancer-associated fibroblasts promote bone invasion in oral squamous cell carcinoma." *British Journal of Cancer* 117(6): 867-875.

Elsdale, T. and J. Bard (1972). "Collagen substrata for studies on cell behavior." *Journal of Cell Biology* 54(3): 626-637.

Farrell, E., M. Aliabouzar, C. Quesada, B. M. Baker, R. T. Franceschi, A. J. Putnam and M. L. Fabiilli (2022). "Spatiotemporal control of myofibroblast activation in acoustically-responsive scaffolds via ultrasound-induced matrix stiffening." *Acta Biomaterialia* 138: 133-143.

Ferrari, M., F. Cirisano and M. C. Moran (2019). "Mammalian Cell Behavior on Hydrophobic Substrates: Influence of Surface Properties." *Colloids and Interfaces* 3(2): 16.

Ferraro, F., C. Lo Celso and D. Scadden (2010). Adult stem cells and their niches. Cell Biology of Stem Cells. E. Meshorer and K. Plath. Berlin, Springer-Verlag Berlin. **695:** 155-168.

Fogel, D. B. (2018). "Factors associated with clinical trials that fail and opportunities for improving the likelihood of success: A review." *Contemporary Clinical Trials Communications* 11: 156-164.

Fong, H., I. Chun and D. H. Reneker (1999). "Beaded nanofibers formed during electrospinning." *Polymer* 40(16): 4585-4592.

Friedman, S. L. (2004). "Mechanisms of Disease: mechanisms of hepatic fibrosis and therapeutic implications." *Nature Clinical Practice Gastroenterology & Hepatology* 1(2): 98-105.

Gabbiani, G. (2003). "The myofibroblast in wound healing and fibrocontractive diseases." *Journal of Pathology* 200(4): 500-503.

Gaggioli, C., S. Hooper, C. Hidalgo-Carcedo, R. Grosse, J. F. Marshall, K. Harrington and E. Sahai (2007). "Fibroblast-led collective invasion of carcinoma cells with differing roles for RhoGTPases in leading and following cells." *Nature Cell Biology* 9(12): 1392-U1392.

Garcia, A. J., M. D. Vega and D. Boettiger (1999). "Modulation of cell proliferation and differentiation through substrate-dependent changes in fibronectin conformation." *Molecular Biology of the Cell* 10(3): 785-798.

Gascard, P. and T. D. Tlsty (2016). "Carcinoma-associated fibroblasts: orchestrating the composition of malignancy." *Genes & Development* 30(9): 1002-1019.

Geesin, J. C., L. J. Brown, J. S. Gordon and R. A. Berg (1993). "Regulation of collagen-synthesis in human dermal fibroblasts in contracted collagen gels by ascorbic-acid, growth factors, and inhibitors of lipid-peroxidation." *Experimental Cell Research* 206(2): 283-290.

Geiger, B., A. Bershadsky, R. Pankov and K. M. Yamada (2001). "Transmembrane extracellular matrix-cytoskeleton crosstalk." *Nature Reviews Molecular Cell Biology* 2(11): 793-805.

Gelse, K., E. Poschl and T. Aigner (2003). "Collagens - structure, function, and biosynthesis." *Advanced Drug Delivery Reviews* 55(12): 1531-1546.

Ghibaudo, M., L. Trichet, J. Le Digabel, A. Richert, P. Hersen and B. Ladoux (2009). "Substrate Topography Induces a Crossover from 2D to 3D Behavior in Fibroblast Migration." *Biophysical Journal* 97(1): 357-368.

Gil, E. S., S.-H. Park, J. Marchant, F. Omenetto and D. L. Kaplan (2010). "Response of Human Corneal Fibroblasts on Silk Film Surface Patterns." *Macromolecular Bioscience* 10(6): 664-673.

Gonzalez-Diaz, E. C. and S. Varghese (2016). "Hydrogels as Extracellular Matrix Analogs." *Gels* 2(3): 18.

Greiner, A. and J. H. Wendorff (2007). "Electrospinning: A fascinating method for the preparation of ultrathin fibres." *Angewandte Chemie-International Edition* 46(30): 5670-5703.

Grinnell, F. (1994). "Fibroblasts, myofibroblasts, and wound contraction." *Journal of Cell Biology* 124(4): 401-404.

Grinnell, F., C. H. Ho, E. Tamariz, D. J. Lee and G. Skuta (2003). "Dendritic fibroblasts in three-dimensional collagen matrices." *Molecular Biology of the Cell* 14(2): 384-395.

Grinnell, F., L. B. Rocha, C. Iucu, S. Rhee and H. M. Jiang (2006). "Nested collagen matrices: A new model to study migration of human fibroblast populations in three dimensions." *Experimental Cell Research* 312(1): 86-94.

Guo, S. and L. A. DiPietro (2010). "Factors Affecting Wound Healing." *Journal of Dental Research* 89(3): 219-229.

Halloran, C. and J. Slavin (2002). "Pathophysiology of Wound Healing." *Surgery (Oxford)* 20(Issue 5): 1-5.

Han, C. C., T. Y. Liu and R. Yin (2020). "Biomarkers for cancer-associated fibroblasts." *Biomarker Research* 8(1): 8.

Hanafusa, H., S. Torii, T. Yasunaga and E. Nishida (2002). "Sprouty1 and Sprouty2 provide a control mechanism for the Ras/MAPK signalling pathway." *Nature Cell Biology* 4(11): 850-858.

Harley, B. A. C., H. D. Kim, M. H. Zaman, I. V. Yannas, D. A. Lauffenburger and L. J. Gibson (2008). "Microarchitecture of three-dimensional scaffolds influences cell migration behavior via junction interactions." *Biophysical Journal* 95(8): 4013-4024.

Harper, R. A. and G. Grove (1979). "Human-skin fibroblasts derived from papillary and reticular dermis - differences in growth-potential invitro." *Science* 204(4392): 526-527.

Hearnden, V., H. Lomas, S. MacNeil, M. Thornhill, C. Murdoch, A. Lewis, J. Madsen, A. Blanazs, S. P. Armes and G. Battaglia (2009). "Diffusion Studies of Nanometer Polymersomes Across Tissue Engineered Human Oral Mucosa." *Pharmaceutical Research* 26(7): 1718-1728.

Heldin, C. H. (2013). "Targeting the PDGF signaling pathway in tumor treatment." *Cell Communication and Signaling* 11: 18.

Hinz, B. (2007). "Formation and function of the myofibroblast during tissue repair." *Journal of Investigative Dermatology* 127(3): 526-537.

Hinz, B., G. Celetta, J. J. Tomasek, G. Gabbiani and C. Chaponnier (2001). "Alpha-smooth muscle actin expression upregulates fibroblast contractile activity." *Molecular Biology of the Cell* 12(9): 2730-2741.

Htwe, S. S., H. Harrington, A. Knox, F. Rose, J. Aylott, J. W. Haycock and A. M. Ghaemmaghami (2015). "Investigating NF-kappa B signaling in lung fibroblasts in 2D and 3D culture systems." *Respiratory Research* 16: 144.

Hu, M., Z. H. Ling and X. Ren (2022). "Extracellular matrix dynamics: tracking in biological systems and their implications." *Journal of Biological Engineering* 16(1): 13.

Hughes, L. A., J. Gaston, K. McAlindon, K. A. Woodhouse and S. L. Thibeault (2015). "Electrospun fiber constructs for vocal fold tissue engineering: Effects of alignment and elastomeric polypeptide coating." *Acta Biomaterialia* 13: 111-120.

Hui, E., L. Moretti, T. H. Barker and S. R. Caliari (2021). "The Combined Influence of Viscoelastic and Adhesive Cues on Fibroblast Spreading and Focal Adhesion Organization." *Cellular and Molecular Bioengineering* 14(5): 427-440.

Hwang, T. J., D. Carpenter, J. C. Lauffenburger, B. Wang, J. M. Franklin and A. S. Kesselheim (2016). "Failure of Investigational Drugs in Late-Stage Clinical Development and Publication of Trial Results." *Jama Internal Medicine* 176(12): 1826-1833.

Ishii, G., A. Ochiai and S. Neri (2016). "Phenotypic and functional heterogeneity of cancer-associated fibroblast within the tumor microenvironment." *Advanced Drug Delivery Reviews* 99: 186-196.

Ivarsson, M., A. McWhirter, T. K. Borg and K. Rubin (1998). "Type I collagen synthesis in cultured human fibroblasts: Regulation by cell spreading, platelet-derived growth factor and interactions with collagen fibers." *Matrix Biology* 16(7): 409-425.

Jiang, H. M. and F. Grinnell (2005). "Cell-matrix entanglement and mechanical anchorage of fibroblasts in three-dimensional collagen matrices." *Molecular Biology of the Cell* 16(11): 5070-5076.

Jiang, T., E. J. Carbone, K. W. H. Lo and C. T. Laurencin (2015). "Electrospinning of polymer nanofibers for tissue regeneration." *Progress in Polymer Science* 46: 1-24.

Jiang, Y., S. Lu and Y. Zeng (2011). "Dermal fibroblast behaviour on micropatterned substrates with different pattern geometries." *Journal of Tissue Engineering and Regenerative Medicine* 5(5): 402-409.

Jolliffe, I. T. and J. Cadima (2016). "Principal component analysis: a review and recent developments." *Philosophical Transactions of the Royal Society a-Mathematical Physical and Engineering Sciences* 374(2065): 16.

Jones, D. L. and A. J. Wagers (2008). "No place like home: anatomy and function of the stem cell niche." *Nature Reviews Molecular Cell Biology* 9(1): 11-21.

Kabir, T. D., R. J. Leigh, H. Tasena, M. Mellone, R. D. Coletta, E. K. Parkinson, S. S. Prime, G. J. Thomas, I. C. Paterson, D. H. Zhou, J. McCall, P. M. Speight and D. W. Lambert (2016). "A miR-335/COX-2/PTEN axis regulates the secretory phenotype of senescent cancer-associated fibroblasts." *Aging-Us* 8(8): 1608-1635.

Kahounova, Z., D. Kurfurstova, J. Bouchal, G. Kharaishvili, J. Navratil, J. Remsik, S. Simeckova, V. Student, A. Kozubik and K. Soucek (2018). "The fibroblast surface markers FAP, anti-fibroblast, and FSP are expressed by cells of epithelial origin and may be altered during epithelial-to-mesenchymal transition." *Cytometry Part A* 93A(9): 941-951.

Kalluri, R. (2016). "The biology and function of fibroblasts in cancer." *Nature Reviews Cancer* 16(9): 582-598.

Kalluri, R. and M. Zeisberg (2006). "Fibroblasts in cancer." *Nature Reviews Cancer* 6(5): 392-401.

Kanehisa, M. and S. Goto (2000). "KEGG: Kyoto Encyclopedia of Genes and Genomes." *Nucleic Acids Research* 28(1): 27-30.

Karouzakis, E., R. E. Gay, S. Gay and M. Neidhart (2009). "Epigenetic control in rheumatoid arthritis synovial fibroblasts." *Nature Reviews Rheumatology* 5(5): 266-272.

Khan, S., M. Ul-Islam, M. Ikram, M. W. Ullah, M. Israr, F. Subhan, Y. Kim, J. H. Jang, S. Yoon and J. K. Park (2016). "Three-dimensionally microporous and highly biocompatible bacterial cellulose-gelatin composite scaffolds for tissue engineering applications." *Rsc Advances* 6(112): 110840-110849.

Kim, Y., A. E. Rice and J. M. Denu (2003). "Intramolecular dephosphorylation of ERK by MKP3." *Biochemistry* 42(51): 15197-15207.

Konig, A. and L. Brucknertuderman (1991). "Epithelial-mesenchymal interactions enhance expression of collagen-VII in vitro." *Journal of Investigative Dermatology* 96(6): 803-808.

Kono, T., T. Tanii, M. Furukawa, N. Mizuno, J. Kitajima, M. Ishii, T. Hamada and K. Yoshizato (1990). "Cell-cycle analysis of human dermal fibroblasts cultured on or in hydrated type-1 collagen lattices." *Archives of Dermatological Research* 282(4): 258-262.

Kopelovich, L. (1982). "Genetic predisposition to cancer in man: in vitro studies." *International Review of Cytology-a Survey of Cell Biology* 77: 63-88.

Kresse, H. and E. Schonherr (2001). "Proteoglycans of the extracellular matrix and growth control." *Journal of Cellular Physiology* 189(3): 266-274.

Kuang, S. H., K. Kuroda, F. Le Grand and M. A. Rudnicki (2007). "Asymmetric self-renewal and commitment of satellite stem cells in muscle." *Cell* 129(5): 999-1010.

Kuperwasser, C., T. Chavarria, M. Wu, G. Magrane, J. W. Gray, L. Carey, A. Richardson and R. A. Weinberg (2004). "Reconstruction of functionally normal and malignant human breast tissues in mice." *Proceedings of the National Academy of Sciences of the United States of America* 101(14): 4966-4971.

Law, K. Y. (2014). "Definitions for Hydrophilicity, Hydrophobicity, and Superhydrophobicity: Getting the Basics Right." *Journal of Physical Chemistry Letters* 5(4): 686-688.

Lawlor, K. T. and P. Kaur (2015). "Dermal Contributions to Human Interfollicular Epidermal Architecture and Self-Renewal." *International Journal of Molecular Sciences* 16(12): 28098-28107.

Lazard, D., X. Sastre, M. G. Frid, M. A. Glukhova, J. P. Thiery and V. E. Koteliansky (1993). "Expression of smooth muscle-specific proteins in myoepithelium and stromal myofibroblasts

of normal and malignant human breast-tissue." *Proceedings of the National Academy of Sciences of the United States of America* 90(3): 999-1003.

LeBleu, V. S. and E. G. Neilson (2020). "Origin and functional heterogeneity of fibroblasts." *Faseb Journal*: 18.

Leitinger, B. and E. Hohenester (2007). "Mammalian collagen receptors." *Matrix Biology* 26(3): 146-155.

Lendahl, U., L. Muhl and C. Betsholtz (2022). "Identification, discrimination and heterogeneity of fibroblasts." *Nature Communications* 13(1): 14.

Levy, V., C. Lindon, B. D. Harfe and B. A. Morgan (2005). "Distinct stem cell populations regenerate the follicle and interfollicular epidermis." *Developmental Cell* 9(6): 855-861.

Li, H. P., E. T. Courtois, D. Sengupta, Y. L. Tan, K. H. Chen, J. J. L. Goh, S. L. Kong, C. Chua, L. K. Hon, W. S. Tan, M. Wong, P. J. Choi, L. J. K. Wee, A. M. Hillmer, I. B. Tan, P. Robson and S. Prabhakar (2017). "Reference component analysis of single-cell transcriptomes elucidates cellular heterogeneity in human colorectal tumors." *Nature Genetics* 49(5): 708-+.

Li, M., A. M. Rezakhanlou, C. Chavez-Munoz, A. Lai and A. Ghahary (2009). "Keratinocyte-releasable factors increased the expression of MMP1 and MMP3 in co-cultured fibroblasts under both 2D and 3D culture conditions." *Molecular and Cellular Biochemistry* 332(1-2): 1-8.

Li, X. R., J. W. Xie, J. Lipner, X. Y. Yuan, S. Thomopoulos and Y. N. Xia (2009). "Nanofiber Scaffolds with Gradations in Mineral Content for Mimicking the Tendon-to-Bone Insertion Site." *Nano Letters* 9(7): 2763-2768.

Li, Y.-F., H. Gregersen, J. V. Nygaard, W. Cheng, Y. Yu, Y. Huang, M. Dong, F. Besenbacher and M. Chen (2015). "Ultraporous nanofeatured PCL-PEO microfibrous scaffolds enhance cell infiltration, colonization and myofibroblastic differentiation." *Nanoscale* 7(36): 14989-14995.

Lin, T. H., Q. M. Chen, A. Howe and R. L. Juliano (1997). "Cell anchorage permits efficient signal transduction between Ras and its downstream kinases." *Journal of Biological Chemistry* 272(14): 8849-8852.

Liu, J., H. Y. Zheng, P. S. P. Poh, H. G. Machens and A. F. Schilling (2015). "Hydrogels for Engineering of Perfusable Vascular Networks." *International Journal of Molecular Sciences* 16(7): 15997-16016.

Liu, Y., Y. Ji, K. Ghosh, R. A. F. Clark, L. Huang and M. H. Rafailovichz (2009). "Effects of fiber orientation and diameter on the behavior of human dermal fibroblasts on electrospun PMMA scaffolds." *Journal of Biomedical Materials Research Part A* 90A(4): 1092-1106.

Livak, K. J. and T. D. Schmittgen (2001). "Analysis of relative gene expression data using real-time quantitative PCR and the 2(T)(-Delta Delta C) method." *Methods* 25(4): 402-408.

Lorenz, H. P., M. T. Longaker, L. A. Perkocha, R. W. Jennings, M. R. Harrison and N. S. Adzick (1992). "Scarless wound repair - a human fetal skin model." *Development* 114(1): 253-259.

Lou, P.-J., M.-Y. Chiu, C.-C. Chou, B.-W. Liao and T.-H. Young (2010). "The effect of poly (ethylene-co-vinyl alcohol) on senescence-associated alterations of human dermal fibroblasts." *Biomaterials* 31(7): 1568-1577.

Love, M. I., W. Huber and S. Anders (2014). "Moderated estimation of fold change and dispersion for RNA-seq data with DESeq2." *Genome Biology* 15(12): 38.

Lowery, J. L., N. Datta and G. C. Rutledge (2010). "Effect of fiber diameter, pore size and seeding method on growth of human dermal fibroblasts in electrospun poly(epsilon-caprolactone) fibrous mats." *Biomaterials* 31(3): 491-504.

Lugo-Cintron, K. M., M. M. Gong, J. M. Ayuso, L. A. Tomko, D. J. Beebe, M. Virumbrales-Munoz and S. M. Ponik (2020). "Breast Fibroblasts and ECM Components Modulate Breast Cancer Cell Migration through the Secretion of MMPs in a 3D Microfluidic Co-Culture Model." *Cancers* 12(5): 19.

Lutolf, M. P. and H. M. Blau (2009). "Artificial Stem Cell Niches." *Advanced Materials* 21(32-33): 3255-3268.

Lynch, M. D. and F. M. Watt (2018). "Fibroblast heterogeneity: implications for human disease." *Journal of Clinical Investigation* 128(1): 26-35.

Marini, F. and H. Binder (2019). "pcaExplorer: an R/Bioconductor package for interacting with RNA-seq principal components." *Bmc Bioinformatics* 20: 8.

Marinkovich, M. P., D. R. Keene, C. S. Rimberg and R. E. Burgeson (1993). "Cellular-origin of the dermal-epidermal basement-membrane." *Developmental Dynamics* 197(4): 255-267.

Mascharak, S., H. E. DesJardins-Park, M. F. Davitt, M. Griffin, M. R. Borrelli, A. L. Moore, K. Chen, B. Duoto, M. Chinta, D. S. Foster, A. H. Shen, M. Januszyk, S. H. Kwon, G. Wernig, D. C. Wan, H. P. Lorenz, G. C. Gurtner and M. T. Longaker (2021). "Preventing Engrailed-1 activation in fibroblasts yields wound regeneration without scarring." *Science* 372(6540): 362-+.

Masters, K. S., D. N. Shah, G. Walker, L. A. Leinwand and K. S. Anseth (2004). "Designing scaffolds for valvular interstitial cells: Cell adhesion and function on naturally derived materials." *Journal of Biomedical Materials Research Part A* 71A(1): 172-180.

Matera, D. L., A. T. Lee, H. L. Hiraki and B. M. Baker (2021). "The Role of Rho GTPases During Fibroblast Spreading, Migration, and Myofibroblast Differentiation in 3D Synthetic Fibrous Matrices." *Cellular and Molecular Bioengineering* 14(5): 381-396.

Matera, D. L., W. Y. Wang, M. R. Smith, A. Shikanov and B. M. Baker (2019). "Fiber Density Modulates Cell Spreading in 3D Interstitial Matrix Mimetics." *Acs Biomaterials Science & Engineering* 5(6): 2965-2975.

Mauch, C., A. Hatamochi, K. Scharffetter and T. Krieg (1988). "Regulation of collagen-synthesis in fibroblasts within a 3-dimensional collagen gel." *Experimental Cell Research* 178(2): 493-503.

McMurtrey R.J (2016). "Analytic Models of Oxygen and Nutrient Diffusion, Metabolism Dynamics, and Architecture Optimization in Three-Dimensional Tissue Constructs with Applications and Insights in Cerebral Organoids". *Tissue Engineering Part C: Methods* 22(3): 221-249.

Melling, G. E., S. E. Flannery, S. A. Abidin, H. Clemmens, P. Prajapati, E. E. Hinsley, S. Hunt, J. W. F. Catto, R. Della Coletta, M. Mellone, G. J. Thomas, E. K. Parkinson, S. S. Prime, I. C. Paterson, D. J. Buttle and D. W. Lambert (2018). "A miRNA-145/TGF-beta 1 negative

feedback loop regulates the cancer-associated fibroblast phenotype." *Carcinogenesis* 39(6): 798-807.

Mi, H. Y., A. Muruganujan, J. T. Casagrande and P. D. Thomas (2013). "Large-scale gene function analysis with the PANTHER classification system." *Nature Protocols* 8(8): 1551-1566.

Miki, Y., K. Ono, S. Hata, T. Suzuki, H. Kumamoto and H. Sasano (2012). "The advantages of co-culture over mono cell culture in simulating in vivo environment." *Journal of Steroid Biochemistry and Molecular Biology* 131(3-5): 68-75.

Millet, M., E. Bollmann, C. R. Goulet, G. Bernard, S. Chabaud, M. E. Huot, F. Pouliot, S. Bolduc and F. Bordeleau (2022). "Cancer-Associated Fibroblasts in a 3D Engineered Tissue Model Induce Tumor-like Matrix Stiffening and EMT Transition." *Cancers* 14(15): 18.

Mine, S., N. O. Fortunel, H. Pageon and D. Asselineau (2008). "Aging Alters Functionally Human Dermal Papillary Fibroblasts but Not Reticular Fibroblasts: A New View of Skin Morphogenesis and Aging." *Plos One* 3(12): 13.

Mio, T., Y. Adachi, D. J. Romberger, R. F. Ertl and S. I. Rennard (1996). "Regulation of fibroblast proliferation in three-dimensional collagen gel matrix." *In Vitro Cellular & Developmental Biology-Animal* 32(7): 427-433.

Miron-Mendoza, M., J. Seemann and F. Grinnell (2010). "The differential regulation of cell motile activity through matrix stiffness and porosity in three dimensional collagen matrices." *Biomaterials* 31(25): 6425-6435.

Mozaffari, A. and M. P. Gashti (2022). "Air Plasma Functionalization of Electrospun Nanofibers for Skin Tissue Engineering." *Biomedicines* 10(3): 9.

Muda, M., U. Boschert, R. Dickinson, J. C. Martinou, I. Martinou, M. Camps, W. Schlegel and S. Arkinstall (1996). "MKP-3, a novel cytosolic protein-tyrosine phosphatase that exemplifies a new class of mitogen-activated protein kinase phosphatase." *Journal of Biological Chemistry* 271(8): 4319-4326.

Muhl, L., G. Genove, S. Leptidis, J. P. Liu, L. Q. He, G. Mocci, Y. Sun, S. Gustafsson, B. Buyandelger, I. V. Chivukula, A. Segerstolpe, E. Raschperger, E. M. Hansson, J. L. M. Bjorkegren, X. R. Peng, M. Vanlandewijck, U. Lendahl and C. Betsholtz (2020). "Single-cell analysis uncovers fibroblast heterogeneity and criteria for fibroblast and mural cell identification and discrimination." *Nature Communications* 11(1): 18.

Muniyandi, P., V. Palaninathan, S. Veeranarayanan, T. Ukai, T. Maekawa, T. Hanajiri and M. S. Mohamed (2020). "ECM Mimetic Electrospun Porous Poly (L-lactic acid) (PLLA) Scaffolds as Potential Substrates for Cardiac Tissue Engineering." *Polymers* 12(2).

Nakagawa, S., P. Pawelek and F. Grinnell (1989). "Extracellular-matrix organization modulates fibroblast growth and growth-factor responsiveness." *Experimental Cell Research* 182(2): 572-582.

Nan, L., Y. Zheng, N. Liao, S. Li, Y. Wang, Z. Chen, L. Wei, S. Zhao and S. Mo (2019). "Mechanical force promotes the proliferation and extracellular matrix synthesis of human gingival fibroblasts cultured on 3D PLGA scaffolds via TGF- expression." *Molecular Medicine Reports* 19(3): 2107-2114.

Nelson, C. M. and M. J. Bissell (2006). Of extracellular matrix, scaffolds, and signaling: Tissue architecture regulates development, homeostasis, and cancer. Annual Review of Cell and Developmental Biology. Palo Alto, Annual Reviews. **22:** 287-309.

Niewiarowski, S. and S. Goldstein (1973). "Interaction of cultured human fibroblasts with fibrin - modification bydrugs and aging in-vitro." *Journal of Laboratory and Clinical Medicine* 82(4): 605-610.

Nur-E-Kamal, A., I. Ahmed, J. Kamal, M. Schindler and S. Meiners (2005). "Three dimensional nanofibrillar surfaces induce activation of Rac." *Biochemical and Biophysical Research Communications* 331(2): 428-434.

Nurmik, M., P. Ullmann, F. Rodriguez, S. Haan and E. Letellier (2020). "In search of definitions: Cancer-associated fibroblasts and their markers." *International Journal of Cancer* 146(4): 895-905.

Ohlund, D., A. Handly-Santana, G. Biffi, E. Elyada, A. S. Almeida, M. Ponz-Sarvise, V. Corbo, T. E. Oni, S. A. Hearn, E. J. Lee, I. I. C. Chio, C. I. Hwang, H. Tiriac, L. A. Baker, D. D. Engle, C. Feig, A. Kultti, M. Egeblad, D. T. Fearon, J. M. Crawford, H. Clevers, Y. Park and D. A. Tuveson (2017). "Distinct populations of inflammatory fibroblasts and myofibroblasts in pancreatic cancer." *Journal of Experimental Medicine* 214(3): 579-596.

Orimo, A., P. B. Gupta, D. C. Sgroi, F. Arenzana-Seisdedos, T. Delaunay, R. Naeem, V. J. Carey, A. L. Richardson and R. A. Weinberg (2005). "Stromal fibroblasts present in invasive human breast carcinomas promote tumor growth and angiogenesis through elevated SDF-1/CXCL12 secretion." *Cell* 121(3): 335-348.

Ozdemir, B. C., T. Pentcheva-Hoang, J. L. Carstens, X. F. Zheng, C. C. Wu, T. R. Simpson, H. Laklai, H. Sugimoto, C. Kahlert, S. V. Novitskiy, A. De Jesus-Acosta, P. Sharma, P. Heidari, U. Mahmood, L. Chin, H. L. Moses, V. M. Weaver, A. Maitra, J. P. Allison, V. S. LeBleu and R. Kalluri (2014). "Depletion of Carcinoma-Associated Fibroblasts and Fibrosis Induces Immunosuppression and Accelerates Pancreas Cancer with Reduced Survival." *Cancer Cell* 25(6): 719-734.

Pape, J., M. Emberton and U. Cheema (2021). "3D Cancer Models: The Need for a Complex Stroma, Compartmentalization and Stiffness." *Frontiers in Bioengineering and Biotechnology* 9: 8.

Pardo, A. and M. Selman (2006). "Matrix metalloproteases in aberrant fibrotic tissue remodelling." *Proceedings of the American Thoracic Society* 3(4): 383-388.

Park, H., J. W. Lee, K. E. Park, W. H. Park and K. Y. Lee (2010). "Stress response of fibroblasts adherent to the surface of plasma-treated poly(lactic-co-glycolic acid) nanofiber matrices." *Colloids and Surfaces B-Biointerfaces* 77(1): 90-95.

Pelham, R. J. and Y. L. Wang (1997). "Cell locomotion and focal adhesions are regulated by substrate flexibility." *Proceedings of the National Academy of Sciences of the United States of America* 94(25): 13661-13665.

Plikus, M. V., X. J. Wang, S. Sinha, E. Forte, S. M. Thompson, E. L. Herzog, R. R. Driskell, N. Rosenthal, J. Biernaskie and V. Horsley (2021). "Fibroblasts: Origins, definitions, and functions in health and disease." *Cell* 184(15): 3852-3872.

Poobalarahi, F., C. F. Baicu and A. D. Bradshaw (2006). "Cardiac myofibroblasts differentiated in 3D culture exhibit distinct changes in collagen I production, processing, and matrix

deposition." *American Journal of Physiology-Heart and Circulatory Physiology* 291(6): H2924-H2932.

Pozzi, M., K. K. Wary, F. G. Giancotti and H. A. Gardner (1998). "Integrin alpha 1 beta 1 mediates a unique collagen-dependent proliferation pathway in vivo." *Journal of Cell Biology* 142(2): 587-594.

Pruss, R. M. and H. R. Herschman (1977). "Variants of 3T3 cells lacking mitogenic response to epideral growth-factor - (receptors mitogens colchicine selection)." *Proceedings of the National Academy of Sciences of the United States of America* 74(9): 3918-3921.

Ramos-Rodriguez, D. H., S. MacNeil, F. Claeyssens and I. O. Asencio (2021). "The Use of Microfabrication Techniques for the Design and Manufacture of Artificial Stem Cell Microenvironments for Tissue Regeneration." 8(5): 50.

Ramos-Rodriguez, D. H., S. MacNeil, F. Claeyssens and I. Ortega Asencio (2021). "Fabrication of Topographically Controlled Electrospun Scaffolds to Mimic the Stem Cell Microenvironment in the Dermal-Epidermal Junction." *ACS biomaterials science & engineering*.

Ramos, T., M. Ahmed, P. Wieringa and L. Moroni (2015). "Schwann cells promote endothelial cell migration." *Cell Adhesion & Migration* 9(6): 441-451.

Reneker, D. H. and I. Chun (1996). "Nanometre diameter fibres of polymer, produced by electrospinning." *Nanotechnology* 7(3): 216-223.

Renshaw, M. W., X. D. Ren and M. A. Schwartz (1997). "Growth factor activation of MAP kinase requires cell adhesion." *Embo Journal* 16(18): 5592-5599.

Rhee, S. (2009). "Fibroblasts in three dimensional matrices: cell migration and matrix remodeling." *Experimental and Molecular Medicine* 41(12): 858-865.

Rhee, S. and F. Grinnell (2007). "Fibroblast mechanics in 3D collagen matrices." *Advanced Drug Delivery Reviews* 59(13): 1299-1305.

Rosenfeldt, H. and F. Grinnell (2000). "Fibroblast quiescence and the disruption of ERK signaling in mechanically unloaded collagen matrices." *Journal of Biological Chemistry* 275(5): 3088-3092.

Russell, S. B., J. D. Russell, K. M. Trupin, A. E. Gayden, S. R. Opalenik, L. B. Nanney, A. H. Broquist, L. Raju and S. M. Williams (2010). "Epigenetically Altered Wound Healing in Keloid Fibroblasts." *Journal of Investigative Dermatology* 130(10): 2489-2496.

Rutledge, G. C., J. L. Lowery and C. L. Pai (2009). "Characterization by Mercury Porosimetry of Nonwoven Fiber Media with Deformation." *Journal of Engineered Fibers and Fabrics* 4(3): 155892500900400301.

Santocildes M.R (2014). Electrospun Poly(Caprolactone) and Strontium-Substituted Bioactive Glass for Bone Tissue Engineering. *White Rose Ethesis Online*. https://etheses.whiterose.ac.uk/5690/

Sahai, E., I. Astsaturov, E. Cukierman, D. G. DeNardo, M. Egeblad, R. M. Evans, D. Fearon, F. R. Greten, S. R. Hingorani, T. Hunter, R. O. Hynes, R. K. Jain, T. Janowitz, C. Jorgensen, A. C. Kimmelman, M. G. Kolonin, R. G. Maki, R. S. Powers, E. Pure, D. C. Ramirez, R. Scherz-Shouval, M. H. Sherman, S. Stewart, T. D. Tlsty, D. A. Tuveson, F. M. Watt, V. Weaver, A. T.

Weeraratna and Z. Werb (2020). "A framework for advancing our understanding of cancer-associated fibroblasts." *Nature Reviews Cancer* 20(3): 174-186.

Schafer, I. A., M. Pandy, R. Ferguson and B. R. Davis (1985). "Comparative observation of fibroblasts derived from the papillary and reticular dermis of infants and adults - growth-kinetics, packing density at confluence and surface-morphology." *Mechanisms of Ageing and Development* 31(3): 275-293.

Scholzen, T. and J. Gerdes (2000). "The Ki-67 protein: From the known and the unknown." *Journal of Cellular Physiology* 182(3): 311-322.

Schor, S. L., J. A. Haggie, P. Durning, A. Howell, L. Smith, R. A. S. Sellwood and D. Crowther (1986). "Occurrence of a fetal fibroblast phenotype in familial breast cancer." *International Journal of Cancer* 37(6): 831-836.

Schroeder, A., O. Mueller, S. Stocker, R. Salowsky, M. Leiber, M. Gassmann, S. Lightfoot, W. Menzel, M. Granzow and T. Ragg (2006). "The RIN: an RNA integrity number for assigning integrity values to RNA measurements." *Bmc Molecular Biology* 7: 14.

Sheng, W., G. Z. Wang, Y. L. Wang, J. Y. Liang, J. P. Wen, P. S. Zheng, Y. J. Wu, V. Lee, J. Slingerland, D. Dumont and B. B. Yang (2005). "The roles of versican V1 and V2 isoforms in cell proliferation and apoptosis." *Molecular Biology of the Cell* 16(3): 1330-1340.

Smitha, B. and M. Donoghue (2011). "Clinical and histopathological evaluation of collagen fiber orientation in patients with oral submucous fibrosis." *Journal of oral and maxillofacial pathology : JOMFP* 15(2): 154-160.

Smithmyer, M. E., S. E. Cassel and A. M. Kloxin (2019). "Bridging 2D and 3D culture: Probing impact of extracellular environment on fibroblast activation in layered hydrogels." *Aiche Journal* 65(12): e16837.

Somodi, S. and R. Guthoff (1995). "Visualization of keratocytes in the human cornea with fluorescence microscopy." *Ophthalmologe* 92(4): 452-457.

Song, X. Q. and T. Xie (2002). "DE-cadherin-mediated cell adhesion is essential for maintaining somatic stem cells in the Drosophila ovary." *Proceedings of the National Academy of Sciences of the United States of America* 99(23): 14813-14818.

Song, X. Q., C. H. Zhu, C. Doan and T. Xie (2002). "Germline, stem cells anchored by adherens junctions in the Drosophila ovary niches." *Science* 296(5574): 1855-1857.

Sorrell, J. M., M. A. Baber and A. I. Caplan (1996). "Construction of a bilayered dermal equivalent containing human papillary and reticular dermal fibroblasts: use of fluorescent vital dyes." *Tissue engineering* 2(1): 39-49.

Sorrell, J. M., M. A. Baber and A. I. Caplan (2004). "Site-matched papillary and reticular human dermal fibroblasts differ in their release of specific growth factors/cytokines and in their interaction with keratinocytes." *Journal of Cellular Physiology* 200(1): 134-145.

Sriram, G., P. L. Bigliardi and M. Bigliardi-Qi (2015). "Fibroblast heterogeneity and its implications for engineering organotypic skin models in vitro." *European Journal of Cell Biology* 94(11): 483-512.

Stachewicz, U., R. J. Bailey, W. Wang and A. H. Barber (2012). "Size dependent mechanical properties of electrospun polymer fibers from a composite structure." *Polymer* 53(22): 5132-5137.

Stanton, M. M., A. Parrillo, G. M. Thomas, W. G. McGimpsey, Q. Wen, R. M. Bellin and C. R. Lambert (2015). "Fibroblast extracellular matrix and adhesion on microtextured polydimethylsiloxane scaffolds." *Journal of Biomedical Materials Research Part B-Applied Biomaterials* 103(4): 861-869.

Stanton, M. M., J. M. Rankenberg, B.-W. Park, W. G. McGimpsey, C. Malcuit and C. R. Lambert (2014). "Cell Behavior on Surface Modified Polydimethylsiloxane (PDMS)." *Macromolecular Bioscience* 14(7): 953-964.

Taylor, G. (1969). "Electrically driven jets." *Proceedings of the Royal Society of London Series a-Mathematical and Physical Sciences* 313(1515): 453-&.

Thonemann, B., G. Schmalz, K. A. Hiller and H. Schweikl (2002). "Responses of L929 mouse fibroblasts, primary and immortalized bovine dental papilla-derived cell lines to dental resin components." *Dental Materials* 18(4): 318-323.

Tibbitt, M. W. and K. S. Anseth (2009). "Hydrogels as Extracellular Matrix Mimics for 3D Cell Culture." *Biotechnology and Bioengineering* 103(4): 655-663.

Tomasek, J. J., G. Gabbiani, B. Hinz, C. Chaponnier and R. A. Brown (2002). "Myofibroblasts and mechano-regulation of connective tissue remodelling." *Nature Reviews Molecular Cell Biology* 3(5): 349-363.

Tracy, L. E., R. A. Minasian and E. J. Caterson (2016). "Extracellular Matrix and Dermal Fibroblast Function in the Healing Wound." *Advances in Wound Care* 5(3): 119-136.

Tse HM, Gardner G, Dominguez-Bendala J, Fraker CA. The Importance of Proper Oxygenation in 3D Culture (2021). *Frontiers in Bioengineering and Biotechnology.* 2021 Mar 30;9:634403.

Tuan, T. L., L. C. Keller, D. Sun, M. E. Nimni and D. Cheung (1994). "Dermal fibroblasts activate keratinocyte outgrowth on collagen gels." *Journal of Cell Science* 107: 2285-2289.

Urban, N. and T. H. Cheung (2021). "Stem cell quiescence: the challenging path to activation." *Development* 148(3): 11.

Ushiki, T. (2002). "Collagen fibers, reticular fibers and elastic fibers. A comprehensive understanding from a morphological viewpoint." *Archives of Histology and Cytology* 65(2): 109-126.

Van Norman, G. A. (2019). "Limitations of Animal Studies for Predicting Toxicity in Clinical Trials Is it Time to Rethink Our Current Approach?" *Jacc-Basic to Translational Science* 4(7): 845-854.

Van Norman, G. A. (2020). "Limitations of Animal Studies for Predicting Toxicity in Clinical Trials Part 2: Potential Alternatives to the Use of Animals in Preclinical Trials." *Jacc-Basic to Translational Science* 5(4): 387-397.

Vashaghian, M., B. Zandieh-Doulabi, J.-P. Roovers and T. H. Smit (2016). "Electrospun Matrices for Pelvic Floor Repair: Effect of Fiber Diameter on Mechanical Properties and Cell Behavior." *Tissue Engineering Part A* 22(23-24): 1305-1316.

Wang, J., S. Vasaikar, Z. Shi, M. Greer and B. Zhang (2017). "WebGestalt 2017: a more comprehensive, powerful, flexible and interactive gene set enrichment analysis toolkit." *Nucleic Acids Research* 45(W1): W130-W137.

Wang, P. H., B. S. Huang, H. C. Horng, C. C. Yeh and Y. J. Chen (2018). "Wound healing." *Journal of the Chinese Medical Association* 81(2): 94-101.

Weigelt, B., A. T. Lo, C. C. Park, J. W. Gray and M. J. Bissell (2010). "HER2 signaling pathway activation and response of breast cancer cells to HER2-targeting agents is dependent strongly on the 3D microenvironment." *Breast Cancer Research and Treatment* 122(1): 35-43.

Wight, T. N., I. Kang, S. P. Evanko, I. A. Harten, M. Y. Chang, O. M. T. Pearce, C. E. Allen and C. W. Frevert (2020). "Versican-A Critical Extracellular Matrix Regulator of Immunity and Inflammation." *Frontiers in Immunology* 11: 12.

Wong, C. H., K. W. Siah and A. W. Lo (2019). "Estimation of clinical trial success rates and related parameters." *Biostatistics* 20(2): 273-286.

Woodley, J. P., D. W. Lambert and I. O. Asencio (2022). "Understanding Fibroblast Behavior in 3D Biomaterials." *Tissue Engineering Part B-Reviews* 28(3): 569-578.

Woodley, J. P., D. W. Lambert and I. O. Asencio (2023). "Reduced Fibroblast Activation on Electrospun Polycaprolactone Scaffolds." *Bioengineering-Basel* 10(3): 20.

Wu, Y. J., D. P. La Pierre, J. Wu, A. J. Yee and B. B. Yang (2005). "The interaction of versican with its binding partners." *Cell Research* 15(7): 483-494.

Wynn, T. A. (2007). "Common and unique mechanisms regulate fibrosis in various fibroproliferative diseases." *Journal of Clinical Investigation* 117(3): 524-529.

Wynn, T. A. (2008). "Cellular and molecular mechanisms of fibrosis." *Journal of Pathology* 214(2): 199-210.

Wynn, T. A. and T. R. Ramalingam (2012). "Mechanisms of fibrosis: therapeutic translation for fibrotic disease." *Nature Medicine* 18(7): 1028-1040.

Xia, S. L., B. Lal, B. Tung, S. Wang, C. R. Goodwin and J. Laterra (2016). "Tumor microenvironment tenascin-C promotes glioblastoma invasion and negatively regulates tumor proliferation." *Neuro-Oncology* 18(4): 507-517.

Xie, J. W., X. R. Li, J. Lipner, C. N. Manning, A. G. Schwartz, S. Thomopoulos and Y. N. Xia (2010). ""Aligned-to-random" nanofiber scaffolds for mimicking the structure of the tendon-to-bone insertion site." *Nanoscale* 2(6): 923-926.

Yamada, M., E. Kato, A. Yamamoto and K. Sakurai (2016). "A titanium surface with nano-ordered spikes and pores enhances human dermal fibroblastic extracellular matrix production and integration of collagen fibers." *Biomedical Materials* 11(1).

Yamaguchi, H. and R. Sakai (2015). "Direct Interaction between Carcinoma Cells and Cancer Associated Fibroblasts for the Regulation of Cancer Invasion." *Cancers* 7(4): 2054-2062.

Yamashita, Y. M., D. L. Jones and M. T. Fuller (2003). "Orientation of asymmetric stem cell division by the APC tumor suppressor and centrosome." *Science* 301(5639): 1547-1550.

Yang, S.-P., H.-S. Wen, T.-M. Lee and T.-S. Lui (2016). "Cell response on the biomimetic scaffold of silicon nano- and micro-topography." *Journal of Materials Chemistry B* 4(10): 1891-1897.

Yarden, Y. and M. X. Sliwkowski (2001). "Untangling the ErbB signalling network." *Nature Reviews Molecular Cell Biology* 2(2): 127-137.

Yeung, T., P. C. Georges, L. A. Flanagan, B. Marg, M. Ortiz, M. Funaki, N. Zahir, W. Y. Ming, V. Weaver and P. A. Janmey (2005). "Effects of substrate stiffness on cell morphology, cytoskeletal structure, and adhesion." *Cell Motility and the Cytoskeleton* 60(1): 24-34.

Zhang, J. W., C. Niu, L. Ye, H. Y. Huang, X. He, W. G. Tong, J. Ross, J. Haug, T. Johnson, J. Q. Feng, S. Harris, L. M. Wiedemann, Y. Mishina and L. H. Li (2003). "Identification of the haematopoietic stem cell niche and control of the niche size." *Nature* 425(6960): 836-841.

Zhang, W. and H. T. Liu (2002). "MAPK signal pathways in the regulation of cell proliferation in mammalian cells." *Cell Research* 12(1): 9-18.

Zhu, X. Y. and R. K. Assoian (1995). "Integrin-dependent activation of MAP kinase - a link to shape-dependent cell-proliferation." *Molecular Biology of the Cell* 6(3): 273-282.